6-30-2016

Iron Uptake And Accumulation Is A Target Of Nickel Toxicity During The Lag Phase In Escherichia Coli

Geoffrey Tuttle Ford
University of South Carolina

IRON UPTAKE AND ACCUMULATION IS A TARGET OF NICKEL TOXICITY DURING THE LAG PHASE IN *ESCHERICHIA COLI*

by

Geoffrey Tuttle Ford

Bachelor of Science
Presbyterian College, 2009

Submitted in Partial Fulfillment of the Requirements

For the Degree of Doctor of Philosophy in

Chemistry

College of Arts and Sciences

University of South Carolina

2016

Accepted by:

F. Wayne Outten, Major Professor

James Sodetz, Committee Member

Ken Shimazu, Committee Member

Erin Connely, Committee Member

Lacy Ford, Senior Vice Provost and Dean of Graduate Studies

DEDICATION

To my parents and my brothers, and most of all to my fiancé and future wife, Amanda.

ACKNOWLEDGEMENTS

I would like to acknowledge my advisor, Dr. F. Wayne Outten, for his guidance and assistance these past years, and for providing me the means and opportunities to reach my objectives. He has had the greatest influence on me as a scientist and mentor; without his aid I would not be the scientist that I am today. I am also grateful for the aid of my doctoral committee, Dr. James Sodetz, Dr. Ken Shimizu, and Dr. Erin Connolly. Together through the years they have given their advice and assisted me at each step towards my doctorate.

I would also like to express my thanks to my fellow colleagues in the Outten labs, both past and present, for their help and assistance. I would also like to thank Dr. Tom Makris and his lab members for their assistance with experiments and use of equipment. In addition to this, I would also like to thank Beth Bair at the USC Center for Elemental Mass Spectrometry for all of her help and support. Finally, I would like to express my gratitude to Dr. Arezue Bourojerdi at Claflin University for her collaboration with various projects. I also cannot thank enough the staff and administrators in the Department of Chemistry and Biochemistry here at USC. With their help I was able to see what is beyond the walls here at USC and was given the opportunity to travel and interact with others in my field.

Lastly, the my influences beyond graduate school were irreplaceable. My family and my brothers never failed to keep me focused on my goals and objectives. The meeting of my fiancé and future wife, Amanda, has also taught me that without any doubt

there will always be someone by my side to support and help me through any obstacle. I cannot express my gratitude to all the people that have been with me since the beginning.

ABSTRACT

Various transition metals are essential to all forms of life, and are only required in trace amounts. But this dependence comes as a double-edged sword. All organisms must maintain a careful intracellular quota that does not traverse outside an acceptable range. One transition metal in particular is nickel. The importance of this transition metal has been debated widely and its function varies greatly between organisms, including bacteria. However, the adverse effects caused by over exposure to this metal have been the center of much experimentation in recent years. Still, the mechanisms of nickel toxicity and the subsequent effects on cellular health, particularly the stability of the iron metallome, in bacteria remains poorly understood. The overall aim of these studies was to further elucidate the effects of nickel toxicity on the overall state of iron homeostasis during the lag phase of growth, using *Escherichia coli* as the model organism. We therefore developed a growth scheme that forced cells pre-adapted to growth on glucose to alter their central carbon metabolism to accommodate growth on gluconate. This shift allotted an additional stress on the iron metallome, given that the 6-phosphogluconate dehydratase enzyme vital to gluconate metabolism requires a [4Fe-4S] cluster for proper function. Our data demonstrated that the activity of this enzyme is absent in the presence of nickel, and thereby inhibited growth on gluconate during nickel exposure. ICP-MS and EPR analyses further confirmed nickel exposure during the lag phase inhibited iron uptake, and several genes central to iron uptake and Fe-S cluster synthesis were expressed through the lag phase. Finally, wild type cells were observed to ultimately

adapt to the nickel stress and grow to stationary phase. It was determined that these nickel treated cells developed a new phenotype that was resistant to nickel toxicity. The ferric reductase YqjH was linked to the development of this nickel resistance. A nickel-hypersensitive DyqjH mutant, however, did not develop resistance to nickel toxicity as the wild type strain had done. Finally, YqjH has been linked to both iron and nickel homeostasis, suggesting a possible role for YqjH during nickel stress.

TABLE OF CONTENTS

LIST OF TABLES

LIST OF FIGURES

CHAPTER 1

INTRODUCTION

1.1 Importance of Transition Metals

The biologically relevant, transition metals function as essential components serving in a variety of roles concerning cellular metabolism (Fig. 1.1). These transition metals are utilized as cofactors in metalloproteins, which are designed for catalysis, electron transport, structural support, or as sensors of redox processes and other cellular environmental conditions. Often, a select metalloprotein shows specificity for a given metal cation, and maximum activity occurs only with the native metal cofactor, but exceptions are not uncommon. Additionally, metalloproteins are often inhibited by non-native transition metals and have long been the subject of many studies. It is estimated that one-third to one-half of all proteins incorporate metal ions into their holo forms for proper function.[1,2] Despite their importance, each transition metal requires a complex system of import, export, intracellular transport, storage, and regulation to maintain a proper cellular quota (Fig. 1.2). This metal quota in bacteria is strongly dictated by environmental conditions as well as cellular and metabolic requirements, which in turn alters the repertoire of metalloproteins that require and regulate that metal. When the intracellular concentration of a given metal moves either above or below its acceptable

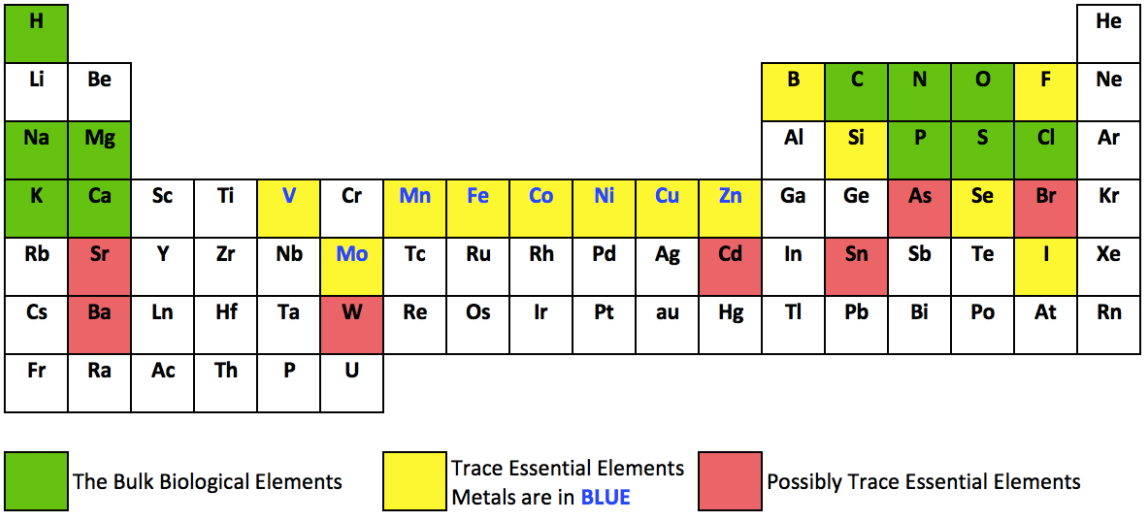

Figure 1.1. **Illustration of the elements identified as essential for life**. The above highlighted elements have been found in nature as essential (and possibly essential) for life in eukaryotes and prokaryotes. The transition metals have the chemical symbol in blue font.

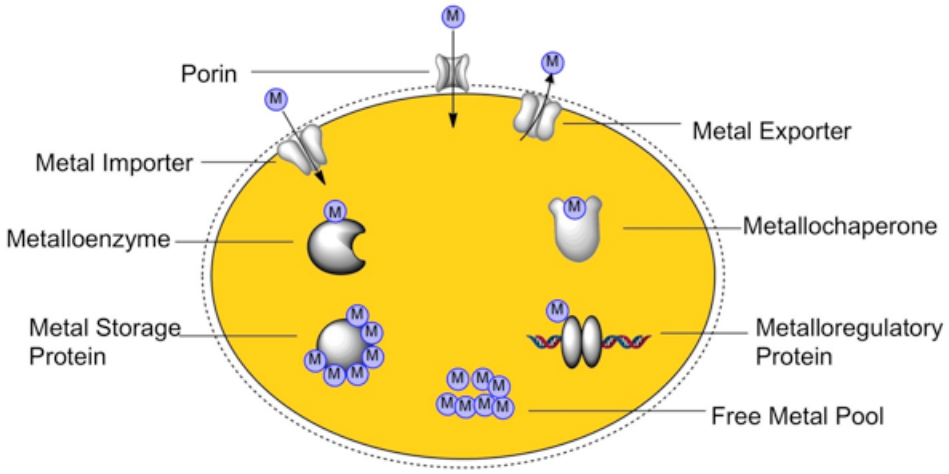

Figure 1.2. **Generalized Metal Homeostasis**. The systems involved in metal homeostasis include proteins utilized for import, intracellular transport, storage, regulation, labile pools, and export, in addition to a variety of metalloproteins specific to each metal species. These systems work in tandem to maintain intracellular quotas for proper cellular health.

cellular range, various downstream effects can lead to cellular damage and even death, through a variety of mechanisms

1.2 The Physiological Role of Iron

Iron is one of the most ubiquitous and essential transition metals found in life. Its availability in nature and its favorable redox activity were key to its selection as a major metal cofactor for a vast majority of metalloproteins. Iron-dependent metalloproteins are often involved in enzyme catalysis and electron transfer pathways, and are found in a variety of cofactors, such as Fe-S cluster centers, di-iron centers, or heme. As with all trace metals, intracellular iron levels are regulated via an intricate system of proteins and small molecules involved in mobilization, transport, intracellular trafficking, cofactor assembly, and storage (e.g. the ferritins).[3-5] In *E. coli*, transcriptional and post-transcriptional regulation of iron homeostasis is mediated by the metalloregulatory protein Fur and the small RNA RyhB.[6] Additionally, the IscR metalloregulatory protein, where the active, holo form is loaded with an Fe-S cluster, regulates a number of iron-utilizing and iron cofactor biogenesis systems in response to Fe-S cluster demand and somewhat overlaps the Fur regulon.[7] Together Fur, IscR, and RhyB coordinate the acquisition and use of iron by *E. coli*.

Due to its importance to cellular and physiological function, a lack of this metal is often detrimental, and iron starvation is a regulatory signal to alter organismal behavior to find more iron. For example, in many pathogenic bacteria, a lack of available iron not only signals growth within a host cell or tissue, but also activates a number of virulence

genes in order to obtain iron from host sources.[8,9] In other instances, iron starvation can inhibit cellular growth and evokes a "stringent response" due to decreased amino and nucleic acid production, de-represses the Fur regulon, and increases sensitivity to other external forces.[10,11] However, in contrast to the consequences of iron starvation, the opposite instance of iron toxicity can be caused by the over-abundance of intracellular iron levels and is an ever-present concern to many organisms, especially in the case of obligate and facultative aerobes. One detrimental consequence of iron toxicity is the occurrence of Fenton chemistry involving iron-dependent proteins and labile iron pools, and the subsequent production of radical oxygen species that leads to the damaging of various cellular components.[12,13] Iron is able to reversibly and easily traverse to and from the ferrous and ferric oxidation state at physiological pHs, a factor that allows this metal to fill a number of physiological roles. However, this comes as a double-edged sword. In the presence of an oxidative environment combined with high levels of labile iron (iron that is not coordinated to large biochemical compounds, such as proteins), these iron species can be freely oxidized from the ferrous state to the ferric state and produce a number of reactive oxygen species, or ROS. These compounds then lead to subsequent damaging of DNA, lipids, and other proteins that greatly damage the cell.[14,15]

Additionally, the systems of regulation that control intracellular quotas for a variety of other biologically relevant metals have been linked to iron homeostasis and vice versa.[16] For example, the transition metals copper and cobalt have been tied to the disruption of iron homeostasis in a variety of bacteria through an assortment of mechanisms.[17-19] Cobalt has demonstrated the ability, *in vitro*, to inactivate several Fe-S enzymes and to interfere with the Isc pathway (which is involved in Fe-S cluster

assembly).[17] Exposure to cobalt also increased the expression of iron uptake genes controlled by Fur.[17] Another transition metal, copper, has been shown to also disrupt the Fe-S clusters of enzymes involved in branched amino acid synthesis, and produced reactive oxygen species via a reaction similar to Fenton Chemistry with iron.[18] To complicate matters, copper is also an essential transition metal. This implies that in order for a cell to successfully maintain iron homeostasis, it must also coordinate the systems involved with the homeostasis of other transition metals. The scope of this study is to therefore characterize and elucidate any such effects of nickel toxicity has on iron homeostasis and determine the mechanisms of these actions.

1.3 The Physiological Role of Nickel

The transition metal nickel plays an important, albeit still ambiguous, role in organismal health, from bacteria up to humans. In comparison to iron, nickel is the 24th most abundant element overall and the 5th/6th most abundant first row transition metal (found at levels similar to another essential transition metal, zinc); whereas iron is the 4th most abundant element overall and the most abundant transition metal.[20] However, the functionalization of nickel as a cofactor in metalloproteins is not nearly as ubiquitous as the iron cofactors, e.g. heme, iron sulfur clusters, etc. This is partially due to some of the atomic and electrochemical differences between the iron and nickel ion. Unlike the reversibility of iron ions, nickel is not commonly a redox active metal at physiological pHs, and when detected it is often found in the divalent (2+) oxidation state in aqueous equilibria. Nonetheless, a trivalent (3+) nickel state has been observed under proper

conditions and coordination, such as with the Ni-SODs and the previously described Ni-Fe hydrogenases.[21-23] Furthermore, iron and nickel can complex with ligands in several different geometries, with both preferring the octahedral complex, but a coordinated nickel ion has also been observed to be stable in a square planar geometry.[24-26] Nickel has also been suggested to form stronger complexes with various ligand-forming elements based on the Irving-Williams series, and therefore, has the potential ability to displace iron from such complexes. The Irving-Williams series surmises the relative stability of complexes formed by various transition metal cations, primarily divalent species.[27] This order of stability can be expressed as such: Mn(II) < Fe(II) < Co(II) < Ni(II) < Cu(II) > Zn(II). The log stabilities of various transition metal complexes with amino acids and other common cellular metabolites have been illustrated in Figure 1.3 in order to demonstrate these preferences. Additionally, a link between iron and nickel homeostasis could be due to competition for ligands within the cell. Nickel could also be more suitable for physiological roles where iron is not preferred, and vice versa, but this leaves the potential for nickel to compete with iron and toxify cells when in excess like other biologically relevant metals.[16]

The significance of nickel in relation to health in eukaryotic systems has long been in question with specific, nickel-dependent roles remaining unknown. However, specific roles in bacteria have been identified, albeit sparingly. In *E. coli*, nickel is primarily employed as a cofactor in enzymes such as the Ni-Fe hydrogenase isozymes, as well as in the enzyme glyoxylase I.[28-30] In virulent bacterial species, such as *Helicobacter pylori* or various *Klebsiella* species, a mono-nuclear nickel center is coordinated by histidine residues and is utilized as a cofactor in the enzyme urease for the

A

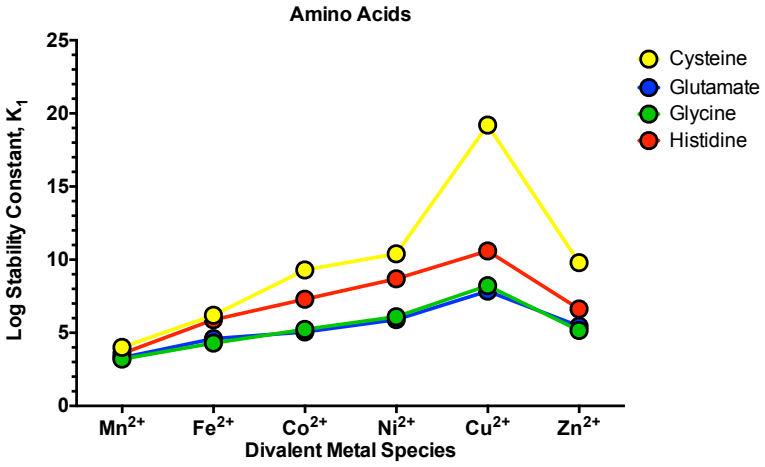

B

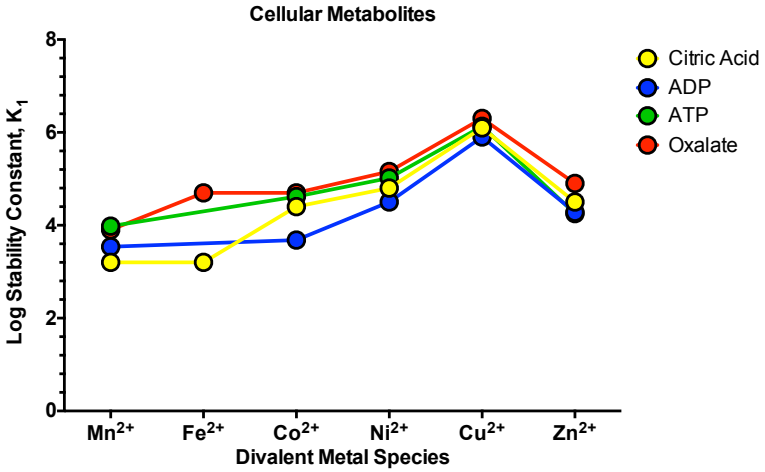

Figure 1.3. **The Irving-Williams Series as demonstrated the stability constants of selected transition metals with various ligands**. (A) The measured log stability constants of amino acids with selected transition metals. (B) The measured log stability constants of various cellular metabolites with selected transition metals.

breakdown of urea and production of ammonia.[31-34]

When necessary, E. coli will actively uptake nickel through the *nikABCDE* transport systems. This system is primarily active during anaerobic growth in order to help provide the cell with competent levels of nickel (primarily for expression of and assimilation into the Ni-Fe hydrogenases) while simultaneously preventing overimportation leading to proposed toxic consequences.[35,36] Overall, the most readily studied nickel-containing enzymes in *E. coli* have been the various Ni-Fe hydrogenase isozymes. Each isozyme is believed to fill a designated enzymatic niche during anaerobiosis, and is involved in either the oxidation of hydrogen gas as a source for reduction power during anaerobic growth, or the reversible reaction using protons as a final electron acceptor. Additionally, a double mutation of the *hydBC* genes (as part of the operon encoding for Ni-Fe Hydrogenase I multimer) fails to grow under anaerobic conditions when supplied solely with H_2(g) as an electron source and fumarate as a carbon source, representing the importance of this enzyme under these conditions.[37]

In contrast to anaerobiosis, nickel plays no vital physiological role during the growth of nonpathogenic *E. coli* under aerobic conditions. Nickel is not actively imported into the cell via its primary uptake system, the gene products of the *nikABCDE* operon, due to aerobic repression by its high affinity nickel-binding, self-repressor NikR and by FNR, a global regulator of aerobic-anaerobic metabolism.[38] Simultaneously, expression of the nickel exporter, RcnA, is activated at sub-micromolar levels of cytoplasmic nickel.[39,40] RcnR, the constitutive repressor of the RcnA nickel efflux transporter, has a high binding affinity of 25 and 5nM to nickel and cobalt, respectively.[41] Repression of RcnA by the RcnR regulator is lost in the presence of nickel, activating the

rcnA gene product and ultimately increasing nickel efflux by RcnA. Working together, these systems of uptake and efflux help *E. coli* to maintain low levels of intracellular nickel under aerobic conditions and at sufficient levels under anaerobic conditions, to ensure that nickel toxicity is minimalized.

The presence of chromosomally-located, nickel efflux systems like the RcnRA operon implies that nickel toxicity is a common occurrence in bacteria, regardless of the environmental conditions. The previously discussed mechanisms to counter the toxic effects of nickel were evolved by bacteria in order to restrict nickel uptake or increase nickel efflux when necessary. For instance, the deletion of the RcnRA proteins led to increased intracellular levels of nickel and cobalt.[16,42] Despite recent evidence in eukaryotic models, increased mutagenesis of DNA in bacterial models of nickel toxicity is less pronounced, and these effects depended on the model system used and the presence of co-mutagenic compounds.[42.43] Moreover, the degree of nickel toxicity and the resulting effects were heavily affected by both cell culture density, growth media, and other external factors, e.g. aerobic versus anaerobic, in which cells are cultured.[44,45] For example, during anaerobic growth in a complex media, such as Luria broth, millimolar levels of nickel were required to produce toxic effects.[44] As such, the mechanisms behind nickel toxicity have remained largely unknown, and identified targets of direct nickel toxicity are still few in number and vary by mechanism. Nonetheless, links between nickel and iron homeostasis have been established. For example, the proteins RcnR and RcnA were observed to fall under control by the Fur regulon, and RcnR expression was induced by iron.[16] Additionally, the expression of the putative ferric reductase enzyme YqjH, from *E. coli*, was also activated in the presence of nickel as well

as during iron starvation.[46] Finally, nickel homeostasis shares a number of similarities with cobalt homeostasis; through the aforementioned RcnRA efflux pathway, and that both are non-specifically transported through the Mg(II)-transporter CorA protein under aerobic conditions.[17,47,48] The link between cobalt and iron homeostasis was previously discussed, where cobalt was demonstrated to interfere with iron homeostasis by inhibiting Fe-S cluster assembly.[17] While nickel appear to fill physiological roles not suitable solely for iron, and vice versa, this does not erase the potential for nickel to compete with iron and toxify cells when in excess like other biologically relevant metals.[16] These examples hint that additional targets involved in iron homeostasis may still exist, and the link between these two metals is stronger than perceived and may carry an overall greater effect on cellular health.

1.4 **Mechanisms of Nickel Toxicity**

Despite its apparent toxicity at all levels of life, the mechanisms of nickel toxicity remain relatively ambiguous as mentioned briefly above. However, specific targets have begun to be discovered and the subsequent mechanisms of nickel toxicity have begun to be characterized.[42,49] By focusing on these select targets, several proposed mechanisms of nickel toxicity were recently postulated by Macomber et al.[42] Additional targets of nickel toxicity that may be involved in iron homeostasis that have yet to be identified may very well fall within one of these mechanisms or possibly through a novel mechanism yet to be seen.

First, nickel may displace a stipulated metal ion from the catalytic center of a metalloprotein (Fig. 1.4A). This was been observed *in vitro* with the iron-dependent metalloenzyme taruine/α-ketoglutarate dioxygenase (TauD), and with variable effect *in vitro* with a magnesium-dependent DNA polymerase I in *E. coli*.[50,51] Furthermore, in the prescribed cases above, inhibition of enzyme activity was increased if the metal-free apo-enzyme was treated with nickel prior to activation with the native metal ion. Recalling the premise and order of the Irving-Williams series, nickel's affinity for ligands (i.e. thiols like cysteine) is higher as compared to those with ferrous iron. Given that a convincing link has been observed between nickel and iron homeostasis, this indicates the need for careful regulation of each metal so that one does not perturb the other.[16,46] However, despite the observance of higher ligand affinities of nickel (according to Irving and Williams) and the observance that nickel inhibition of metalloproteins is increased if exposure occurs with a metalloprotein's apo form, nickel is unable to displace the coordinated iron centers of enzymatic Fe-S metalloproteins. This comes in stark contrast where as other softer metals such as Cu(II), Ag(I), Pb(II), and Zn(II) were able to do so with relative ease and very low concentrations.[45] Overall, considering these results, nickel may instead be considered an opportunistic metal toxicant. So that in order to maximize the effects of nickel toxicity of a potential enzymatic target, the presence of the metal may have to occur at an early stage in the maturation of the metalloprotein in question. This further increases the possibilities that when such exposure to nickel is sufficiently early in the iron cofactor biogenesis or enzyme maturation process, then new targets of nickel toxicity could be discerned with toxicity occurring by this mechanism.

In a second proposal, nickel may also bind to the catalytic residues of non-metalloenzymes, as further predicted by the Irving-William series (Fig. 1.3 and 1.4B). All enzymes maintain an active site or center that utilizes nearby amino acid residues to form a variety of intermediates and products during enzymatic turnover. Many of these residues contain nitrogen, oxygen, and sulfur atoms involved in the reactions; all of which may serve as a potential ligand to the Ni(II) ion. Two such non-metal dependent enzymes in *E. coli* are the tRNA-modifying enzymes cytosine-5-methyltransferase and uracil-5-methyltransferase.[52] The presence of cysteine residues in the active sites of these two proteins are possibly the reason for an ~80% loss in activity when the protein is in the presence of 1μM nickel. Furthermore, nickel is purported to have a higher affinity for ligands such as sulfur (thiol) and nitrogen, as opposed to ferrous iron, according to the Irving-Williams series (Fig. 1.3).

Nickel may also allosterically inhibit a protein's function (Fig. 1.4C). Recently, the metalloenzyme fructose-1,6-bisphosphate aldolase (FbaA) in *E. coli*, a critical enzyme utilized early in glycolysis, is a target of nickel toxicity. It was shown that nickel was able to displace a non-catalytic zinc ion in FbaA.[49] FbaA contains two zinc ions, one vital to the catalytic activity, and a second ion whose role is less defined but is still important for enzyme function and stability of the catalytic center.[53] It was observed *in vitro* that the presence of 2.5μM nickel ion displaced the secondary structural zinc center; which is coordinated with an aspartate and two glutamate residues.[49] By contrast, the catalytic zinc center is coordinated to 3 histidine residues. Furthermore, growth in minimal media with glucose as the sole carbon source was severely inhibited in the presence of 8μM nickel added during early exponential phase of growth.[49] Interestingly,

while zinc is theorized to have an affinity for ligands that is greater than nickel, nickel appeared to selectively displace a zinc center coordinate with primarily oxygen ligands but unable to displace a zinc coordinated with primarily nitrogen ligands. Overall, this mechanism follows a similar reasoning to the first prescribed mechanism, only instead the nickel ion complexes with residues outside the catalytic center and allosterically inhibits the enzyme or possibly destabilizes the catalytic center. This is also possibly a more common mechanism due to the lack of an already coordinated metal ion or that, if present, the coordination of a non-catalytic metal ion is not nearly as tightly bound as active center metals.

Finally, nickel, in both soluble (ionic) and insoluble (particulate) forms, may cause some form of oxidative damage at the cellular level, despite its poor redox activity as compared to iron. However, past studies in eukaryotic cell lines have demonstrated that inorganic nickel compounds can produce reactive oxygen species that mediate oxidative damage against various cellular macromolecules like DNA and lipids, especially where sulfur is ligated to the nickel ion.[54] Oxidative damage to DNA has long been suggested as a possible mechanism of nickel toxicity in eukaryotic models, either by oxidative damage to the DNA directly or an inhibition of DNA repair.[55,56] Evidence for nickel-media oxidative damage in bacteria has been more forthcoming in recent years, but is still relatively inconclusive. However, the possibility of oxidative damage occurring likewise in microorganisms remains nonetheless. *In vivo* and *in vitro* observations have been made involving the direct oxidative cleavage of DNA bases by a nickel complex, and nickel exposure increased expression superoxide dismutases, SODs (Fig. 1.4D).[57-60] SOD proteins are responsible for the protecting the cell from oxidative

A

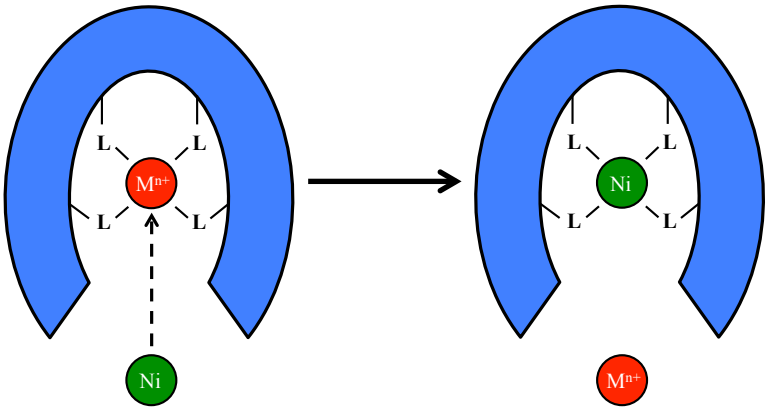

B

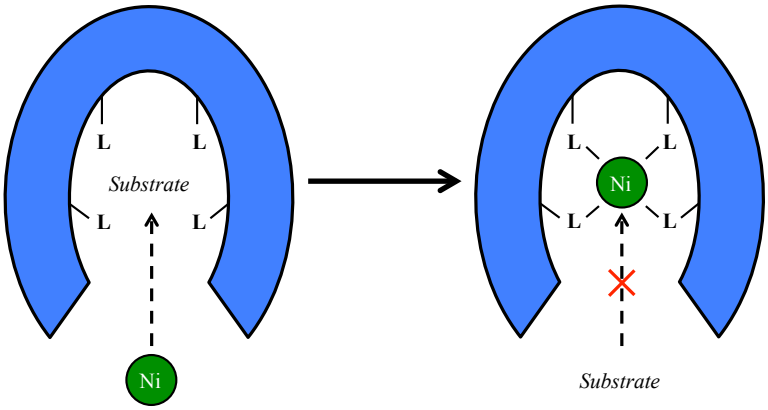

C

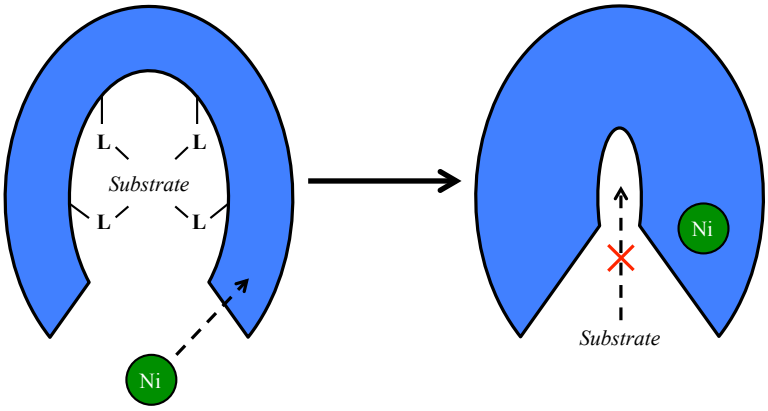

D

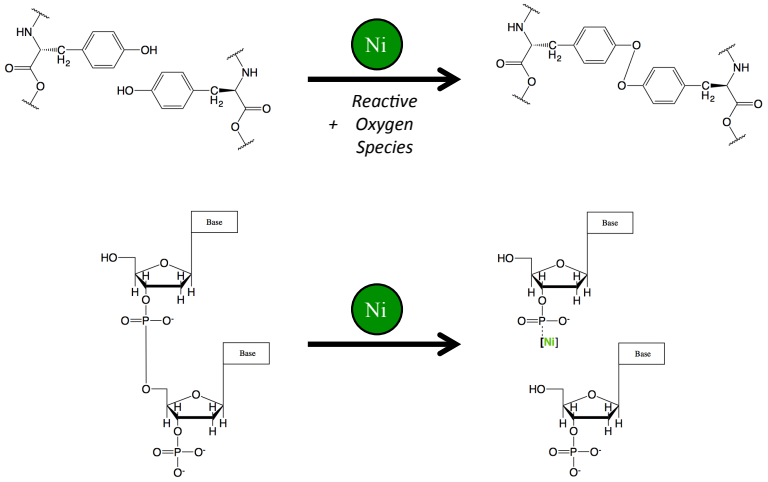

Figure 1.4. **Potential Mechanisms of Nickel Toxicity**. (A) Nickel displaces the native metal cation of a metalloenzyme. (B) Nickel inhibits non-metalloenzymes by chelating the active center residues involved in the enzyme mechanism and blocks substrate binding. (C) Nickel allosterically inhibits an enzyme by bind to amino acid residues outside of the catalytic center. (D) Nickel toxicity leads to mediated oxidative damage.

damage by consuming generated reactive oxygen species. Additionally, the deletion of the cytoplasmic Mn- and Fe-SODs in *E. coli* increased sensitivity to nickel, further suggesting the generation of reactive oxygen species as possible consequence of nickel toxicity in *E. coli*.[61] The oxidation of tyrosine residues to form cross-linked structures in a protein model was observed in the presence of a nickel complex with a peroxyacid mediator (Fig. 1.4D).[62] Lastly, a secondary but more indirect method of oxidative damage is also a possibility. Given the links between iron and nickel homeostasis and the toxicity mechanism involved with the possible displacement of iron centers from metalloproteins, oxidative damage via Fenton chemistry could occur due the increased levels of labile iron within the cell.

1.5 **Biomedical Importance**

Nickel is an important trace metal in higher species such as mammals, despite the primary function(s) remaining undetermined**.** Nickel deficiency has been linked to depressed growth, lower reproductive performance, and altered distribution of other trace metals (e.g. iron and zinc) and vitamin B_{12} in mammals such as rats and goats.[63] On the other hand, overexposure to of nickel in eukaryotic organisms, including humans, can cause disorders ranging from mild allergic reactions to carcinogenesis by possibly targeting and/or inhibiting proteins belonging to the iron/2-oxoglutarate-dependent dioxygenase family (2-ODDs), which includes proteins responsible for DNA repair and the regulation of the hypoxia-inducing factor (HIF).[56,64-66] Another example in eukaryotes demonstrated that nickel exposure interfered with cytosolic and mitochondrial

aconitase activity, proteins that contain Fe-S clusters.[67] There is further evidence that suggests soluble nickel may disrupt the regulation and homeostasis of iron in eukaryotic species. For example, nickel was able decrease intracellular iron levels in A549 human lung cells by competing with iron for uptake by DMT-1, the ubiquitous divalent metal transporter known for iron import, therefore inducing IRP-1 binding activity and reducing the translational rates of various iron homeostasis genes due to a lack of available iron.[64] As mentioned above, nickel was able to alter the cellular metabolism of iron as well as oxygen in human cells by activating the hypoxia-inducing factor 1 (HIF-1). One model suggested that nickel is able to substitute in for the iron center in a heme-containing protein; thereby blocking the oxygen-binding capability of the cells and inducing the hypoxic state and eventual downstream signaling cascade.[55,68] Overall, the blocking of iron uptake potentially caused the cells to be starved for iron due simply to the presence of the nickel. Finally, the effects of nickel toxicity can be caused by ingested soluble nickel compounds absorbed in the gut or from inhaled nickel particulates in the respiratory system, such as the particularly toxic nickel carbonyl .[56,64] Therefore, unlike mercury or arsenic, the form of the nickel species appears to bear no weight on its ability to toxify cells.

Regardless of the severity of nickel toxicity in humans, ranging from dermatological to cancerous, it is important to develop effective treatments for these conditions. To accomplish this, a strong understanding of the mechanisms of nickel toxicity is required. The effects of nickel toxicity in bacteria are well known, but only recently has it been determined how and why simple organisms such as bacteria are able to overcome nickel toxicity. Our studies aim to provide a further molecular and

biochemical understanding of the mechanisms of nickel toxicity in *E. coli*, and the prospective effect of nickel on iron homeostasis.

1.6 References

1. Thomson, A. J. and Gray, H. B. (1998) Bio-inorganic chemistry. *Curr Op Chem Biol*, 155-158.

2. Ascone, I., Meyer-Klaucke, W., and Murphy, L. (2003) Experimental aspects of biological X-ray absorption spectroscopy. *J Synchro Radiat* 10, 16-22.

3. Guerinot, M. L. (1994) Microbial Iron Transport. *Ann Rev Microbiol* 48, 743-772.

4. Stintzi, A., Barnes, C., Xu, J., and Raymond, K. N. (2000) Microbial iron transport via a siderophore shuttle: a membrane ion transport paradigm. *Proc Natl Acad Sci USA* 97, 10691-10696.

5. Ayala-Castro, C., Saini, A., and Outten, F. W. (2008) Fe-S cluster assembly pathways in bacteria. *Microbiol Mol Biol Rev* 72, 110-125.

6. Katigbak, J. and Zhang, Y. (2013) Iron Binding Site in a Global Regulator in Bacteria-Ferric Uptake Regulator (Fur) Protein: Structure, Mössbauer Properties, and Functional Implication. *J Phys Chem Lett* 3, 3503-3508.

7. Giel, J. L., Rodlonov, D., Liu M., Blattner, F. R., and Kiley, P. J. (2006) IscR-depdendent gene expression link iron-sulphur cluster assembly to the control of O_2-regulated genes in *Escherichia coli*. *Mol Microbiol* 60, 1058-1075.

8. Calderwood, S. B. and Makalanos, J. J. (1987) Iron regulation of Shiga-like toxin expression in *Escherichia coli* is mediate by the *fur* locus. *J Bacteriol* 169, 4759-4764.

9. Litwin, C.M. and Calderwood, S. B. (1993) Role of iron regulation of virulence genes. *Clin Microbiol Rev* 6, 137-149.

10. McHugh, J. P., Rodríguez-Quiñones, F., Abdul-Tehrani, H., Svistunenko, D. A., Poole, R. K., Cooper, C. E., and Andrews, S. C. (2003) Global Iron-dependent gene regulation in *Escherichia coli*. A new mechanism for iron homeostasis. *J Biol Chem* 278, 29478-29486.

11. Miethke, M., Westers, H., Blom, E. J., Kuipers, O. P., and Marahiel, M. A. (2006) Iron Starvation Triggers the Stringent Response and Induces Amino Acid Biosynthesis for Bacillibactin Production in *Bacillus subtilis*. *J Bacteriol* 188, 8655-8657.

12. Touati, D., Jacques, M., Tardat, B., Bouchard, L., and Despied, S. (1995) Lethal oxidative damage and mutagenesis are generated by iron in delta *fur* mutants of *Escherichia coli*: protective role of superoxide dismutase. *J Bacteriol* 177, 2305-2314.

13. Winterbourn, C. C. (1995) Toxicity of iron and hydrogren peroxide: the Fenton Reaction. *Toxicol Lett* 82, 969-974.

14. Cabiscol, E., Tamarit, J., and Ros, J. (2000) Oxidative stress in bacteria and protein damage by reactive oxygen species. *Int Microbiol* 3, 3-8.

15. Kashimari, Z. N. and Mankar, S. A. (2014) Free radicals and oxidative stress in bacteria. *Int J Curr Microbiol Appl Sci* 3, 26-33.

16. Koch, D., Nies, D. H., and Grass, G. (2007) The RcnRA (YohLM) system of *Escherichia coli*: a connection between nickel, cobalt, and iron homeostasis. *BioMetals* 20, 759-771.

17. Ranquet, C., Ollagnier-de-Choudens, S., Loiseau, L., Barras, R., and Fontecave, M. (2007) Cobalt stress in *Escherichia coli* – The Effect on the Iron-Sulfur Proteins. *J Biol Chem* 282, 30442-30451.

18. Macomber, L. and Imlay, J. A. (2009) The iron-sulfur clusters of dehydratases are primary intracellular targets of copper toxicity. *Proc Natl Acad Sci USA* 106, 8344-8349.

19. Chillappagari, S., Seubert, A., Trip, H., Kulpers, O. P., Marahiel, M. A. and Miethke, M. (2010) Copper stress affects iron homeostasis by destabilizing iron-sulfur cluster formation in *Bacillus subtillis*. *J Bacteriol* 192, 2512-2524.

20. Fleischer (1953) Recent Estimates of the Abundances of the Elements in the Earth's Crust. *Geological Survey Circular*, 1-7.

21. Ragsdale, S. W. (2006) Nickel biochemistry. *Curr Op Chem Biol* 2, 208-215.

22. Neupane, K. P., Gearty, K., Francis, A., and Shearer, J. (2007) Probing variable axial ligation in nickel superoxide dismutases utilizing metallopeptide-based models: insight into the superoxide disproportion mechanism. *J Am Chem Soc* 129, 14605-14618.

23. Sheng, Y., Abreu, I. A., Cabelli, D. E., Maroney, M. J., Miller, A. F., Teixeira, M., and Valentine, J. S. (2014) Superoxide Dismutases and Superoxide Reductases. *Chem Rev* 114, 3854-3918.

24. Harding, M. M. (2001) Geometry of metal-ligand interactions in proteins. *Acta Crystallogr D: Biol Chem* 57, 401-411.

25. Dokmanic, I., Sikic, M., and Tomic, S. (2008) Metals in proteins: correlation between the metal-ion type, coordination number, and the amino-acid residues involved in the coordination. *Acta Crystallogr D: Biol Chem* 64, 257-263.

26. Rulisek, L. and Vondrasek, J. (2009) Coordination geometries of selected transition metal ions (Co2+, Ni2+, Cu2+, Zn2+, Cd2+, and Hg2+) in metalloproteins. *J Inorg Biochem* 71, 115-127.

27. Irving, H. and Williams, R. J. P. (1984) Order of stability of metal complexes. *Nature* 162, 746-747.

28. Ballentine , S. P. and Boxer, D. H. (1986) Isolation and characterisation of a soluble active fragment of hydrogenase isoenzyme 2 from the membranes of anaerobically grown *Escherichia coli*. *Eur J Biochem* 156, 277-284.

29. Menon, N. K., Robbins, J., Wendt, J. C., Shanmugam, K. T., and Przybyla, A. E. (1991) Mutational analysis and characterization of the *Escherichia coli hya* operon, which encodes [NiFe] hydrogenase 1. *J Bacteriol* 173, 4851-4861.

30. Clugston, S. L., Barnard, J. F., Kinach, R., Miedema, D., Ruman, R., Daub, E., and Honek, J. F. (1998) Overproduction and characterization of a dimeric non-zinc glyoxylase I from *Escherichia coli*: evidence for optimal activation by nickel ions. *Biochem* 37, 8754-8763.

31. Hausinger, R. P. (1987) Nickel utilization by microorganisms. *Microbiol Rev* 51, 22-42.

32. Park, I. S. and Hausinger, R. P. (1993) Site-directed mutagenesis of *Klebsiella aerogenes* urease: identification of histidine residues that appear to function in nickel ligation, substrate binding, and catalysis. *Prot Sci* 2, 1034-1041.

33. Jabri, E., Carr, M. B., Hausinger, R. P., and Karplus, P. A. (1995) The crystal structure of urease from *Klebsiella aerogenes*. *Science* 268, 998-1004.

34. Li, Y. and Zamble, D. B. (2009) Nickel Homeostasis and Nickel Regulation: An Overview. *Chem Rev* 109, 4617-4643.

35. Chivers, P. T. and Sauer, R. T. (2000) Regulation of high affinity nickel uptake in bacteria. Ni2+-Dependent interaction of NikR with wild-type and mutant operator sites. *J Biol Chem* 275, 19735-19741.

36. Rowe, J. L., Starnes, G. L., and Chivers, P. T. (2005) Complex Transcriptional control links NikABCDE-Dependent Nickel Transport with Hydrogenase Expression in *Escherichia coli*. *J Bacteriol* 187, 6317-6323.

37. Dubini, A., Pye, R. L., Jack, R. L., Palmer, T., & Sargent, F. (2002). How bacteria get energy from hydrogen: a genetic analysis of periplasmic hydrogen oxidation in *Escherichia coli*. *Int J Hydrogen Energ* 27, 1413-1420

38. Chivers, P. T. and Sauer, R. T. (2002) NikR repressor: high-affinity nickel binding to the C-terminal domain regulates binding to operator DNA. *Chem Biol* 9, 1141-1148.

39. Rodrigue, A., Effantin, G., and Mandrand-Berthelot, M. A. (2005) Identification of *rcnA* (*yohM*), a Nickel and Cobalt Resistance Gene in *Escherichia coli*. *J Microbiol* 187, 2912-2916.

40. Iwig, J. S., Rowe, J. L., and Chivers, P. T. (2006) Nickel homeostasis in *Escherichia coli* – the *rcnR-rcnA* efflux pathway and its linkage to NikR function. *Mol Microbiol* 62, 252-262.

41. Iwig, J. S., Leitch, S., Herbst, R. W., Maroney, M. J., and Chivers, P. T. (2008) Ni(II) and Co(II) Sensing by *Escherichia coli* RcnR. *J Am Chem Soc* 130, 7592-7606.

42. Macomber, L. and Hausinger, R. P. (2011) Mechanisms of nickel toxicity in microorganisms. *Metallomics* 3, 1152-1162.

43. Kasprzak, K. S., Sunderman, F. W. Jr, and Salnikow, K. (2012) Nickel carcinogenesis. *Mutation Res* 553, 67-97.

44. Wu, L. F., Navarro, C., de Pina, K., Quénard, M., and Mandrand, M. A. (1994) Antagonistic Effect of Nickel on the Fermentative Growth of *Escherichia coli* K-12 and Comparison of Nickel and Cobalt Toxicity on the Aerobic and Anaerobic Growth. *Environ Health Perspect* 102, 297-300.

45. Xu, F. F. and Imlay, J. A. (2012) Silver(I), mercury(II), cadmium(II), and zinc(II) target exposed enzymic iron-sulfur clusters when they toxify *Escherichia coli*. *Appl Environ Microbiol* 78, 3614-3621.

46. Wang, S., Wu, Y. and Outten, F. W. (2011) Fur the the novel regulator YqjI control transcription of the ferric reductase gene *yqjH* in *Escherichia coli*. *J Bacteriol* 193, 563-574.

47. Thorgerson, M. P. and Downs, D. M. (2007) Cobalt targets multiple metabolic processes in *Salmonella enterica*. *J Bacteriol* 189, 7774-7781.

48. Wang, S. Z., Chen, Y., Sun, Z. H., Zhou, Q., and Sui, S. F. (2006) *Escherichia coli* CorA periplasmic domain functions as a homotetramer to bind substrate. *J Biol Chem* 281, 26813-26820.

49. Macomber, L., Elsey, S. P., and Hausinger, R. P. (2011). Fructose-1,6-bisphosphate aldolase (class II) is the primary site of nickel toxicity in *Escherichia coli*. *Mol Microbiol* 82, 1291-1300.

50. Snow, E. T., Xu, L. S., and Kinney, P. L. (1993) Effects of nickel ions on polymerase activity and fidelity during DNA replication *in vitro*. *Chem Biol Interact* 88*,* 155-173.

51. Kalliri, E., Gryska, P. A., and Hausinger, R. P. (2005) Kinetic and spectroscopic investigation of CoII, NiII, and N-oxalylglycine inhibition of the FeII/alpha-ketoglutarate dioxygenase, TauD. *Biochem Biophys Res Commun* 338, 191-197.

52. Hurwitz, J., Gold, M., and Anders, M. (1964) The enzymatic methylation of ribonucleic acid and deoxyribonucleic acid. IV. The properties of the soluble ribonucleic acid-methylating enzymes. *J Biol Chem* 239, 3474-3482.

53. Hall, D. R., Leonard, G. A., Reed, C. D., Watt, C. I., Berry, A., Hunter, W. N. (1999) The crystal structure of *Escherichia coli* class II fructose-1, 6-bisphosphate aldolase in complex with phosphoglycolohydroxamate reveals details of mechanism and specificity. *J Mol Biol* 287, 383–394.

54. Haung, X., Zhuang, Z, Frenkel, K., Klein, C. B., and Costa, M. (1994) The role of nickel and nickel-mediated reactive oxygen species in the mechanism of nickel carcinogenesis. *Environ Health Perspect* 102, 281-284.

55. Denkhaus, E. and Salnikov, K. (2002) Nickel essentiality, toxicity, and carcinogenicity. *Crit Rev Oncol Hematol* 42*,* 35-56.

56. Kasprzak, K. S., Sunderman, F. W., and Salnikov, K. (2003) *Mutation Research Fund Mol Mech Mut* 533, 67-97.

57. Kawanishi, S., Inoue, S., and Yamamoto, K. (1994) Active oxygen speciesin DNA damage induced by carcinogenic metal compounds. *Environ Health Perspect* 102, 17-20.

58. Van Nostrand, J. D., Arthur, J. M., Kilpatrick, L. E., Neely, B. A., Bertsch, P. M. and Morris, P. J. (2008) Changes in protein expression in *Burkholderia vietnamiensis* PR1 301 at pH 5 and 7 with and without nickel. *Microbiol* 154, 3813-3824.

59. Cheng, Z., Wei, Y. Y., Sung, W. W., Glick, B. R., and McConkey, B. J. (2009) Proteomic analysis of the response of the plant growth-promoting bacterium *Pseudomonas putida* UW4 to nickel stress. *Proteome Sci* 7, 1-8.

60. Tan, J., Zhu, L., and Wang, B. (2009) DNA binding and cleavage activity of quercetin nickel(II) complex. *Dalton Trans* 24, 4722-4728.

61. Geslin, C., Llanos, J. Prieur, D., Jeanthon, C. (2001) The manganese and iron superoxide dismutases protect *Escherichia coli* from heavy metal toxicity. *Res Microbiol* 152, 901-925.

62. Gill, G., Richter-Rusli, A. A., Ghosh, M., Burrows, C. J., and Rokita, S. E. (1997) Nickel-dependent oxidative cross-linking of a protein. *Chem Res Toxicol* 10, 302-309.

63. Nielsen, F. H. (1991) Nutritional requirements for boron, silicon, vanadium, nickel, and arsenic: current knowledge and speculation. *FASEB J* 5, 2661-2667.

64. Davidson, T., Chen, H., Garrick, M. D., D'Angelo, G., and Costa, M. (2005) Soluble nickel interferes with cellular iron homeostasis. *Mol Cell Biochem* 279, 157-162.

65. Chen, H. and Costa, M. (2009) Iron- and 2-oxoglutarate-dependent Dioxygenases: an emerging group of molecular targets for nickel toxicity and carcinogenicity. *BioMetals* 22, 191-196.

66. Mulware, S. J. (2013) Trace elements and carcinogenicity: a subject in review. *3 Biotech* 3, 85-96.

67. Chen, H., Davidson, T., Singleton, S., Garrick, M. D., and Costa, M. (2005) Nickel decreases cellular iron level and converts cytosolic aconitase to iron-regulatory protein 1 in A549 cells. *Toxicol Appl Pharmacol* 206, 275-287.

68. Li, Q., Chen, H., Huang, X., and Costa, M. (2010) Effects of 12 metal ions on iron regulatory protein 1 (IRP-1) and hypoxia-inducible factor-1 alpha (HIF-1a) and HIF-regulated genes. *Toxicol Appl Pharmacol* 213, 245-255.

CHAPTER 2

ESCHERICHIA COLI IS MORE SUSCEPTIBLE TO NICKEL TOXICITY DURING LAG PHASE AND SUGGESTS NEW TARGETS OF NICKEL TOXICITY

Abstract

The lag phase is a period of equilibration and adaptations, where cells must first acclimate to a new environment. During this period, bacteria must synthesize and integrate the proper cellular components necessary for rapid growth, or a period known as the exponential phase. The overall duration of the lag phase depends on the metabolic changes and micronutrient accumulation necessary to adapt to the new environment. We set out to investigate the effects of nickel toxicity on lag phase in *E. coli* in various media requiring metabolic rewiring to accommodate new carbon sources. We have established that the degree of nickel toxicity is dependent upon a number of factors, but it is primarily dependent on the timing of the nickel exposure. Moreover, the choice of the pre-stress and stress media, as well as the carbon source further influenced the degree of nickel toxicity. An immediate exposure to nickel at the time of inoculation caused a marked increase in the lag phase duration, along with an increase in overall doubling time once cells exit the lag phase. In contrast, if nickel exposure was delayed until the cells entered the exponential phase, the overall effects were much less severe. Furthermore, nickel toxicity was dependent on the uptake of nickel into the cell and nickel efflux was

critical for adaptation to the nickel stress. Unlike other transition metals, such as copper and silver, nickel did not trigger a bactericidal effect but was instead only observed to be bacteriostatic; once the nickel obstacle has been overcome or removed, *E. coli* cells were able to move into the exponential phase of growth. Lastly, nickel resistance was observed in strains that were pre-exposed to only the highest levels of nickel and then re-exposed under the same conditions; however, this occurrence was not found in cells exposed to 40μM Ni(II) and lower.

2.1 **Introduction**

Bacteria are constantly subjected to changing environmental conditions, and they must quickly and efficiently alter their metabolic profile in order to adapt to these constant changes to survive. This leads to bacteria cycling through a variety of "growth phases" in response to environmental changes. Bacterial growth during a batch culturing is traditionally broken down into the following four phases; lag, exponential, stationary, and death (likely via programmed cell death or PCD) (Fig. 2.1). Lag phase is described as a period of adaptation, repair, and no growth; cells are actively accumulating the necessary macro- and micronutrients for the synthesis of cellular compounds required for rapid growth or in response to a requirement of key metabolites.[1,2] The exponential and stationary phases are described as the start and end of rapid bacterial growth and division, respectively, where bacteria begin to exponentially divide and then slow down due to a build-up of waste products, such as acetic acid, and a growing lack of the necessary nutrients required for this sustained growth.[3,4] Finally, the death phase occurs once a

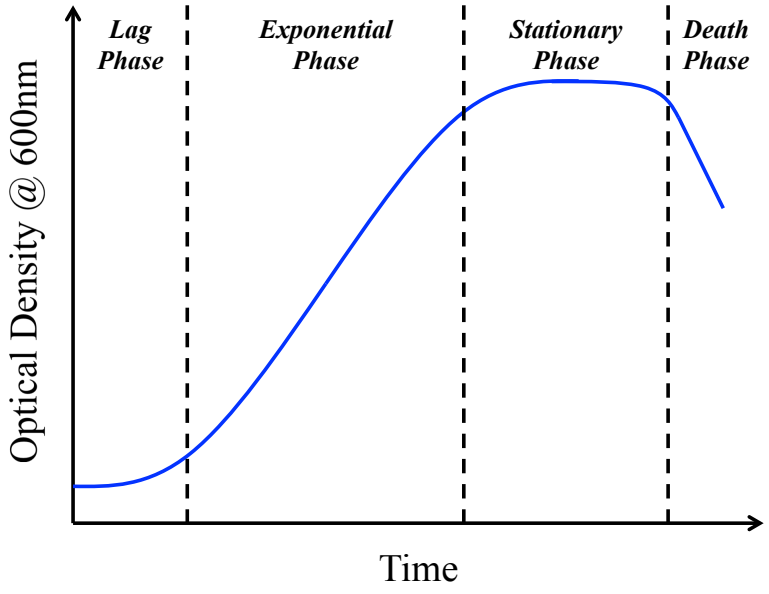

Figure 2.1. **Bacterial Growth Phases**. A bacterial culture progress through four traditionally defined phases of growth: Lag, Exponential, Stationary, and Death. Phases can be defined by the ratio of cell division against cell death.

medium is unable to sustain living cells and a bacterial cell's ability to counteract these toxic compounds fails. PCD, has been postulated as the mechanism behind this phase, possibly in order to free up necessary nutrients for other cells or to prevent detrimental mutations.[5,6] Alternatively, each phase can be characterized primarily by the rate of growth or the metabolic activity of the bacteria (Fig. 2.1). The exponential phase has been one of the most studied phases of growth since cells are rapidly dividing, metabolically homogenous, and the consumption of nutrients and metabolites is at its height. Therefore, the exponential phase is an advantageous point during culture growth to test the bacteriostatic or bactericidal effects of select chemicals or compounds, and observe their effect on rapid bacterial growth and metabolism. By contrast, the lag phase is much less understood and studies require optimization in order to utilize popular "-omics" methods (i.e. genomics, proteomics, metallomics, metabolomics) commonly applied during exponential phase growth.[2] First described near the start of the 20th century, it is defined as the period of adaptation for cells adjusting to a new growth medium.[1,7] The extent or length of this period,defined as l, is dependent on a number of factors. These factors include temperature, growth medium, nutrient availability, the presence of oxygen, and the magnitude of the inoculation itself.[1,2] New and improved models for phase prediction have been developed in order to simplify the exploration of this important yet still mysterious phase.

The selection of the base media is an important factor when studying culture growths, having large effect on the overall length of the lag phase period.[1] The availability of a carbon source, macronutrients such as nitrogen and sulfur, the presence of oxygen, and micronutrients such as the transition metals all influence this period of

adaptation, especially if the bacterial cells must synthesize the compounds themselves. The exact composition of a growth medium can be variable but a common base medium is complex Lennox Broth, or LB, which is composed of tryptone, yeast extract, and NaCl in a 2:1:1 ratio by mass. This rich media contains plentiful quantities of the nutrients, both macro- and micro-, required by *E. coli* for optimal growth, including high levels of catabolizable amino acids used as carbon sources.[4] In contrast to this is a chemically-defined such as M9 minimal media, which is composed primarily of phosphate and ammonium salts to ensure a final buffered pH of approximately 7, no carbon source, and low yet sustainable amounts of essential micronutrients like iron. A carbon source, increased amounts of micronutrients (e.g. biologically-relevant metals and vitamins), and other macronutrients (e.g. sulfur), can be supplemented to the base minimal media for studying the varying effects of each addition. Overall, growth in an M9 minimal media often forces the cells to synthesize the necessary base materials, such as nucleic and amino acids, required for rapid growth and is, of itself, a stress on cellular growth.

Selection of the carbon source for use in chemically-defined minimal media can be based on a number of factors, such as the point of entry into the central metabolic pathways that are active under aerobic or anaerobic growth. Glucose, gluconate, and glycerol all enter the Embden-Meyerhof-Parnas pathway, also known as Glycolysis, at a variety of points, as seen in Figure 2.2.[8-10] Glucose moves through the entire Glycolysis pathway and into the Kreb's Cycle as acetate. Glycerol is actively taken up and phosphorylated to glycerol-3-phosphate before entering the second half of glycolysis as dihydroxyacetone phosphate.[10] Finally, gluconate is actively transported by a two different systems, GntI and GntII, into the cell to be phosphorylated to gluconate-6-phosphate.[8,11-13] While

gluconate primarily follows the Entner-Doudoroff pathway (green arrows in Figure 2.2, a small amount can be used for the Pentose Phosphate Pathway (PPP, blue arrows in Figure 2.2) and re-enter glycolysis by being recycling as fructose-6-phosphate during nucleotide precursor synthesis. Recent studies have shown that the fructose bisphosphate aldolase II enzyme, FbaA II, is a target of nickel toxicity.[14] This enzyme is required for the proper catabolism of glucose via glycolysis.[15] FbaA activity was severely inhibited *in vitro* and *in vivo* in the presence of nickel and growth on glucose or fructose minimal media was drastically slowed.[14] As seen in Figure 2.2, glycerol bypasses the block in FbaA activity since it enters Glycolysis at a later step. Gluconate will also largely bypass the FbaA-dependent step of Glycolysis and enter at the later stages. However, the portion of gluconate that is siphoned into the Pentose Phosphate Pathway for metabolism would be dependent on FbaA later downstream as the products of the PPP feed back into glycolysis as fructose-6-phosphate, a point prior to aldolase function of the FbaA enzyme.

To review, nickel plays a small, but still important, role in bacterial cell health, primarily during anaerobiosis. Despite its relatively small role, bacteria have developed various systems of control specific to nickel since given its toxic effects when control over this metal is lost and intracellular levels increase. An overview of nickel homeostasis, including uptake, regulation, and export, has been previously reviewed by Higgins et al., as represented in Figure 2.3, as well as by others.[16-18] The physiological role in *E. coli* of nickel is tied to the presence and availability of oxygen. During aerobiosis there is no need for nickel and its uptake it shut down, whereas during anaerobiosis the requirement of nickel by the Fe-Ni hydrogenases are important during energy production.[88] The primary system of nickel uptake into *E. coli* during growth

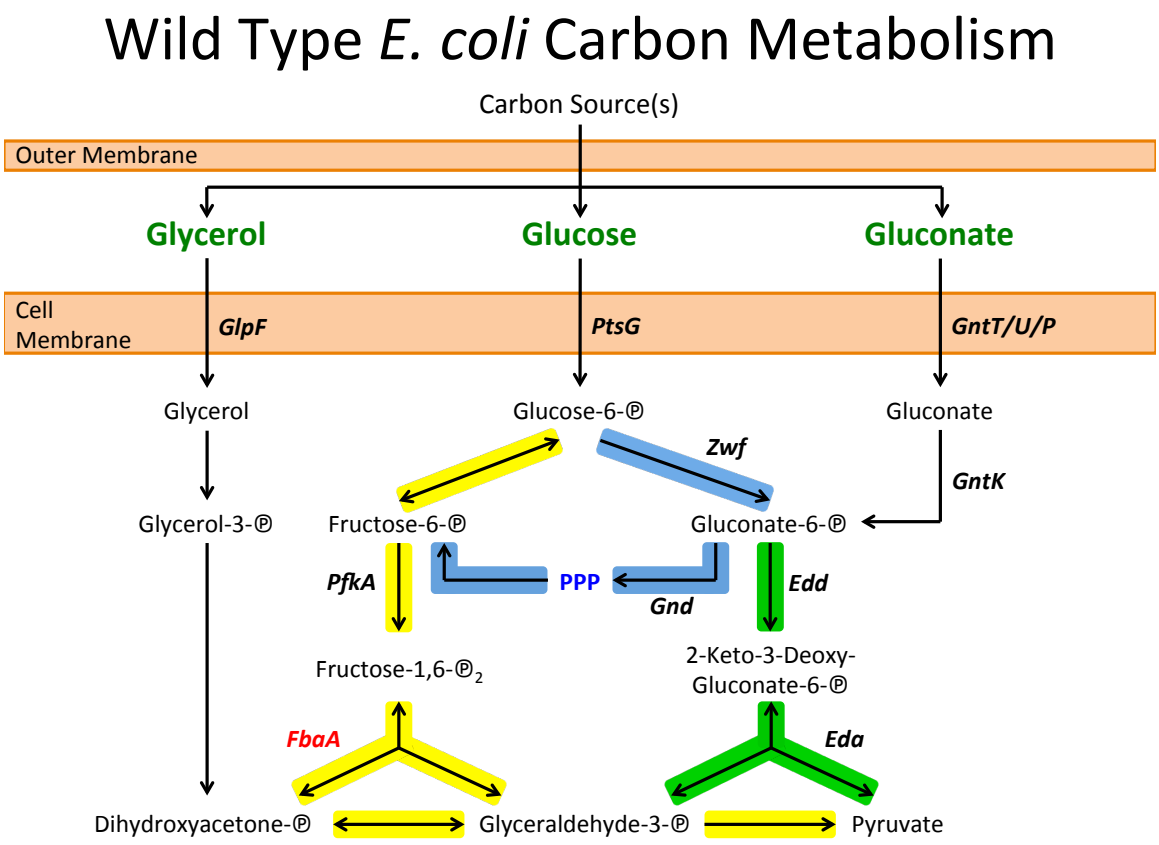

Figure 2.2. ***E. coli* MG1655 wild-type Carbon Metabolism**. The metabolic pathways used for initial catabolism of glycerol, glucose, and gluconate are shown. Glucose enters the cell and is phosphorylated to glucose-6-phosphate in order to proceed through glycolysis (yellow arrows). Glycerol is phosphorylated to glycerol-3-phosphate and ultimately to dihydroxyacetone-phosphate. Gluconate is phosphorylated to gluconate-6-phosphate and proceeds largely through the Entner-Doudoroff pathway (green arrows). Both glucose and gluconate can enter the Pentose Phosphate Pathway (blue arrows) for production of NADPH and nucleotide precursors. The nickel-inhibited glycolytic enzyme FbaA is shown in red.

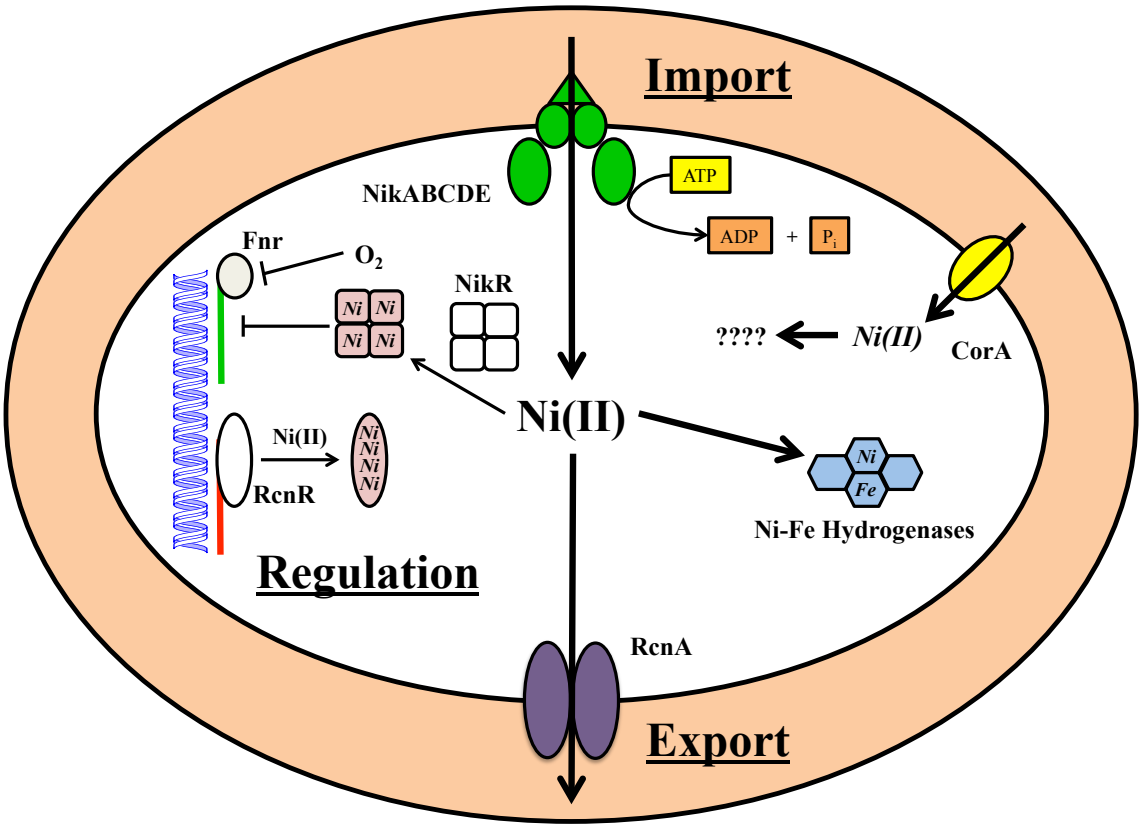

Figure 2.3. Nickel Homeostasis in *E. coli*. An overview of nickel homeostasis in E. coli, showing the key systems involved in nickel import, export, and regulation. Ni-Fe hydrogenases are shown as the primary targets for nickel assimilation, with support from the SlyD chaperone.

under anaerobic conditions includes the gene products of the *nikABCDE* operon, under the regulation of its own regulator, NikR, and the aerobic-anaerobic metabolism regulatory FNR.[19] NikR is encoded at the end of the nikABCDE operon and includes its own promoter sequence in order to maintain low levels of constitutive expression. Additionall, NikR maintains two sites for high- and low-affinity nickel binding that affect its overall level of repression on the *nikABCDE* operon. The high affinity site binds nickel ion in the picomolar range to maintain a low constitutive repression of the *nikABCDE* operon, whereas, the low affinity site binds nickel in the nanomolar range to induce greater repression of the *nikABCDE* system, which is a likely occurrence during active nickel uptake.[19-21] Overall, NikR prevents intracellular levels from becoming too high to cause toxicity but also allots for a proper level of intracellular nickel when the metal is required by the cell.

In addition to the control of nickel importation, excessive levels of nickel are further prevented by the RcnRA system, encoding the regulatory protein and a nickel-cobalt efflux transporter, respectively.[82,23] As discussed previously, RcnA binds nickel in the low nanomolar range (25nM) and operates in league with NikR to maintain low levels of intracellular nickel.[23,24] While the down-regulation of the nikABCDE operon remains relatively high during growth under aerobic conditions (due to the FNR regulator), no such effect is seen on RcnRA expression. Instead, regulation is primarily controlled by the presence of nickel, but there exists evidence that iron homeostasis may also play a role via the Fur regulatory protein.[25] This suggests that nickel entry into the cell during aerobic growth is likely non-specific, and nickel toxicity is a constant threat to bacteria such as *E. coli*. One possible point of entry for nickel into *E. coli* during aerobic growth

includes a constitutively-express Mg(II)-transporter, CorA.[26] Purified CorA was shown to be able to bind Co(II) and Ni(II), in addition to Mg(II), however these affinities for Co(II) and Ni(II) lower.[27] In addition, deletion of the *corA* gene helped to restore bacterial growth under aerobic conditions in minimal N-glucose media with 50μM Ni(II).[28] The presence of the CorA transporter, therefore, offers a strong target for focusing on nickel import under aerobic conditions for *E. coli* growths under different conditions as well.

The demonstrated link between iron and nickel homeostasis suggests that nickel toxicity may stem from detrimental effects on iron homeostasis that are caused by nickel overexposure. Therefore, the importance for the characterization and elucidation of these effects cannot be understated. Here, we explored various growth conditions in order to explore nickel toxicity and what targets may exist during the lag phase of *E. coli*

2.2 Materials and Methods

Bacterial Strains, Growth Media, and Growth Conditions. Strains used in this study are all derivatives of the parent wild-type strain *E. coli* MG1655 (Table 2.1). The MG1655 Δ*corA*::*kan*^{R} strain was constructed by P1 transduction using donor strains purchased from the CGSC at Yale University. The mutation was confirmed using colony PCR. For bacterial growths, an individual colony was transferred from fresh Lennox broth (LB) agar plates into a 4mL volume of LB and grown for 4 to 5hrs at 37°C with shaking at 200rpm. As described, cells from this culture were pelleted and washed twice

Table 2.1. **Bacterial Strains and Plasmids utilized in this study**.

Strain or Plasmid	Relevant Genotype or Phenotype	Reference or Source
E. coli Strains		
MG1655	Wild Type, *E. coli* K12 F-, λ^-, *ilvG-rfb*-50 *rph*-1	Laboratory Strain
GTF007	MG1655 Δ*rcnA::kan*^{R}	40
GTF032	MG1655 0μM Ni-treated	This Study
GTF037	MG1655 40μM Ni-treated	This Study
GTF038	MG1655 50μM Ni-treated	This Study
GTF054	MG1655 Δ*corA761::kan*^{R}	This Study
GTF059	MG1655 Δ*gnd727::kan*^{R}	This Study

in sterile 1X M9 minimal media salts; then the OD_{600} was normalized to 1.0. Normalized cells were diluted 1:200 into the specified pre-stress growth. For carbon source shifts, the pre-stress growth consisted of M9 glucose minimal media containing 1X M9 minimal salts (BD Difco), 0.2% (w/v) glucose (Acros Organics), 0.2% (w/v) magnesium chloride, 0.1mM calcium sulfate, and 0.5µg/mL Thiamine HCl (Sigma-Aldrich). Cultures were incubated overnight for 18 – 20hr, at 37°C and 200rpm, then washed and pelleted twice in sterile 1X M9 salts as described above. The resulting cell suspensions were normalized to an OD_{600} of 2.0 and diluted 1:50 into M9 gluconate minimal media with 0.2% (w/v) potassium gluconate (Alfa Aesar) to give an initial OD_{600} of 0.04. Nickel chloride (Sigma-Aldrich) was added to a specified final concentration in the M9 gluconate minimal media, from 0µM up to 50µM. Other reagents added to M9 glucose or M9 gluconate media are described in the appropriate figure legends. The growth scheme for carbon source shifting is represented in Figure 2.4.

Cell growth was monitored by UV-Vis absorption at 600nm and plotted versus time (in hours). Lag phase duration, l, was determined using the online fitting program, DMFit (www.ifr.ac.uk/safety/DMfit), applying the no-asymptote fitted model and parameters.[29] Stationary phase OD_{600} measurements were omitted for best fit of the model. Doubling time of the cells during the exponential phase of growth, where the steepest linear fit line could be applied at the point of inflection, was determined using the Online Doubling Calculator (http://www.doubling-time.com/compute.php).[30] All growths were cultured according to the growth scheme described in Figure 2.4 on the next page, unless otherwise noted.

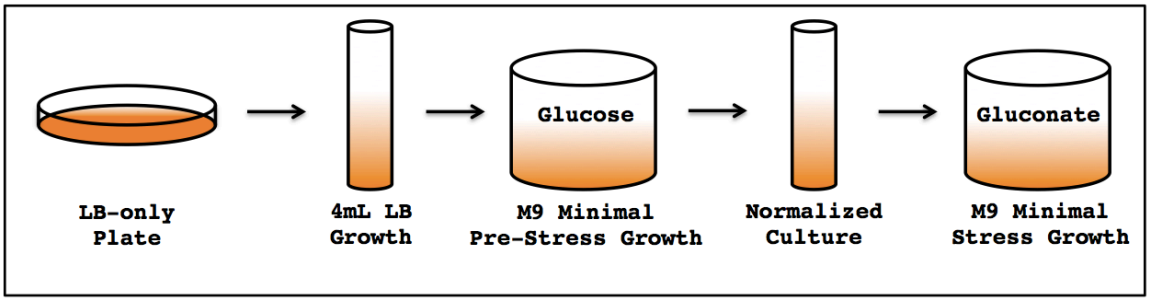

Figure 2-4. **Growth scheme for shift of cultures from growth on glucose to growth on gluconate**. Strains were plated on an LB agar plate (antibiotic applied when necessary) and incubated overnight at 37°C. Single colonies were individually inoculated into 4mL of LB media and incubated at 37°C, 200rpm for 4-5hrs. Cells were washed and pelleted twice using ice-cold, 1x M9 salts, then normalized to an OD_{600} of 1.0 and diluted 200x into growth media containing 1x M9 salts, 0.2% glucose (w/v), 0.02% $MgSO_4$, 100mM $CaCl_2$, and 0.5g/L Thiamine-HCl. Further supplementation of the media was indicated per specified growth. This growth was incubated at 37°C, 200rpm overnight for 18-20hrs. Cells were washed and pelleted twice using ice-cold, 1x M9 salts, normalized to an OD_{600} of 2.0, then diluted 50x into media containing 1x M9 salts, 0.2% gluconate (w/v), 0.02% $MgSO_4$, 100mM $CaCl_2$, and 0.5g/L Thiamine-HCl. Any further supplementation of the media was indicated per specified growth.

6-phosphogluconate Dehydratase Assays. Preparatory cell growth in LB and glucose minimal media was conducted as described above**.** Cultures were grown in 2L M9 gluconate minimal media with or without 50µM nickel chloride in a 4L culture flask at 37°C and 200rpm. For sample collection, a 150mL volume of cells was removed, washed, and pelleted twice using an ice-cold 1X M9 salt solution. Resulting cell pellets were resuspended in 1mL of cold 1X M9 salt solution; a small portion of each sample was diluted 40x to measure the final OD_{600}. The collected cell suspension was transferred to clean 1.5mL Eppendorf tubes, and the volume was recorded. After centrifugation, the supernatant was discarded and the pellets were frozen and stored at -80°C until ready to assay.

The production of pyruvate from gluconate via the combined activity of the 6-phosphogluconate dehydratase (Edd) and 2-keto-3-deoxy-6-phosphogluconate aldolase (Eda) enzymes was measured in whole cell lysate using a slightly modified form of a previous method.[31,32] Cell samples were prepared by thawing the frozen pellets for 15min on ice, then transferring them into an anaerobic chamber (Coy) with 2.5% H_2(g). Cell pellets were re-suspended in 500µL of anaerobic reaction buffer containing 50mM Tris-HCl, pH 7.65. After anaerobic cell breakage by sonication, a total volume of 400µL of whole cell lysate was transferred to a clean 1.5mL Eppendorf tube. After brief centrifugation to remove the cellular debris, whole cell lysates were kept on ice and the total protein concentration of each sample was determined via Bradford Assay. Next, 30µL of anaerobic 100mM magnesium chloride and 30µL anaerobic of 80mM 6-phosphogluconic acid (Research Products International Corp.) were added to whole cell lysate to provide a final whole cell lysate total protein concentration of 1mg/mL in a final

reaction volume of 300µL. The reactions proceeded for approximately 5min inside the anaerobic chamber and were quenched by the addition of 500µL of boiled reaction buffer followed by incubation in a boiling water bath for 3min. After cooling at room temperature for 1min and then on ice for 5min, denatured protein was removed by centrifugation for 5min at 4°C, 16,000 x g. A total volume of 600µL of cleared, quenched reaction supernatant was transferred into a clean 1.5mL Eppendorf tube. The total production of pyruvate was measured via a second enzymatic reaction by adding 100µL of quenched reaction supernatant to 4µL of 20mM NADH and 2µL l-Lactic dehydrogenase enzyme (80-120units/mg) (Sigma-Aldrich) and diluted to a final reaction volume of 500µL. Consumption of NADH was measured at 340nm after 5min. The final Δ340nm (e_{340} = 6200$mM^{-1}cm^{-1}$) was used to calculate the specific activity for 6-phosphogluconate dehydratase using Equation 1, below, where C = the lysate total protein concentration in mg/mL, t = time of the first (anaerobic) reaction in minutes, V = quenched reaction volume in mL, and ε_{NADH} = 6,220$mM^{-1}cm^{-1}$.

Equation 1: Specific Activity = $(\Delta Abs_{340})/[C * t * V * \varepsilon_{NADH}]$

Isocitrate Dehydrogenase Assays. Whole cell lysate samples previously prepared for Edd assays were further analyzed for Isocitrate Dehydrogenase (IDH) activity using an adapted protocol.[33] IDH assay buffer was made fresh and contained 50mM Tris-HCl, 20mM $MnCl_2$ tetrahydrate (Sigma Aldrich); the buffer pH was adjusted to 7.4. A fresh 1µL aliquot of 2mM $NADP^+$ and fresh 2.4µL aliquot of 10mM DL-Isocitratic Acid trisodium salt (Sigma Aldrich) were added to the IDH buffer. Whole cell

lysate was added to begin the reaction, giving a total final reaction volume of 1mL. The reaction was monitored at 340nm for the evolution of NADPH over time. Specific activity was calculated using a linear portion of the resulting assay, according to Equation 2 below:

Equation 2: Specific Activity = (μmol $NADP^+$ reduced)/hr/mg total protein

Development of nickel resistance, threshold growths, and CFU Counts. To ascertain if resistance to nickel toxicity had developed, wild-type MG1655 cells initially exposed to increasing levels of Ni(II) were collected after each growth had entered the stationary phase and cells were plated on LB plates without nickel. Plates were incubated overnight at 37°C, single colonies were transferred into 2mL LB, and cultured overnight at 37°C and 200rpm. Glycerol stocks were made from these cultures and stored at -80°C. Further experiments requiring these "Ni-adapted" strains (specified by the concentration of Ni(II) exposure) were conducted following the same growth scheme described above, with each strain exposed to increasing levels of nickel. To further determine if nickel toxicity was bacteriostatic or bactericidal, cells were cultured according to the growth scheme in Figure 2-4, but only incubated in the M9 gluconate media with 50μM Ni(II) for 3 hours before collection and inoculation into fresh LB media. Cells were grown at 37°C and 200rpm. The culture growth was monitored by absorbance by 600nm until the culture growth reached an OD_{600} of 0.15. The time elapsed to reach this threshold was recorded. In a dual-purpose experiment, colony formation units were measured after several 1:100 serial dilutions of the same cell growths on to fresh LB-only agar plates.

Plates were incubated over night at 37°C and the colonies were counted the next day in order to calculate the number of colony forming units.

2.3 Results

New targets of nickel toxicity are exposed during the lag phase in E. coli cells. In order to study the effects of nickel toxicity during the lag phase of growth, it was important to develop and refine a growth scheme that would allow us to investigate nickel toxicity in E. coli during lag phase. Recent studies indicate that nickel stress inhibits the zinc-dependent fructose-1,6-bisphosphate aldolase (FbaA) in exponential phase E. coli cells cultured in minimal media containing glucose or fructose.[14] FbaA is a crucial enzyme for the metabolism of these sugars via the Glycolysis pathway. Therefore, it was necessary to bypass the already known targets of nickel toxicity in order to elucidate other potential targets. To begin, cells were first cultured overnight in one of two types of media broth, the complex media LB or the chemically defined M9 minimal media (this first overnight growth will here on be referred to as known as a "pre-stress" growth). LB was selected as a rich, complex media containing multiple carbon sources, optimal levels of small molecule metabolites (i.e. amino acids), and sufficient levels of the biologically relevant metals required for growth. In contrast, M9 minimal media is limited for most nutrients and metals as compared to LB and often provides only a single, controlled carbon source to support growth. Minimal media therefore allowed a much greater control over which nutrients and metals the cells were exposed to as well as the final concentration of those nutrients. Other compounds could also be added to the

minimal media to supplement a different nutritional necessity or allow us to study the varied effect on nickel toxicity.

After an overnight pre-stress growth in a selected media, the cells were washed and normalized, then subsequently inoculated to a "stress" growth that would contain nickel at a specified concentration. When M9 minimal media was utilized during the stress growth phase, the choice for the single carbon was made between glucose, gluconate, and glycerol, due to their various entry points into mainstream carbon metabolism in *E. coli*. This permitted us to determine the overall effect of nickel toxicity as it correlated to a specific carbon source. Glucose was selected as a control carbon source, because of the previously observed defects in cellular growth in this media.[14] Gluconate was specifically chosen in order to bypass the main route for glucose metabolism via its metabolism primarily through the parallel Entner-Doudoroff pathway. Finally, glycerol was selected as an alternative carbon source that also bypasses the first half of glycolysis, and therefore the FbaA enzyme, by using an alternative route versus the Entner-Doudoroff pathway.[10]

Wild type *E. coli* cells were grown overnight in an LB-only pre-stress growth, then inoculated into an M9 minimal media with a selected carbon source. The growths were observed to have drastically different growth phenotypes in response to the nickel toxicity after 24 hours of growth (Fig. 2.5). As a control, these cells were also inoculated, in triplicate, into fresh volumes of LB media with the same range of nickel concentrations. These LB control growths showed no evidence of nickel toxicity with up to 50μM Ni(II) exposure (Fig. 2.5). Growths in glycerol minimal media showed no toxicity phenotype up to 50μM Ni(II) after 24 hours, as opposed to the glucose and

gluconate minimal media growths (Fig 2.5). While nickel toxicity in both the glucose and gluconate M9 minimal media growths correlated to the increasing nickel concentrations, wild type cells cultivated in glucose minimal media showed a much greater degree of toxicity as indicated by the lower culture density by the 24hrs checkpoint (Fig 2.5). We further noted that the control growths for each carbon source, with 0μM added nickel, in gluconate minimal media resulted in an overall lower growth density as compared to the glucose and glycerol minimal media control cultures. This suggests that the transition from LB to gluconate is more metabolically demanding compared to shifting from LB into glucose or LB into glycerol. These results also showed that following a shift from the complex LB media, cells grown on glucose minimal media are more sensitive to nickel than cells grown on glycerol or gluconate as the sole carbon source (data not shown).

For the next step, cells were cultivated overnight first in an M9 minimal media pre-stress growth, as opposed to the LB-only media pre-stress growth. Cells were then transferred to the same type of media with the same carbon source but with a varied range of added nickel (Fig 2.6). Cultures of wild type cells grown in M9 minimal stress media with glucose or gluconate carbon sources at 24hrs were significantly less inhibited and showed a lesser effect of nickel toxicity (Fig. 2.6). This comes as a stark difference to the cultures grown in the LB-only pre-stress media overnight with the subsequent shift into an M9 minimal media (Fig. 2.5) Wild type cells cultured in glycerol showed no relevant toxicity, regardless of the pre-stress media type (LB vs. M9 minimal media with glycerol) (Fig. 2-5 and 2-6). These results suggest that pre-adaptation to the selected stress media minimizes the effects of nickel toxicity (Fig. 2-6) and suggests that the lag phase, where

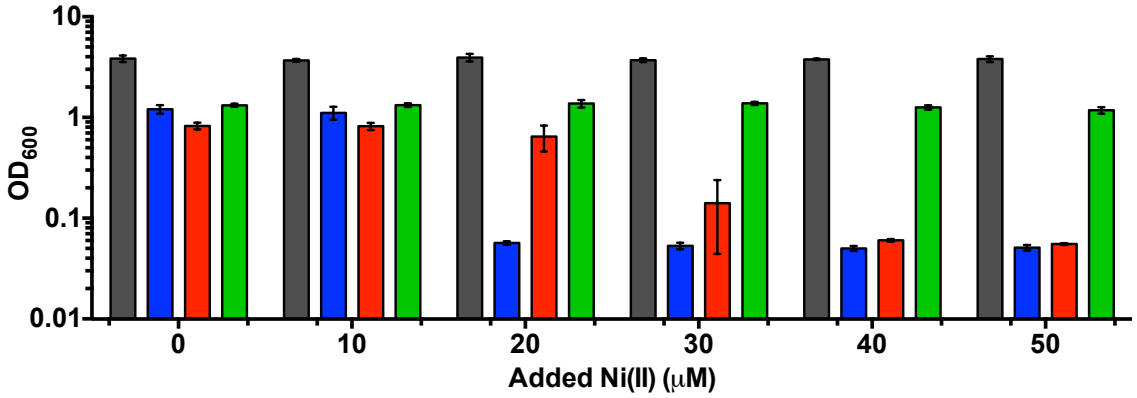

Figure 2.5. **Nickel toxicity varies with carbon source**. *E. coli* MG1655 wild type cells were cultured overnight in LB for 18hrs, then inoculated into various stress media containing $NiCl_2$ (0 to 50μM, in 10μM increments). Cell culture optical density at 600nm was measured and recorded after 24 hours of growth. All growths were repeated in triplicate (n = 3), and error bars indicate one standard deviation from the mean value.

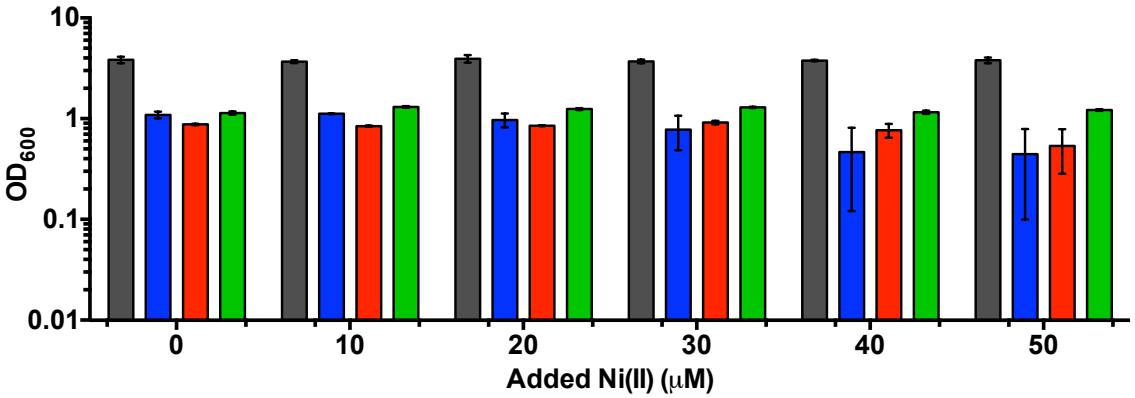

Figure 2.6. **Preadaptation to M9 minimal media and carbon source abolishes nickel toxicity**. MG1655 wild type cells were cultivated overnight in M9 minimal media with a specified carbon source; glucose (blue), gluconate (red), or glycerol (green). After this, cells were washed and inoculated into fresh M9 minimal media infused with the same matching carbon sources and nickel concentrations of 0 to 50μM, in 10μM increments. All growths were repeated in triplicate (n = 3), and error bars indicate one standard deviation from the mean value.

cells adapt to the new environmental conditions, could be a period of nickel sensitivity.

Therefore, our next aim was to test if new targets of nickel toxicity in *E. coli* may be exposed in the lag phase of a growth with a metabolic adaptation to a new carbon source We therefore developed a growth scheme to allow cells to adapt to the stress of the minimal media by culturing cells on glucose M9 minimal media as the overnight pre-stress growth, and then shifted the cells into a gluconate minimal media stress growth with varying levels of nickel. This growth scheme is represented by Figure 2.4 and served as the primary growth scheme for the succeeding growths unless otherwise noted. To test if nickel toxicity was altered during metabolic adaptation, *E. coli* cells were first grown in M9 glucose minimal media overnight to stationary phase and then diluted into M9 gluconate minimal media with varying concentrations of nickel (Fig. 2.7A). In contrast to the previous growth measurements, which only measured final cell density after 24 hours (Figures 2.5 and 2.6), here we measured the increase in cell density over time (by measuring optical density at 600nm) in the presence of nickel. These growth measurements over time allowed us to fit the growth data to obtain lag phase duration as well as the doubling-time during exponential growth. As previously reviewed, gluconate was selected due to its alternative metabolism through the Entner-Doudoroff pathway that bypasses the FbaA enzymatic step in glycolysis (Fig. 2.2). Gluconate uptake, phosphorylation, and downstream metabolism is repressed in cells grown with glucose.[12,13] Therefore, this switch from glucose to gluconate forces the cells to synthesize the [4Fe-4S] 6-phosphogluconate dehydratase (Edd) *de novo* to allow catabolism via the gluconate-inducible Entner-Doudoroff pathway.[8,31] The metabolic shift of wild-type *E. coli* from glucose to gluconate minimal media, paired with exposure

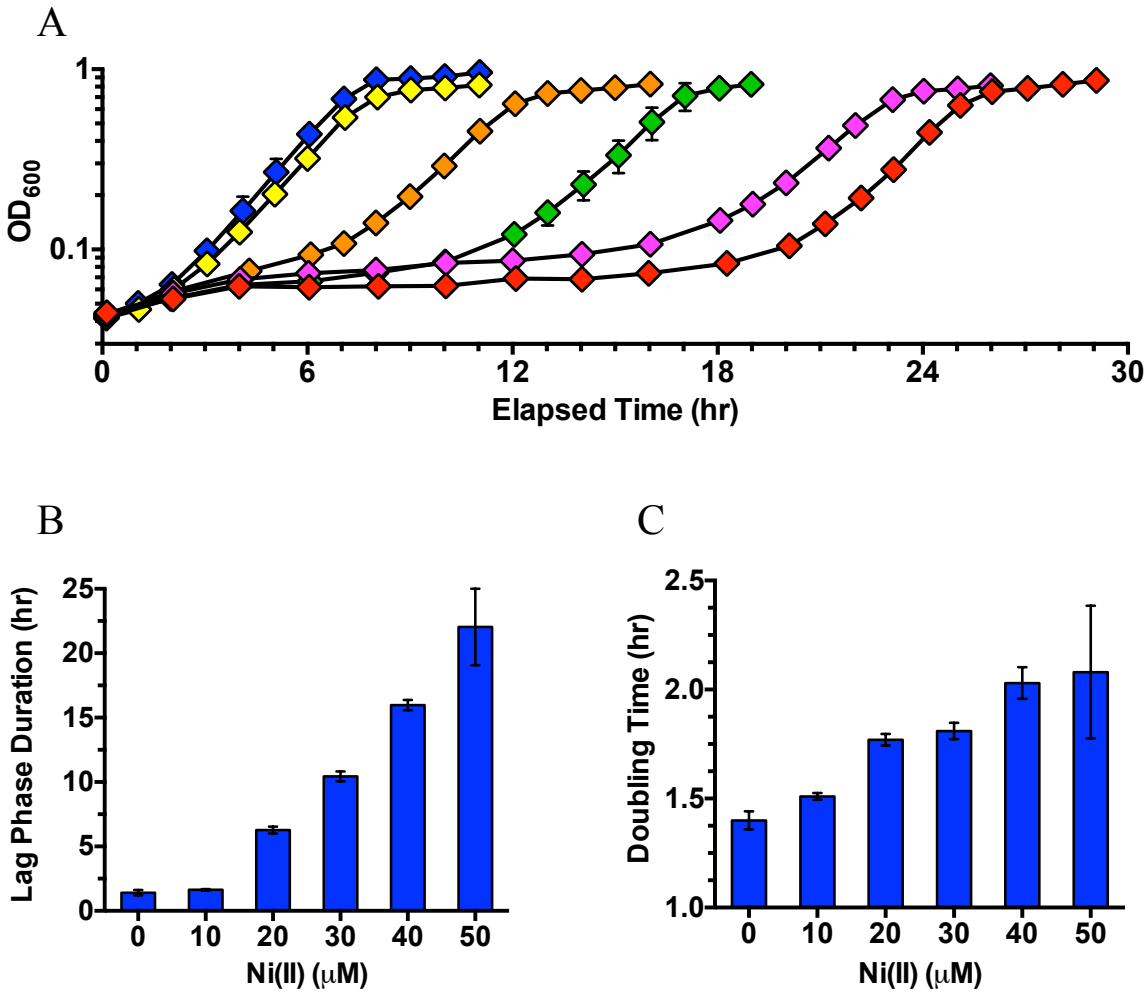

Figure 2.7. **Nickel toxicity extends lag phase duration**. Wild-type MG1655 cells grown overnight in glucose minimal media were diluted into gluconate minimal media in accordance with the scheme in Figure 2-5. The gluconate stress media was supplemented with increasing concentrations of $NiCl_2$. (A) Growth curves of wild type cells exposed to 0, 10, 20, 30, 40, or 50μM $NiCl_2$. (B) Lag phase duration calculated from growth curve data in (A). (C) Doubling times calculated from growth curve data in (A). All growths were repeated in triplicate (n = 3), and error bars indicate one standard deviation from the mean value.

to increasing levels of nickel, caused a more than 10-fold increase in lag phase duration (Fig. 2.7B). Additionally, once the nickel-exposed cells exited the lag phase and entered the exponential growth phase, the presence of nickel only increased the culture doubling time by a maximum of 2-fold with 50μM Ni(II) exposure (Fig. 2.7C).

Recently, it was demonstrated that wild type cells also display a growth defect when nickel was added during early exponential phase in gluconate minimal media.[14] It was shown that during exponential phase growth on gluconate, the nickel-sensitive glycolytic enzyme FbaA is still required to recycle fructose-1,6-bisphospate, produced as a result of the Pentose Phosphate Pathway (PPP), back into glycolysis (Figure 2.2). However, nickel toxicity in the exponential phase on gluconate media was averted by the deletion of Gnd (6-phosphogluconate dehydrogenase), which is the entry point into the PPP (Fig. 2.2).[14] The Δ*gnd* mutation prevents the production of fructose 6-phosphate by the PPP and therefore the need for downstream FbaA activity. We observed similar results using our own MG1655 Δ*gnd::Kan*^{R} strain (Fig. 2.8A). To further test if nickel exposure in lag phase during growth in gluconate minimal media was due to the function of FbaA, via the PPP, we cultured the Δ*gnd* mutant strain according to the growth scheme in Figure 2.4. Under these conditions, the Δ*gnd* mutant strain proved to be just as sensitive to nickel toxicity as the wild type strain (Fig. 2.8B), demonstrating that growth defects during lag phase nickel exposure are not due to inhibition of FbaA activity and that other targets of nickel toxicity are possible.

Having ruled out the inhibition of FbaA by nickel as the cause of the extended lag phase, we next tested if gluconate utilization itself were compromised by nickel toxicity. To determine if the extended lag phase was specifically due to disruption of

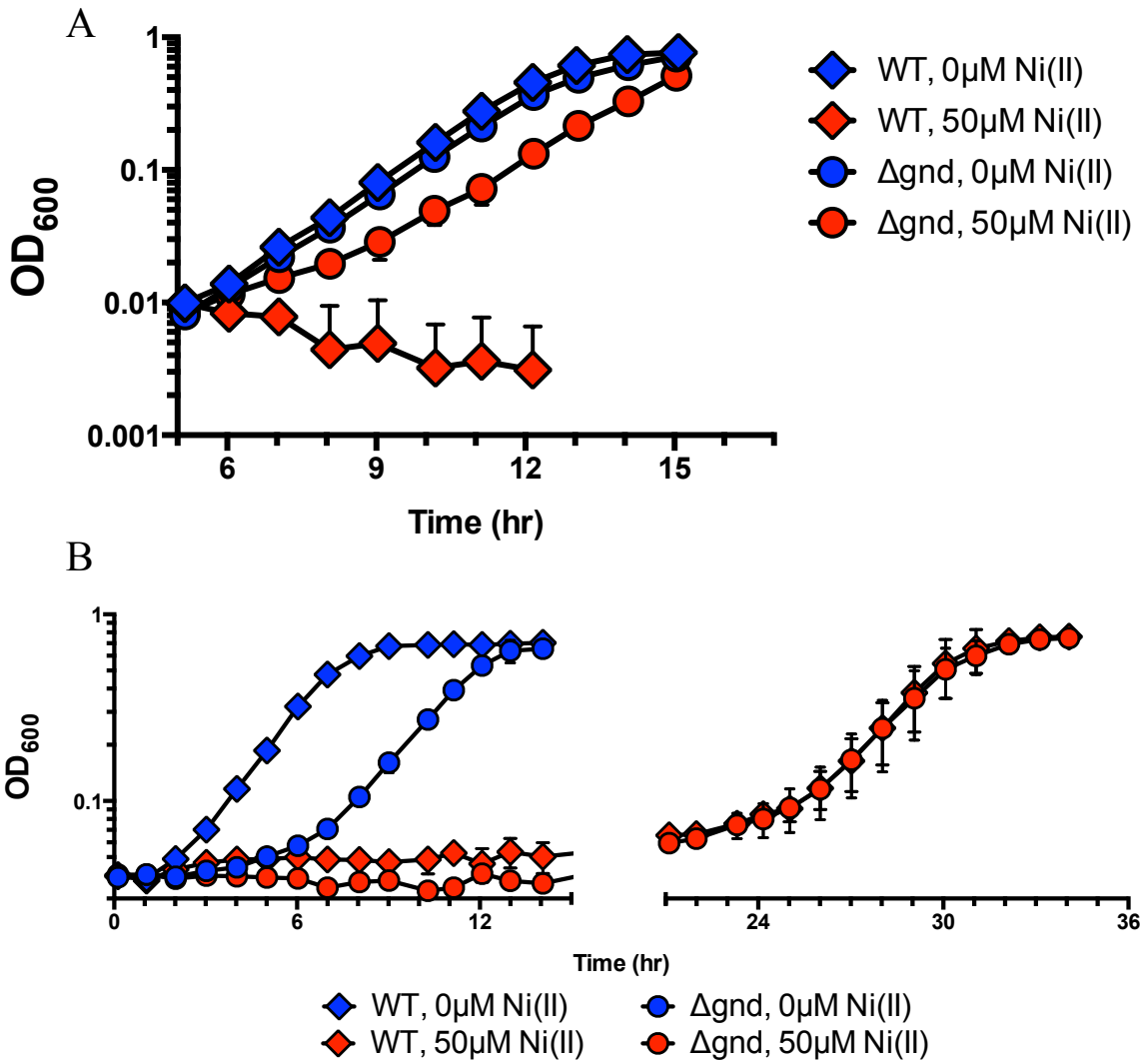

Figure 2.8. **The Δ*gnd* mutant is still sensitive to lag phase nickel exposure.** (A) MG1655 wild type and MG1655 Δ*gnd*::*kan*^{R} cells were grown overnight for 24hrs in M9 gluconate minimal media. These overnight cells were inoculated into fresh M9 gluconate minimal media, grown to early exponential phase (an OD_{600} of approximately 0.10), and then diluted 10-fold into fresh gluconate M9 minimal media with or without 50μM $NiCl_2$. (B) Wild-type MG1655 and the MG1655 Δ*gnd*::*kan*^{R} mutant strains were grown according to the growth scheme in Figure 2-5. Nickel, if present, was added to a final concentration of 50μM and added at the time of inoculation. All growths were repeated in triplicate (n = 3) and error bars indicate one standard deviation from the mean value.

6-phosphogluconte dehydratase activity (Edd, Figure 2.1), enzyme activity was measured throughout the lag and early exponential phases for cells grown in the presence and absence of 50μM Ni(II) (Fig. 2.9A). Control cells grown without nickel showed a rapid increase in Edd activity as the cells exited lag phase and entered the exponential phase at around four hours of growth. However, cells exposed to 50μM Ni(II) showed a striking absence of Edd activity throughout the same time period (Fig. 2.9A). These results suggested that the inability of *E. coli* to metabolize gluconate was a primary cause of the extended lag phase duration under nickel stress. In support of this hypothesis, we observed that when cells grown with 50μM Ni(II) do eventually exit lag phase and move into the exponential phase of growth at 25-30 hours of growth, Edd specific activity has increased approximately 3-fold, although it still has not reached the same level of activity observed in control cells at the same cell density (Fig. 2.9A). As a control, the activity of Isocitrate Dehydrogenase (IDH), a non-iron dependent enzyme with constitutive expression, was selected for assaying under identical growth conditions, both without and in the presence of nickel. The activity of IDH was only mildly affected by nickel exposure (Fig. 2.9B). This suggested that the nickel stress is specifically targeting the *de novo* production of 6-phosphogluconate dehydratase during the lag phase.

Nickel toxicity is diminished in partially adapted *E. coli* cells during the stress growth. In comparison to the gluconate minimal media stress growths with nickel exposure at the time of inoculation, it was important to confirm whether or not this toxicity was linked to the specific phase of growth and if it was during the lag phase cells were the most susceptible to the nickel toxicity. Employing our growth scheme in Figure 2.4, cells were cultured in glucose M9 minimal media overnight and then transferred into

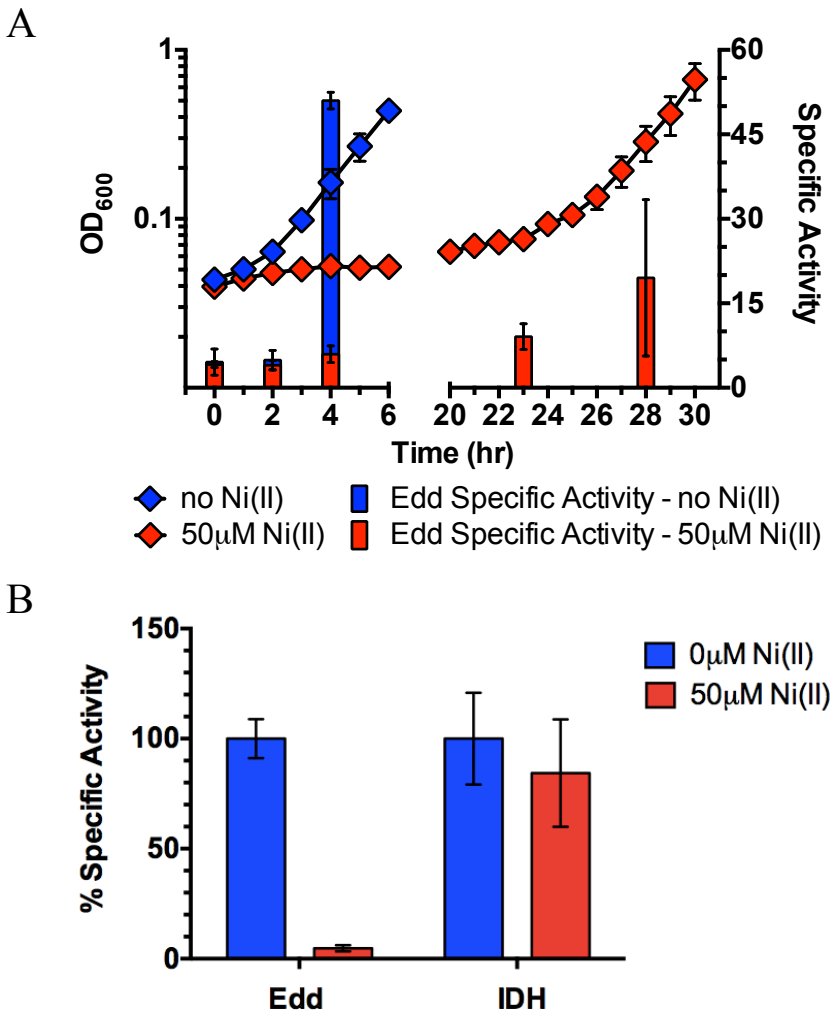

Figure 2.9. **6-phosphogluconate dehydratase (Edd) specific activity is decreased in cells exposed to high levels of nickel during the lag phase**. (A) Edd specific activity (bars) is overlaid with growth curve data (diamonds) from wild-type MG1655 cells grown in gluconate minimal media with 0μM (blue) or 50μM (red) added $NiCl_2$. All growth and activity measurements were repeated in triplicate (n = 3) and error bars indicate one standard deviation from the mean value. (B) Edd and IDH assays were performed as described in the Methods and Materials. The control whole cells lysates (from cells cultured without nickel) were set to 100% of activity. All cells were assayed after 4hrs of growth and assays were repeated in triplicate (n = 3) and error bars indicate one standard deviation from the mean value.

gluconate M9 minimal media as previously described. However, nickel was not added until the cells had reached mid-exponential phase, at around an OD_{600} of 0.25. The data showed in a reduced level of nickel toxicity, as cell growth was only mildly delayed before quickly recovering from the nickel addition, and cells continued to grow through the exponential phase and into the stationary phase (Fig. 2.10). This reduction in nickel toxicity was analogous to the nickel toxicity observed with the growth data in Figure 2.6, where cells pre-adapted overnight to the media showed little to no nickel sensitivity in the subsequent stress growth with nickel exposure.

Nickel uptake and efflux influence nickel toxicity. Cells exposed to up to 50mM Ni(II) were still able to eventually exit the lag phase at approximately 24hrs after inoculation and resume growth despite the high level of toxicity by nickel (Fig. 2.7A). Under aerobic growth conditions, the *nikABCDE* operon encoding the high-affinity nickel transport system is repressed and nickel enters the cell via non-specific, low affinity transport systems, such as the Mg(II) uptake protein CorA, that normally transport other divalent metals.[8,28,35,36] It was also recently established that the amino acid L-histidine inhibits nickel uptake through these non-specific uptake systems by complexing with nickel in the media.[37] We also observed that the simultaneous addition of 500μM L-histidine, with the presence of 50μM Ni(II) at the time of inoculation into the gluconate stress media, completely abolished the extended lag phase phenotype caused by nickel toxicity (Fig. 2.11A). Additional growth studies with the deletion of the *corA* gene prevented the nickel toxicity phenotype observed during lag phase, which was also observed previously in other nickel toxicity studies using a variety of different conditions (Fig. 2.11B).[28] This result confirmed that the CorA transporter is the primary

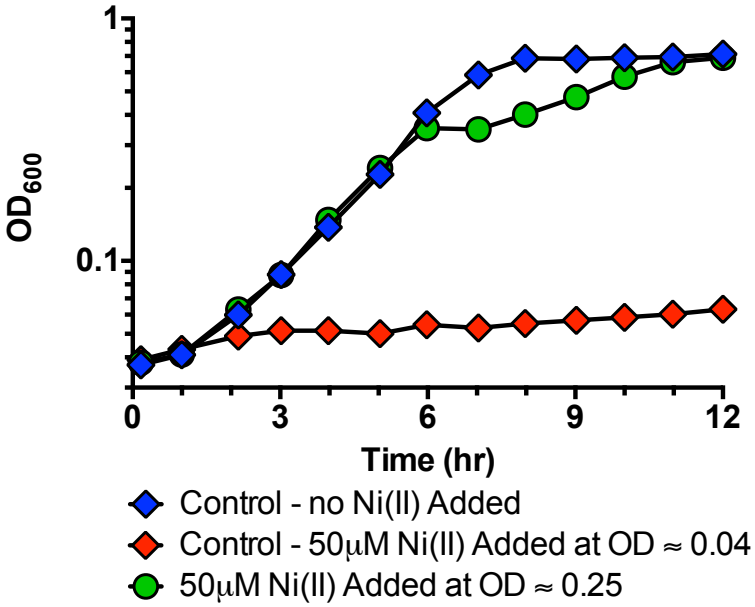

Figure 2.10. **Wild type cells in exponential phase are less sensitive to nickel toxicity compared to cells exposed to nickel while in lag phase**. Wild-type MG1655 cells were cultured following the growth scheme in Figure 2-5. $NiCl_2$ was added to the gluconate media at the time of inoculation (OD_{600} = 0.04, red diamonds) or once the cell cultures had reached an OD_{600} = 0.25 (green circles) and compared to wild-type control cells with no nickel addition (blue diamonds). All growths were repeated in triplicate (n = 3), and error bars indicate one standard deviation from the mean value.

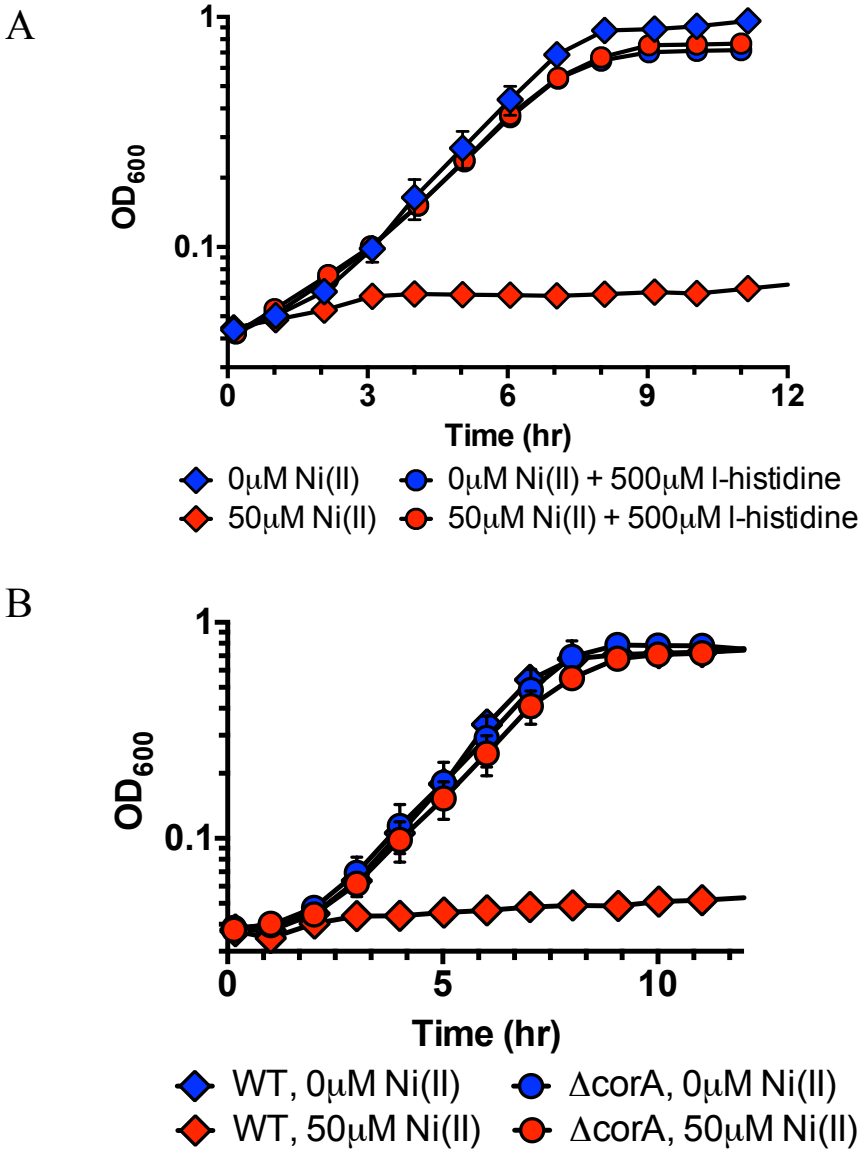

Figure 2.11. **The presence of l-histidine and deletion of *corA* abolished nickel toxicity by chelating nickel ion and preventing uptake, respectively**. (A) Wild type cells were cultured in M9 glucose media overnight, as according to the growth scheme in Figure 2-5, then inoculated into M9 gluconate media alone (diamonds) or with 500μM L-histidine added (circles). 50μM $NiCl_2$ (red symbols) was added at the time of inoculation. Control cultures with no nickel addition are also shown (blue symbols). All growths were repeated in triplicate (n = 3), and error bars indicate one standard deviation from the mean value. (B) Cells were cultured with no added nickel (blue symbols) or with 50μM $NiCl_2$ (red symbols). All growths were repeated in triplicate (n = 3), and error bars indicate one standard deviation from the mean value.

point of entry for nickel into *E. coli* during aerobic growth under out growth scheme. We further tested if intracellular nickel accumulation is required for lag phase nickel toxicity by utilizing an Δ*rcnA* mutant strain lacking the nickel efflux protein, RcnA, which actively exports both nickel and cobalt into the periplasm.[22,23] The Δ*rcnA* strain demonstrated a greater extended lag phase phenotype, well beyond that of the wild-type strain, when shifted from the glucose to gluconate minimal media with 50μM Ni(II) added at the time of inoculation (Fig. 2.12). In contrast to the wild-type strain, the Δ*rcnA* strain failed to adapt to the high nickel stress and resume growth, indicating that the capacity for nickel efflux is critical for the eventual adaptation to the nickel stress. Overall, the chelating effect of L-histidine, or deletion of *corA*, combined with the failure of the Δ*rcnA* strain to adapt to nickel stress suggests that uptake of nickel into the cell is necessary for the full toxicity phenotype, while nickel efflux is a key component of the eventual adaptation and recovery.

Exposure to high levels of nickel selects for a nickel-resistant mutation in E. coli. In cultures grown with nickel exposure as high as 50μM, all wild type cell cultures eventually exited the lag phase, entered into exponential growth, and reached the stationary phase (Fig. 2.7A). To test if this adaptation to nickel stress was transient or the result of permanent selection for a nickel-resistant population, cultures that were subjected to various levels of nickel stress were collected after entry into the stationary phase. These nickel-adapted strains were passaged several times on fresh LB media onlyand re-tested for nickel sensitivity in M9 gluconate minimal media as according to our growth scheme in Figure 2.4. Cultures previously exposed to nickel concentrations conditions up to 40μM nickel did not show any permanent development of resistance to

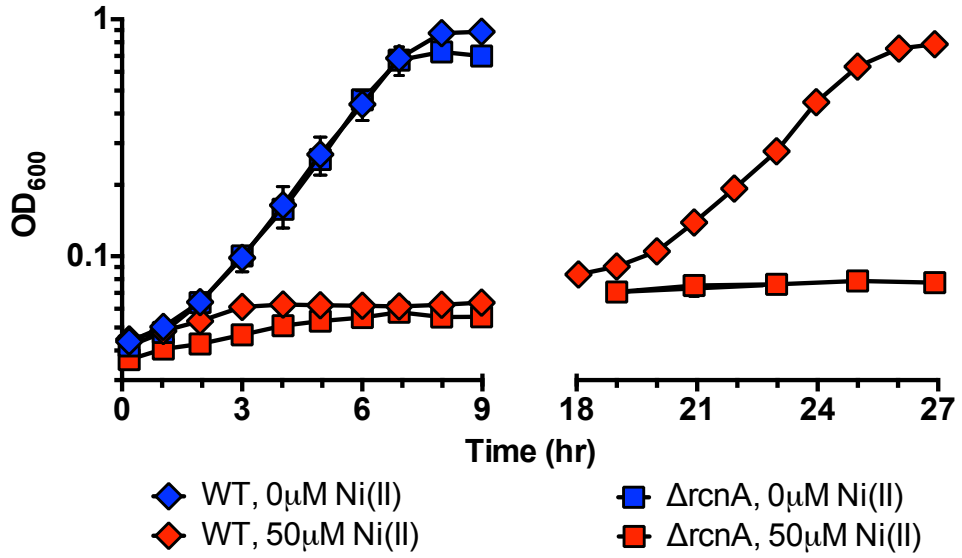

Figure 2.12. **Deletion of the nickel and cobalt-specific exporter RcnA increases nickel toxicity by preventing efflux of nickel from the cell**. Wild-type MG1655 (diamonds) or Δ*rcnA* (squares) strains were cultured according to Figure 2-5, with 50μM $NiCl_2$ added (red symbols) or with no nickel addition (blue symbols) to the gluconate M9 minimal stress media. All growths were repeated in triplicate (n = 3), and error bars indicate one standard deviation from the mean value.

nickel stress when re-tested, and still required the extended periods of lag phase similar to untreated WT cells (data not shown). This indicated that the adaptation was a transient event under these conditions, and was lost once the cells were removed from the nickel stress (Fig. 2.13). However, the nickel-adapted strain that was previously exposed to 50μM Ni(II) showed a significant degree of nickel resistance when re-tested in M9 gluconate minimal media, indicating the presence of a permanent suppressor mutation or mutations in this new strain (Fig. 2.13).

Since nickel toxicity varied by the timing of the nickel exposure, lag phase versus exponential phase cells, we tested if selection for a nickel resistant mutant also depends on the growth phase of nickel exposure. Cells were cultured as previously described with the 50μM nickel exposure delayed until exponential phase. When nickel exposure was delayed until the exponential phase, there was no development of the permanent nickel resistance in these cells when they were subsequently grown in high nickel (Fig. 2.14). This result suggests that selection for a nickel resistant mutant is stronger during lag phase nickel exposure as compared to exponential phase nickel exposure, and generally agrees with the overall greater nickel toxicity during lag phase.

Nickel toxicity is bacteriostatic. With the possible selection of a nickel-resistant genotype following exposure to 50μM Ni(II), we next tested if nickel exerts a bactericidal or bacteriostatic effect under our experimental conditions. The viability of wild-type cells grown in gluconate media with 50μM Ni(II) was monitored over time by measuring subsequent colony formation on solid LB media and via an adapted "Start Growth Time" method.[38] Both of these techniques indicated that nickel toxicity was bacteriostatic, and did not result in significant cell death (Fig. 2.15). Instead, once

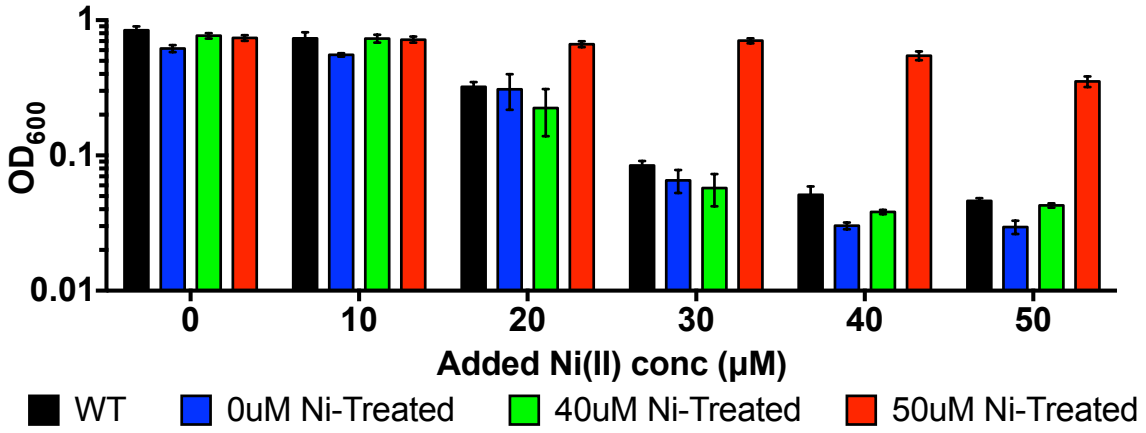

Figure 2.13. **High nickel exposure selects for a nickel resistant genotype**. Wild-type MG1655 cells were previously cultured in varying concentrations of $NiCl_2$ until reaching the stationary phase. After multiple passages through non-selective rich media, these nickel-adapted strains were re-cultured in increasing concentrations of $NiCl_2$ and compared to wild-type control cultures that were not previously exposed to nickel. OD_{600} values shown were measured after 12hrs of growth. All growths were repeated in triplicate (n = 3), and error bars indicate one standard deviation from the mean value.

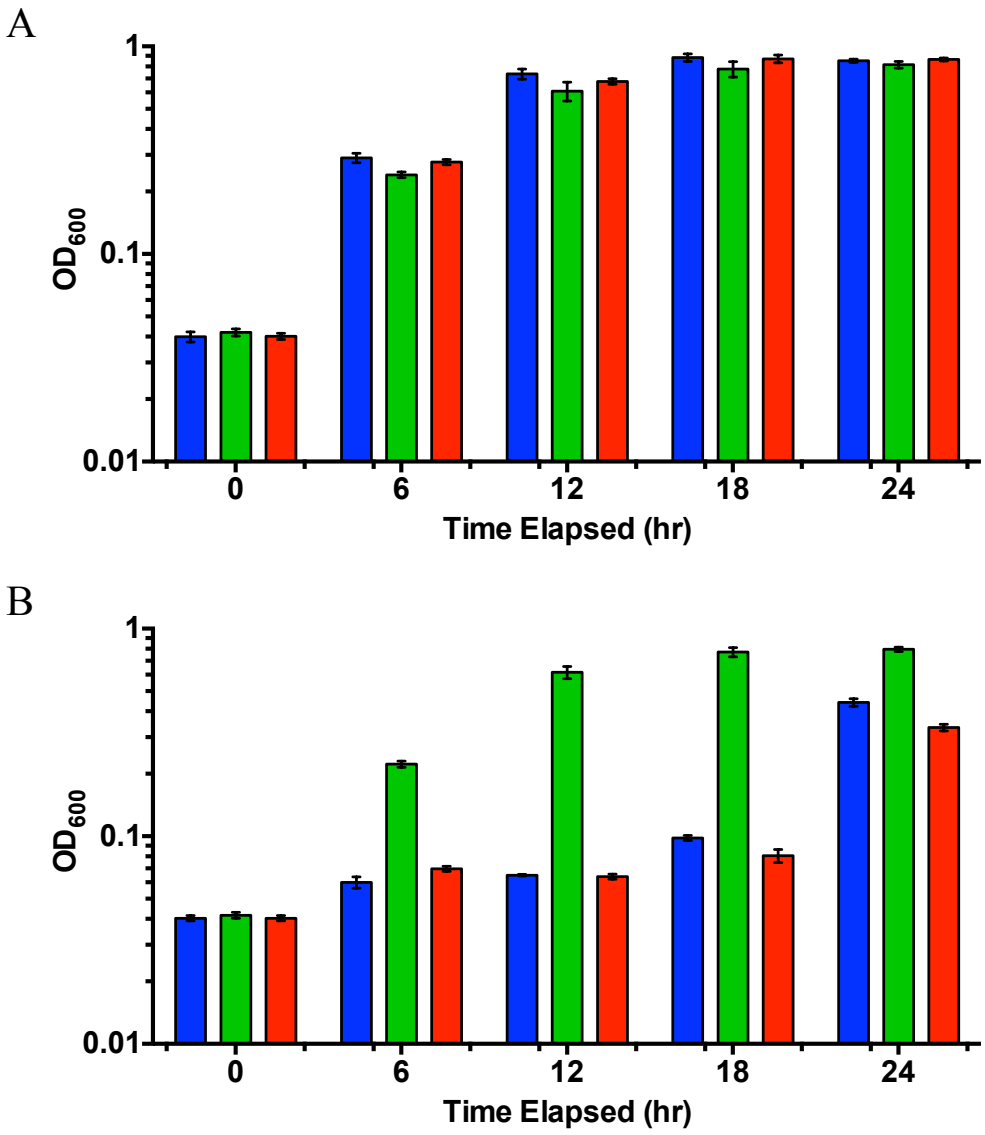

Figure 2.14. **The development of nickel resistance depends on the timing of the nickel exposure**. $NiCl_2$ was added to 50µM to cultures of wild-type MG1655 cells at either an OD_{600} of 0.04 (A,B - green) or 0.25 (A,B - red). The OD_{600} at 0.04 represents an initial, lag phase exposure and the OD_{600} at 0.25 represents a delayed, exponential phase exposure. After multiple passages through non-selective rich media, these nickel-exposed strains were re-cultured as according to the growth scheme in Figure 2-5 in gluconate M9 minimal media with either 0µM (A) or 50µM $NiCl_2$ (B). These growths were compared to wild-type control cultures that were not previously exposed to nickel (A,B - blue) All growths were repeated in triplicate (n = 3), and error bars indicate one standard deviation from the mean value.

removed from the nickel stress, cell growth quickly recovered in the LB media. Regardless of the time of exposure (1 or 3 hours) to 50μM Ni(II), the wild-type strain maintained nearly identical colony counts and reached the designated threshold optical density (at 600nm) in approximately the same amount of time as control cells not exposed to nickel (Fig. 2.15). Therefore, nickel exposure may potentially force cells to enter a dormant state without significant cell death, in accordance with past studies.[14] Growth of the culture population would only resume when the internal nickel stress was alleviated by a transient adaptation to the nickel stress (at lower concentrations) or when a nickel-resistant population is selected and has exited dormancy and begun to grow (observed at high nickel concentrations).

2.4 **Discussion**

The intensity of nickel toxicity is contingent on the media composition and growth conditions. Nickel plays no physiological role in *E. coli* during aerobic growth conditions. The amount of nickel toxicity in stress growths with LB media broth was starkly different from the stress growths in M9 minimal media with the different carbon sources (Fig. 2.2). Virtually no toxicity was observed in LB media stress growths. Nickel chelation via L-histidine was able to completely abolish the nickel toxicity growth phenotype when utilizing our growth scheme in Figure 2.4. It is likely that a similar mechanism occurred with the LB media stress growths with the presence of nickel; given the relatively high concentration of L-histidine, as well as other possible nickel-chelating compounds and amino acids the are present in LB media. Furthermore, growths

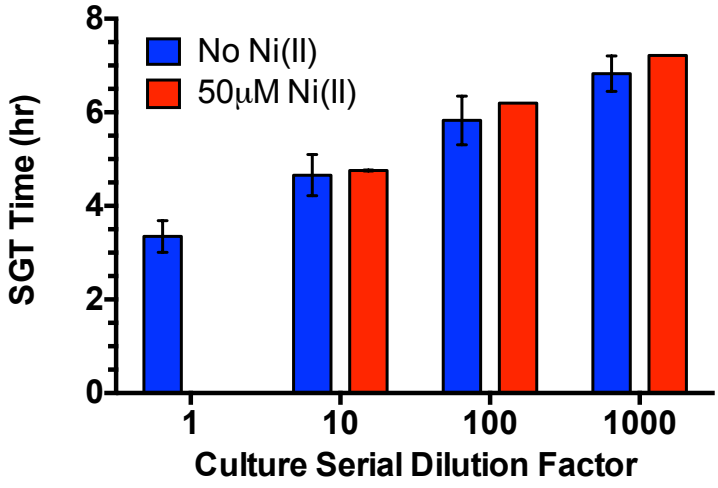

CFU/mL Counts

Control	50μM Ni(II)
4.583×10^7 ($\pm 1.0 \times 10^7$)	4.917×10^7 ($\pm 2.9 \times 10^6$)

Figure 2.15. **Exposure to nickel results in a bacteriostatic effect and does not lead to significant cell death during the first three hours of exposure**. *Top graph*, Wild-type MG1655 cells were incubated for 3hrs in the gluconate media with or without 50μM $NiCl_2$ and then serially diluted into awaiting 3mL volumes of fresh, sterile LB media. Optical density was measured at 600nm every hour via a Start Growth Time (SGT) protocol according to prescribed methods (Hazan *et al.*, 2012). *Bottom table*, the cells also were diluted by 100,000x (final) and then plated on to fresh LB-only agar plates. Plates were incubated overnight at 37°C and then colony forming units (CFUs) were counted the following day. Control cultures were repeated in triplicate (n = 3) and error bars indicate one standard deviation from the mean value.

performed in complex media, such as LB, for studying nickel toxicity have previously required millimolar levels of nickel to induce any amount of toxicity.[25,28] The differences in toxicity for other metals, such as copper and silver, have also been observed between base media types.[37] Furthermore, these results are consistent with our observation that nickel uptake was paramount for full toxicity and that nickel efflux plays an important role in the eventual adaptation of the wild type cells to the nickel stress.

When cells were inoculated into M9 minimal stress media after an overnight growth in LB media, the carbon source selected influenced the degree of nickel toxicity (Fig. 2.2). Each carbon source varies by its point of entry into carbon metabolism.[8-13,15] By altering the carbon source, the relative effect of nickel toxicity on central carbon metabolism could be studied. These results raised the possibility of additional targets of nickel toxicity, especially with the enzymes and pathways involved in the metabolism of each carbon source. Individually, glucose showed the highest level of nickel toxicity, as opposed to glycerol, which showed the least degree of nickel toxicity, as expected (Fig. 2.5). The toxicity from growth on glucose was not surprising considering glucose metabolism passes through the FbaA enzyme, a known target of nickel toxicity. Glycerol, on the other hand, enters glycolysis after the FbaA enzyme. Even more interesting was the delayed growth in gluconate minimal media (Fig. 2.2). Gluconate metabolism follows through the ED pathway and therefore also can bypass the FbaA enzyme as glycerol does, but if gluconate passes into the PPP then it could still feed back into glycolysis at an early enough point to require FbaA. Due to this complication, it was important to ensure that, as according to our growth scheme, gluconate metabolism did not primarily flow back through the Pentose Phosphate pathway and therefore feed into

glycolysis and the FbaA enzyme. In order to achieve this, the Gnd enzyme, the entry point enzyme for gluconate into the PPP, was deleted. We demonstrated that with nickel exposure at the time of inoculation, the *gnd* mutant strain was just as sensitive as the wild type strain to nickel toxicity (Fig. 2.8B). This result suggested that the ED pathway is the primary catabolic pathway for gluconate. Overall, the level of nickel toxicity appeared to be heavily influenced by the timing of nickel exposure in relation to cell adaptation to the carbon sources. Nonetheless, while the resulting toxicity observed in cells grown with glucose was anticipated, but the toxicity levels observed with gluconate as the sole carbon source bring to question the nickel may be targeting when cells are forced to feed on gluconate as an alternative carbon source after adaptation to an alternative source such as glucose.

Cells in the lag phase of growth are more susceptible to nickel toxicity. Nickel toxicity was observed to be the most severe when cells that were formerly adapted to glucose metabolism were inoculated into a gluconate minimal media with 50μM nickel (Fig. 2.7A). Shifting the carbon source from glucose to gluconate requires *de novo* production of the enzymes necessary for the catabolization of gluconate via the ED pathway for energy, such as the Edd enzyme, which are repressed in the presence of glucose.[8] Contrasted to this, the level of nickel toxicity was greatly reduced for cells that were already adapted to the new carbon source prior to nickel exposure, (Fig. 2.5, Fig. 2.10). Edd activity was also significantly lower in whole cell lysates with nickel exposure during the lag phase, as opposed to the relatively unaffected activity of the non-iron enzyme isocitrate dehydrogenase. These results suggest that the pre-adaptation of *E. coli* wild type cells to the gluconate M9 minimal stress media is the reason behind the

diminished nickel toxicity, as the enzymes required for gluconate metabolism, such as the Edd, are likely to be sufficiently expressed, active, and in adequate quantity for metabolic activity and growth to continue even in the presence of high nickel levels. This data also agrees with previous studies that determined holo-Edd enzyme was not directly inhibited by nickel ion and remained active.[39] This could suggest that nickel toxicity may be targeting the non-fully formed inactive Edd enzyme during the lag phase of growth, and therefore, prevents the cell from sufficiently metabolizing gluconate and slowing the transition into the exponential phase of growth. Future work could further confirm this by measuring Edd activity in the whole cell lysate of growths exposed to nickel during the mid-exponential phase of growth. Our studies suggest that nickel targets the maturation of apo-Edd, prior to the assimilation of the [4Fe-4S] cluster required for Edd activity, by possibly blocking or occupying the activity site by binding to available cysteine residues in the metalloenzyme. However, Fe-S cluster biogenesis during the lag phase of growth may also be a target of nickel exposure either directly or by disruption of iron homeostasis. We will explore these possibilities in Chapter 3.

2.5 References

1. Penfold, W. J. (1914) On the Nature of Bacterial Lag. *J Hyg* 14, 215-241.

2. Rolfe, M. D., Rice, C. J., Lucchini, S., Pin, C. Thompson, A., Cameron, A. D. S., Alston, M., Stringer, M. F., Betts, R. P., Baranyi, J., Peck, M. W., and Hinton, J. C. D. (2012) Lag phase is a distinct growth phase that prepares bacteria for exponential growth and involves transient metal accumulation. *J Bacteriol* 194, 686-701.

3. Wilson, P. D. G., Wilson, D. R., Brocklehurst, T. F., Coleman, H. P., Mitchel, G., Waspe, C. R., Jukes, S. A., and Robins, M. M. (2003) Batch growth of

Salmonella typhimurium LT2: stoichiometry and fators leading to cessation of growth. *Int J Food Microbiol* 89, 195-203.

4. Sezonov, G., Joseleau-Petit, D., and D'Ari, R (2007) *Escherichia coli* Physiology in Luria-Bertani Broth. *J Bacteriol* 189, 8746-8749.

5. Finkel, S. E. (2006) Long-term Survival during Stationary Phase: Evolution and the GASP Phenotype. *Natl Rev Microbiol* 4, 113-120.

6. Llorens, J. M. N., Tormo, A., and Martinez-García, E (2010) Stationary phase in gram-negative bacteria. *FEMS Microbiol Rev* 34, 476-495.

7. Müller, M. (1895) Ueber den Einfluss von Fieber temperaturen auf die Wachstumgeschwindigkeit und die Virulenz des *Typhus Bacillus*. *Zeitschrift für Hygiene und Infektionskrankheiten* 20, 245.

8. Eisenberg, R. C., and Dobrogoz, W. J. (1967) Gluconate Metabolism in *Escherichia coli*. *J Bacteriol* 93, 941-949.

9. Verhees, C. H., Kengen, S. W. M., Tuininga, J.E., Schut, G. J., Adams, M. W. W., de Vos, W. M., and van der Oost, J. (2003) The unique features of glycolytic pathways in Archaea. *J Biochem* 375, 231-246.

10. Martinez-Gómez, K., Flores, N., Castañeda, H.M. Martínez-Batallar, G., Hernández-Chávez, G., Ramírez, O. T., Gosset, G., Encarnación, S., and Bolivar, F. (2012) New insights into *Escherichia coli* metabolism: carbon scavenging, acetate metabolism, and carbon recycling responses during growth on glycerol. *Microbial Cell Factories* 11, 1-21.

11. Pouysségur, J. M., Faik, P., and Kornberg, H. L. (1973) Utilization of Gluconate by *Escherichia coli*: Uptake of D-gluconate by a mutant impaired in gluconate kinase activity and by membrane vesicles derived therefrom. *J Biochem* 140, 193-203.

12. Bächi, B., and Kornberg, H. L. (1975) Utilization of Gluconate by *Escherichia coli*: A role of adenosine 3':5'-cyclic monophosphate in the induction of gluconate metabolism. *J Biochem* 140, 123-128.

13. Klemm, P., Tong, S., Nielsen, H., and Conway, T. (1996) The gntP gene of *Escherichia coli* involved in gluconate uptake. *J Bacteriol* 178, 61-67.

14. Macomber, L., Elsey, S. P., and Hausinger, R. P. (2011). Fructose-1,6-bisphosphate aldolase (class II) is the primary site of nickel toxicity in *Escherichia coli*. *Mol Microbiol* 82, 1291-1300.

15. Kim, J. and Copley, S. D. (2007) Why Metabolic Enzymes are Essential or Nonessential for Growth of *Escherichia coli* K12 on Glucose. *Biochem* 46, 12501-12511.

16. Li, Y. and Zamble, D. B. (2009) Nickel Homeostasis and Nickel Regulation: An Overview. *Chem Rev* 109, 4617-4643.

17. Macomber, L. and Hausinger, R. P. (2011) Mechanisms of nickel toxicity in microorganisms. *Metallomics* 3, 1153-1162.

18. Higgins, K. A., Carr, C. E., and Maroney, M. J. (2012) Specific Metal Recognition in Nickel Trafficking. *Biochem* doi: 10.1021/bi300981m

19. Chivers, P. T. and Sauer, R. T. (2002) NikR repressor: high-affinity nickel binding to the C-terminal domain regulates binding to operator DNA. *Chem Biol* 9, 1141-1148.

20. Bloom, S. L. and Zamble, D. B. (2004) Metal-selective DNA-binding response of *Escherichia coli* NikR. *Biochem* 43, 10029-10038.

21. Phillips, C. M., Schreiter, E. R., Guo, Y., Wang, S. C., Zamble, D. B., and Drennan, C. L. (2008) Structural Basis of the Metal Specificity for the Nickel Regulatory Protein NikR. *Biochem* 47, 1938-1946.

22. Rodrigue, A., Effantin, G., and Mandrand-Berthelot, M. A. (2005) Identification of *rcnA* (*yohM*), a Nickel and Cobalt Resistance Gene in *Escherichia coli*. *J Microbiol* 187, 2912-2916.

23. Iwig, J. S., Rowe, J. L., and Chivers, P. T. (2006) Nickel homeostasis in *Escherichia coli* – the *rcnR-rcnA* efflux pathway and its linkage to NikR function. *Mol Microbiol* 62, 252-262.

24. Iwig, J. S., Leitch, S., Herbst, R. W., Maroney, M. J., and Chivers, P. T. (2008) Ni(II) and Co(II) Sensing by *Escherichia coli* RcnR. *J Am Chem Soc* 130, 7592-7606.

25. Koch, D., Nies, D. H., and Grass, G. (2007) The RcnRA (YohLM) system of *Escherichia coli*: A connection between nickel, cobalt, and iron homeostasis. *BioMetals* 20, 759-771.

26. Park, M. H., Wong, B. B., and Lusk, J. E. (1976) Mutants in three genes affecting transport of magnesium in *Escherichia coli*: genetics and physiology. *J Bacteriol* 126, 1096-1103.

27. Wang, S. Z., Chen, Y., Sun, Z. H., Zhou, Q., and Sui, S. F. (2006) *Escherichia coli* CorA periplasmic domain functions as a homotetramer to bind substrate. *J Biol Chem* 281, 26813-26820.

28. Wu, L. F., Navarro, C., de Pina, K., Quénard, M., and Mandrand, M. A. (1994) Antagonistic Effect of Nickel on the Fermentative Growth of *Escherichia coli* K-12 and Comparison of Nickel and Cobalt Toxicity on the Aerobic and Anaerobic Growth. *Environ Health Perspect* 102, 297-300.

29. Baranyi, J. and Roberts, T. A. (1994) A dynamic approach to predicting bacterial growth in food. *Int J Food Microbiol* 23, 277-294.

30. Roth, V (2006) Doubling Time. (http://www.doubling-time.com/compute.php)

31. Zablotny, R. and Fraenkel, D. G. (1967) Glucose and Gluconate Metabolism in a Mutant of *Escherichia coli* Lacking Gluconate-6-Phosphate Dehydrase. *J Bacteriol* 93, 1579-1581.

32. Fraenkel, D. G. and Horecker, B. L. (1964) Pathways of D-glucose metabolism in *Salmonella typhimurium*: a study of a mutant lacking phosphoglucose isomerase. *J Biol Chem* 239, 2765-2771.

33. Outten, F. W., Djaman, O., and Storz, G. (2004) A suf operon requirement for Fe-S cluster assembly during iron starvation in *Escherichia coli*. *Mol Microbiol* 52, 861-872.

34. Cribbs, R. and Englesberg, E. (1964) L-Arabinose negative mutants of the L-ribulokinase structural gene affecting the levels of L-arabinose isomerase in *Escherichia coli*. *Genetics* 49, 95-108.

35. Navarro, C., Wu, L. F., and Mandrand-Berthelot, M. A. (1993) The *nik* operon of *Escherichia coli* encodes a periplasmic binding-protein-dependent transport system for nickel. *Mol Microbiol* 9, 1181-1191.

36. de Pina, K., Navarro, C., McWalter, L., Boxer, D. H., Price, N. C., Kelly, S. M., Mandrand-Berthelot, M. A., and Wu, L. F. (1995) Purification and characterization of the periplasmic nickel-binding protein NikA of *Escherichia coli* K12. *Eur J Biochem* 227, 857-865.

37. Chivers, P. T., Benanti, E. L., Heil-Chapdelaine, V., Iwig, J. S., and Rowe, J. L. (2012) Identification of Ni-$(L\text{-}His)_2$ as a substrate for NikABCDE-dependent nickel uptake in *Escherichia coli*. *Metallomics* 4, 1043-1050.

38. Hazan, R., Que, Y. A., Maura, D., and Rahme, L. G. (2012) A method for high throughput determination of viable bacteria cell counts in 96-well plates. *BMC Microbiol* 12, 1-7.

39. Xu, F. F. and Imlay, J. A. (2012) Silver(I), mercury(II), cadmium(II), and zinc(II) target exposed enzymic iron-sulfur clusters when they toxify *Escherichia coli*. *Appl Environ Microbiol* 78, 3614-3621.

40. Wang, S., Wu, Y. and Outten, F. W. (2011) Fur the the novel regulator YqjI control transcription of the ferric reductase gene *yqjH* in *Escherichia coli*. *J Bacteriol* 193, 563-574.

CHAPTER 3

IRON HOMEOSTASIS IS A PRIMARY TARGET OF NICKEL TOXICITY DURING LAG PHASE

Abstract

The first row transition metals are essential cofactors for key metabolic enzymes but can also be toxic. For example, essential metals can poison other metal homeostasis pathways if present in excess. The lag phase of bacterial growth is a critical period for metal accumulation prior to entry into the exponential phase of growth. We found that nickel inhibits the adaptation of *E. coli* during the lag phase when cells are shifted from glucose to gluconate minimal media. Sensitivity to nickel toxicity was due to loss of activity by the [4Fe-4S] enzyme 6-phosphogluconate dehydratase (Edd). Whole cell metal analysis showed that lag phase nickel exposure diminished iron uptake, suggesting that the lack of Edd activity results from iron deficiency during nickel toxicity. Supplementing cells with excess ferric ion prior to the nickel stress helped to alleviate toxicity and decrease the lag phase period. Finally, enterobactin metabolism was disrupted upon nickel exposure, providing a partial explanation for disrupted iron metabolism. These studies indicate that nickel likely disrupts iron metabolism prior to the assimilation of iron into target proteins, during iron uptake and/or trafficking for iron

cofactor assembly, and helps provide a more detailed molecular understanding of nickel toxicity.

3.1 Introduction

Transition metal ions are essential for cellular metabolism because they operate as cofactors in metalloproteins used for catalysis, electron transport, structural support, or as sensors for oxygen and its byproducts. It is estimated that one-third to one-half of all proteins incorporate metal ions for proper function.[1,2] The intracellular metal quota is dictated by metal bioavailability as well as by cellular and metabolic requirements that can alter the repertoire of metalloproteins that require that metal. When intracellular metal levels move either above or below the acceptable range, various detrimental effects, including cell death, may result due to a variety of mechanisms.[3] In order to maintain the proper cellular metal quota, transition metals require homeostasis systems for transport, intracellular trafficking, and storage.

Iron is a key transition metal involved in numerous enzyme catalysis and electron transfer pathways, for example as part of Fe-S cluster centers, di-iron centers, or heme bound to metalloproteins. Iron primarily exists in the environment in one of two ionic forms: as the highly soluble ferrous Fe(II) ion (approximately 0.1M at a pH of 7.0) or as the terribly insoluble ferric Fe(III) ion (approximately 1×10^{-18} M at a pH of 7.0).[4] While ferrous iron is the most bioavailable form, under oxidative conditions its presence can cause Fenton chemistry inside the cell (Fig. 3.1) and the production of radical species that damage the cell.[5] Iron uptake by *E. coli* is achieved by a variety of systems and

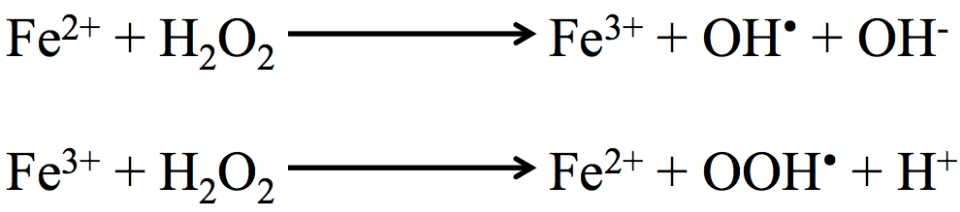

Figure 3.1. **Fenton Reaction with ferrous and ferric iron**. The reaction of peroxide with ferrous iron (Fe^{2+}) or ferric iron (Fe^{3+}) produces a hydroxyl or hydroperoxyl radical species, respectively, that is detrimental to various cellular compounds, proteins, and pathways.

pathways.[4] For example, for growth within a mammalian host, pathogenic variants of *E. coli* are able to scavenge iron from a variety of biological sources, such as heme cofactors, the protein transferritin, and other iron-scavenging proteins.[6] In addition, most strains of *E. coli* employ a set of iron-scavenging chelators called siderophores, which bind ferric ions *ex vivo* for transport into the cell. The binding constants of ferric iron to these siderophore compounds are generally so tight they are able to steal iron from other iron-bound chelators or ligands. For example, the siderophore enterobactin (also known as enterochelin) is commonly synthesized by gram-negative bacteria and has one of the lowest known formation constants ($K_d = 1 \times 10^{-54}$) for ferric iron (Fig. 3.2).[7]

The systems involved in iron uptake are transcriptionally controlled by the Fur metalloregulatory protein.[4,8] Under iron-replete conditions, the Fur protein forms a homo-dimer with a di-iron cofactor between the two monomers that can bind the upstream promoter regions of a variety of genes and repress expression (Fig 3.3).[9] Under low iron conditions, apo-Fur dissociates from target DNA and expression of iron uptake systems is increased.

Previously, it was determined that deletion of the *yqjH* ferric siderophore reductase gene, used for iron acquisition, or deletion of the *sufABCDSE* operon, responsible for stress-responsive Fe-S cluster biogenesis, caused increased sensitivity to nickel stress in LB.[10,11] These results raised the possibility that nickel directly targets iron homeostasis in bacteria. We have extensively tested this hypothesis and determined that nickel does disrupt iron homeostasis in the gram-negative bacterium *Escherichia coli* and that bacterial cells are especially sensitive to nickel stress during lag phase, when cells accumulate iron for subsequent exponential growth. Furthermore, enterobactin

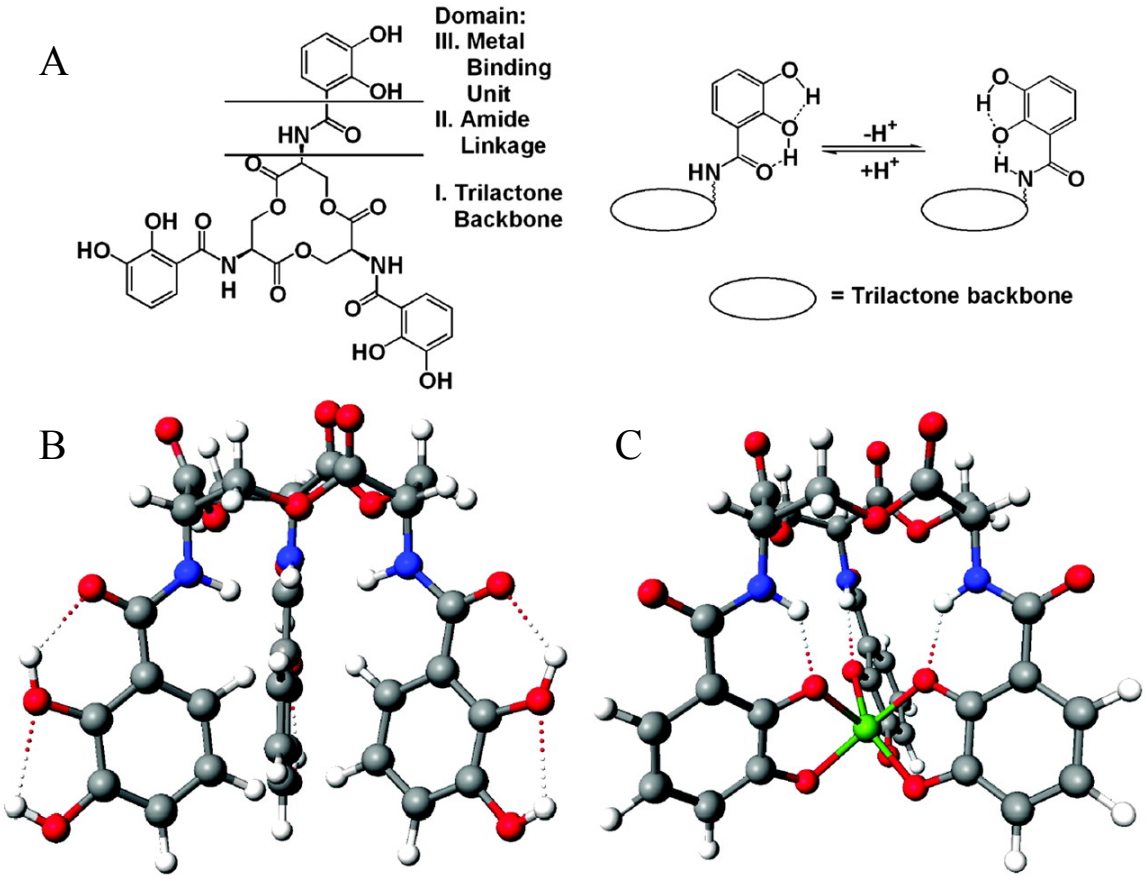

Figure 3.2. **Enterobactin is an iron chelating siderophore produced by *E. coli*.** (A) The various domains of the cyclic enterobactin (enterochelin) compound, showing the protonated and deprotonated catecholate forms. (B) Stick-and-ball model of desferrienterobactin. (C) Stick-and-ball model of ferric enterobactin.

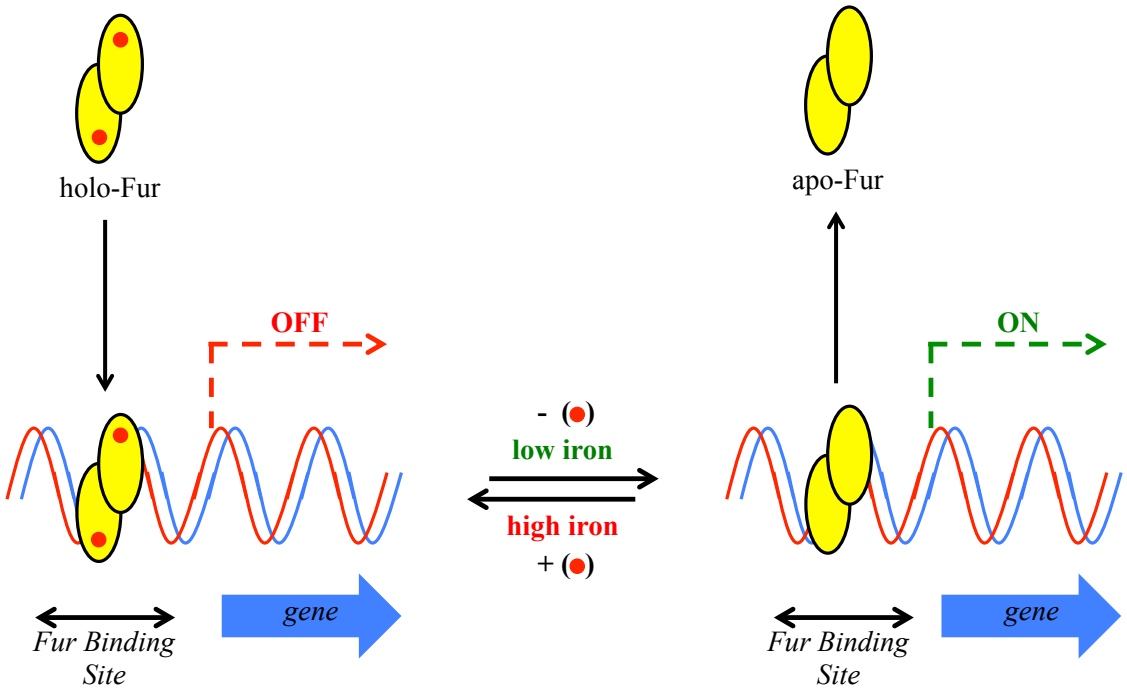

Figure 3.3. **Genetic regulation of the Ferric uptake regulator protein, Fur, under high and low intracellular iron conditions**. When in abundance, iron is bound to the Fur homodimer (as holo-Fur) and blocks genetic expression of targeted genes. When intracellular iron is low, the Fur homodimer loses its iron centers (as apo-Fur), dissociates from the DNA, and is no longer able to repress expression of the target gene.

synthesis is disrupted under nickel exposure so that by increasing the enterobactin synthetic pathway, nickel toxicity was reduced and growth out of the lag phase was partially restored (C. L. Washington Hughes, unpublished data).

3.2 Materials and Methods

Bacterial Strains, Growth Media, and Growth Conditions. Strains used in this study are derivatives of the parent wild-type strain *E. coli* MG1655 (Table 3.1). Where indicated cell growths for phenotype and metal analysis studies were carried out using the following procedure (Fig. 2.4): An individual colony was transferred from fresh Lennox broth (LB) agar plates into a 4mL volume of LB and grown for 4 – 5hrs at 37°C with shaking at 200rpm. Cells from this culture were pelleted and washed twice in sterile 1X M9 minimal media salts; then the OD_{600} was normalized to 1.0. Normalized cells were diluted 1:200 into M9 glucose minimal media containing 1X M9 minimal salts (BD Difco), 0.2% (w/v) glucose (Acros Organics), 0.2% (w/v) magnesium chloride, 0.1mM calcium sulfate, and 0.5µg/mL Thiamine HCl (Sigma-Aldrich). Cultures were incubated overnight for 18 – 20hr, at 37°C and 200rpm, then washed and pelleted twice in sterile 1X M9 salts as described above. The resulting cell suspensions were normalized to an OD_{600} of 2.0 and diluted 1:50 into M9 gluconate minimal media with 0.2% (w/v) potassium gluconate (Alfa Aesar) to give an initial OD_{600} of 0.04. Nickel chloride (Sigma-Aldrich) was added to described final concentrations in the M9 gluconate minimal media, from 0µM up to 50µM. Other reagents added to M9 glucose or M9 gluconate media are described in the appropriate figure legends.

Table 3.1. **Bacterial Strains and Plasmids utilized in this study**

Strain or Plasmid	Relevant Genotype or Phenotype	Reference or Source
E. coli Strains		
MG1655	Wild Type, *E. coli* K12 F-, λ^-, *ilvG- rfb*-50 *rph*-1	Laboratory Strain
CLHW009	MG1655 Φ*fepA-lacZ*	This Study
CLHW010	MG1655 Φ*iscR-lacZ*	This Study
CLHW011	MG1655 Φ*sufA-lacZ*	This Study
CLHW019	MG1655 pWSK29	This Study
CLHW022	MG1655 p*EntCEBA*	This Study
SW071	MG1655 Δ*fepA*	This Study
Plasmids		
pWSK29	Empty vector, tet^R	21
p*EntCEBA*	pEnt1 (pWSK29 with *entCEBA*), tet^R	21

Cell growth was monitored by UV-Vis absorption at 600nm and plotted versus time (in hours). Lag phase duration was determined using the online fitting program, DMFit (www.ifr.ac.uk/safety/DMfit), applying the no-asymptote fitted model and parameters.[12,13] Stationary phase OD_{600} measurements were omitted for best fit of the model. Doubling time of the cells during the exponential phase of growth, where the steepest linear fit line could be applied, was determined using the Online Doubling Calculator (http://www.doubling-time.com/compute.php).[14] All growths were cultured according to Scheme S1, unless otherwise noted.

Inductively Coupled Plasma Mass Spectrometry (ICP-MS). Preparatory cell growth in LB and glucose minimal media was conducted as described above. Cell cultures were then grown in 2L M9 gluconate minimal media with or without 50μM nickel chloride in a 4L culture flask at 37°C and 200rpm. 150mL samples were centrifuged at 3,000 x g for 20min and then pelleted three times at 16,000 x g with intermediate washing in 1mL sterile, ice-cold wash solution consisting of 50mM EDTA tetrasodium salt, 100mM oxalic acid, 100mM NaCl, and 10mM KCl, to remove any cell surface-associated metal ions. Washed cell pellets were re-suspended in a 1mL volume of ice-cold, sterile 1X M9 salts. A small portion of each sample was then diluted 40-fold to record the final OD_{600}. Cell re-suspensions were transferred to an acid-washed, Perfluoroalkoxy (PFA) microcentrifuge tube (Savillex Corporation) and centrifuged at 16,000 x g. After centrifugation, the supernatant was discarded and the cell pellets were frozen in liquid nitrogen. Cell pellets were stored at -80°C until ready for digestion and ICP-MS analysis.

Samples for ICP-MS were thawed for 15min on ice followed by drying at 80°C for 30min. A 400µL volume of trace-metal grade HNO_3 (distilled on site at the Center for Elemental Mass Spectrometry (CEMS), University of South Carolina) was added to each sample tube and digested at 80°C for 4hrs. After digestion, each sample tube was centrifuged for 1min at 16,000 x g and the supernatant was diluted 1:20 into MQ H_2O, giving a final acid matrix of 3.5%. Blanks consisting of 3.5% trace-metal grade HNO_3 only in MQ H_2O (18MW) were simultaneously prepared in the same manner as the samples. A multi-element standard solution (from Inorganic Ventures, provided by Beth Bair) was prepared with variable final concentrations of each metal in the same final acid matrix of 3.5% to establish a limit of detection and a calibration curve for determining the concentrations of each metal analyzed. The isotopes of biologically relevant transition metals with masses of ^{56}Fe, ^{58}Ni, ^{64}Zn, ^{55}Mn, and ^{63}Cu were selected for analysis based on natural abundances. Samples were analyzed under medium resolution to resolve polyatomic interferences (e.g. $^{40}Ar^{16}O$ for ^{56}Fe) on a Thermo Element 2 High Resolution ICP-MS instrument operated by CEMS at the University of South Carolina. A cyclonic spray chamber (Elemental Scientific) was used for delivery of sample into the instrument. Final intracellular metal concentrations were calculated based on total cell numbers present in the EPR tube by using the OD_{600} and previously established cell number conversions.[15]

Whole Cell Electroparamagnetic Resonance (EPR). Preparatory cell growth in LB and glucose minimal media was conducted as described above**.** For whole cell EPR analysis of intracellular labile iron, cultures were grown in 2L of M9 gluconate minimal media with or without 50µM nickel chloride at 37°C and 200rpm for 2hrs. Cell samples

were prepared according to protocols developed by J. Imlay and P. Kiley.[16,17] Cells were collected by centrifugation at 8,000 x g for 20min at 4°C. The sample pellet was re-suspended using 10mL of pre-warmed M9 gluconate media supplemented with 10mM diethylenetriaminepentaacetic acid (DTPA) (Sigma-Aldrich) and 20mM desferrioxamine mesylate salt (DFO) (CalBiochem). 10mL cell re-suspensions were incubated in a 250mL culture flask for 20min at 37°C and 200rpm for proper oxygenation, then pelleted and washed twice using a 50mM Tris HCl, pH 7.4 buffer. After centrifugation, the final pellets were resuspended in 0.5 volumes (relative to the pellet volume) of 50mM Tris HCl, 30% glycerol, pH 7.4 buffer, to give a final glycerol concentration of approximately 10-15%. A 300µL volume of each sample was transferred to a clean EPR tube and stored in liquid nitrogen until analysis. A remaining volume of each cell resuspension was diluted 200x to obtain a final OD_{600}. Ferric-DFO standards were prepared over a range from 0µM to 100µM $FeCl_3$ in 50mM Tris HCl, 1mM DFO, 10% glycerol, pH 7.4. All EPR measurements were performed on a Brüker EMX Plus instrument, at 40K with a receiver gain of 30dB, modulation amplitude of 12.5G, and attenuation of 16dB (5mW). A total of 7 scans per narrow field sweep (750G to 2250G) and 3 scans per wide field sweep (1000G to 4000G) were each averaged. The intensity of the Fe(III)–DFO chelate peak was measured at a g-value of 4.3 (at approximately 1550G). All spectra were double integrated for spin-quantification and compared against the standard calibration curve generated from obtained spectra of the ferric-DFO standards, which were measured under identical instrument conditions. Final intracellular labile iron concentrations were calculated based on total cell numbers present in the EPR tube by using the OD_{600} and

previously established cell number conversions.[15] Additional samples were simultaneously collected and analyzed as described by ICP-MS.

β-Galactosidase Assays for promoter-lacZ fusion strains. Wild-type *E. coli* MG1655 strains containing Φ*fepAp-LacZ* (PK9849), Φ*iscRp-lacZ* (PK7571), and Φ*sufAp-lacZ* (PK7722) were kindly provided by Patricia Kiley (University of Wisconsin – Madison).[18] All cells were initially plated on LB with 30μg/mL kanamycin overnight at 37°C. One colony was transferred to M9 glucose minimal media for approximately 18 hours at 37°C at 200rpm. The cell culture was then diluted 1:50 to a final OD_{600} of 0.04 in 100mL of M9 gluconate minimal media with or without 50μM $NiCl_2$ and grown for 5 hours at 37°C at 200rpm. At various time points cells were collected by centrifugation at 3,000 x g and re-suspended in Z-buffer (0.06M sodium diphosphate, 0.04M monosodium phosphate, 0.01M potassium chloride, 0.001M magnesium sulfate, and 0.05M β-mercaptoethanol). β-galactosidase activity was measured after addition of 200ul of 4mg/mL ortho-Nitrophenyl-ß-galactoside per mL of cells permeabilized with chloroform and SDS according to published protocols.[19] B-galactosidase activity was calculated and reported in Miller Units; see Equation 1 below where t = time of reaction and υ = volume of cells added in mL. Absorbance at 420nm, 550nm, and 600nm were measured using a Beckman-Coulter DU800 UV-Vis Spectrophotometer.

Equation 1: $\text{Miller Unit} = 1000 * [Abs_{420} – (1.75 * Abs_{550})]/[t * \upsilon * Abs_{600}]$

Arnow Assay for Catechol Determination. Methods from Arnow, and Ma were adapted for the quantification of catecholate siderophore production (to include any

catecholate breakdown products) by *E. coli* under nickel stress.[20,21] Wild-type MG1655 and Δ*fepA* strains were cultured according to the scheme in Figure 2.4. Cells were cultured in 0.2% gluconate M9 minimal media with or without 50μM nickel chloride. Every two hours 1mL was collected from each growth, the OD at 650nm was measured and recorded, and then each volume was cleared of cells via centrifugation at 16,000 x g for 1min. A 500μL volume of cleared supernatant was transferred to a clean, 4.0mL polypropylene cuvette. 500μL 0.5N HCl, 500μL of a 10% sodium nitrate/10% sodium molybdate mixture (Sigma-Aldrich), and 500μL 1N NaOH were added to the cuvette. All assay samples were measured against a blank mixture of fresh gluconate M9 minimal media with the above reagents listed for the assay. The absorbance at 515nm was measured and recorded immediately after mixing. Arnow units were calculated using Equation 2 below:

Equation 2: Arnow Unit = 1000 * [Abs_{515}/Abs_{650}]

Enterobactin Purification and Quantification using FPLC. *E. coli* MG1655 Δ*fepA* was plated onto LB and incubated overnight at 37°C. A single colony was cultured according to the scheme in Figure 2-4. Cultured cells were washed, normalized, and diluted to a final optical density of 0.04 in M9 gluconate minimal media, with or without 50μM nickel chloride. Cultures were incubated for 2 hours at 37°C at 200rpm. The cells were centrifuged for 20min at 4°C and 8,000 x g. The supernatant was sterile filtered twice using a fresh 0.22μm filter (Millipore) each time and a total of 1L spent media was collected. Enterobactin and its hydrolysis products were purified using a

modified form of a previously published protocol.[22] Briefly, the sterile, filtered supernatant was loaded onto a DEAE-Sepharose Fast Flow column equilibrated with 10mM sodium phosphate buffer, pH 7.0. 5mL fractions were collected by eluting at 4°C using a step gradient of 0.0M, 0.05M, 0.15M, 1.0M, and 2.0M ammonium chloride. Enterobactin and its hydrolysis products were identified based on the concentration of ammonium chloride at which they eluted and further confirmed by ESI-MS.

3.3 Results

Nickel toxicity targets iron homeostasis by reducing uptake of iron during the lag phase. ICP-MS was utilized to directly monitor the change in total intracellular levels of biologically relevant transition metals during nickel stress (Fig. 3.4). In wild-type cells grown in gluconate minimal media without nickel, total iron levels gradually increased during the lag phase and throughout the transition into exponential phase, before peaking at mid-exponential phase, after which iron content decreased as the cells moved into stationary phase (Fig. 3.4A and data not shown). In contrast, cells cultured in gluconate minimal media with 50μM Ni(II) showed almost no change in total iron levels during the same period (Fig. 3.4A). Interestingly, 30 minutes after inoculation into the gluconate minimal media, intracellular zinc levels had increased nearly two-fold in the nickel-exposed cells (Fig. 3.4B). After this point, the zinc concentration remained elevated for the remainder of growth. In contrast, the total zinc levels in untreated control cell levels increased at a significantly slower rate and to lower total levels than in nickel-exposed cells (Fig. 3.4B). Unlike iron and zinc, the intracellular levels of the

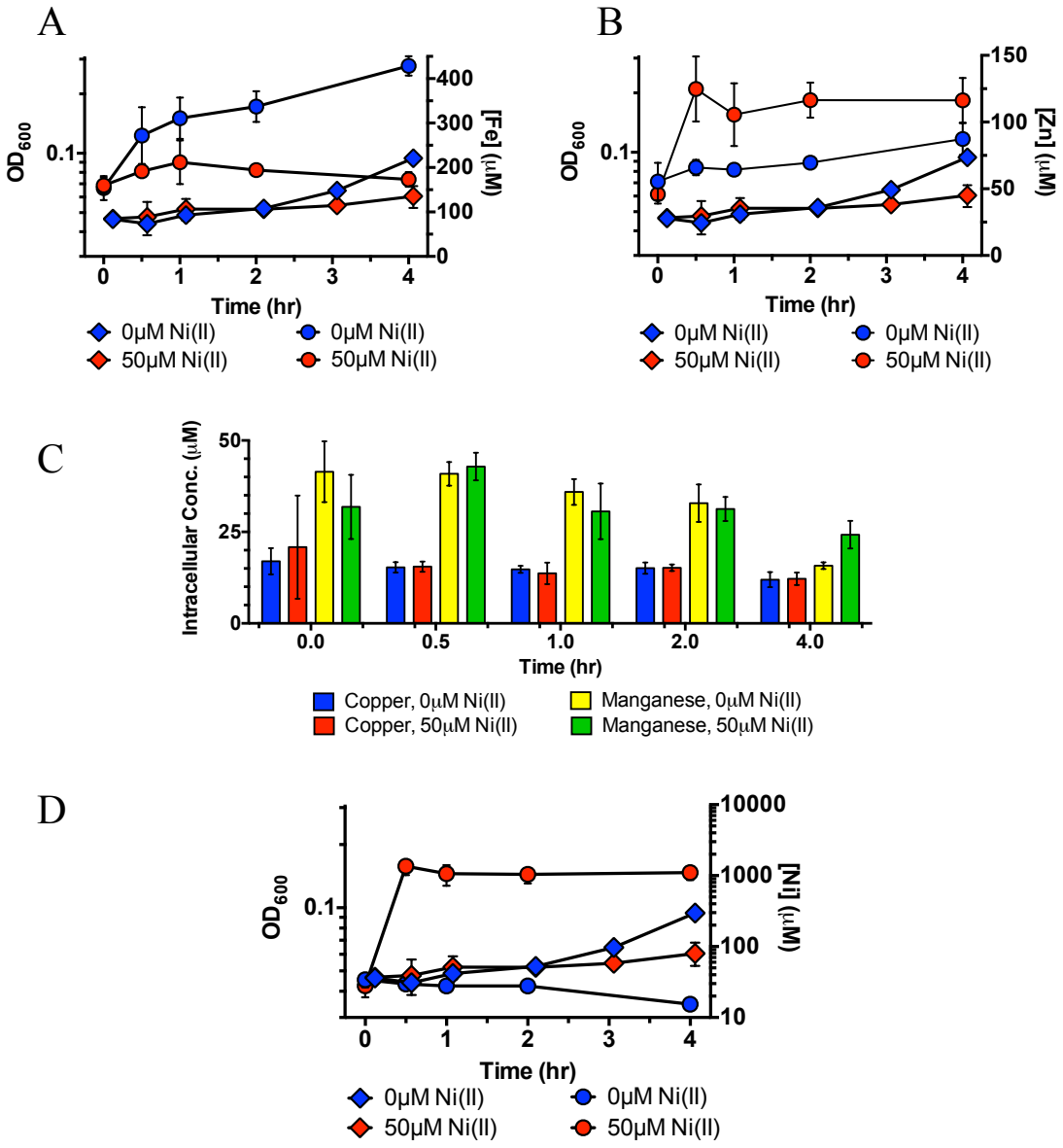

Figure 3.4. **Iron levels are decreased and zinc levels are increased upon exposure to nickel during the lag phase**. (A) Intracellular iron concentrations (right axis) (circles) were measured by ICP-MS. Iron levels are overlaid with the growth data from the same cultures (left axis) (diamonds). (B) Intracellular zinc concentrations (right axis) (circles) were measured by ICP-MS. Zinc levels are overlaid with the growth data from the same cultures (left axis) (diamonds). All measurements were repeated in triplicate (n = 3) and error bars indicate one standard deviation from the mean value. (C) Intracellular levels of manganese and copper were measured by ICP-MS in cells grown according to Scheme S1 with 50μM $NiCl_2$ added at the time of inoculation into the gluconate media. (D) Intracellular nickel concentrations (right axis) (circles) were measured by ICP-MS. Nickel levels are overlaid with the growth data from the same cultures (left axis) (diamonds).

essential metals copper and manganese showed no significant change upon nickel exposure (Fig. 3.4C). Finally, the level of intracellular nickel drastically rose in response to nickel exposure and over a short period of time (less than 1 hour after exposure), as compared to controls cells without nickel exposure (Fig. 3.4D) The rise in nickel levels was not unexpected for nickel exposed cells, but the millimolar levels suggest that nickel uptake is rapid and unchallenged. These results demonstrate that nickel accumulation in cells correlates with a reduction in iron uptake and an increase in zinc accumulation during lag phase.

In addition to measuring the fluctuations in total cellular iron levels, we also monitored changes in the intracellular labile (or "chelatable") iron pool(s) in *E. coli*. This labile iron is likely the source of iron for metallocofactor assembly *in vivo*.[23] The key iron metalloregulatory proteins Fur and IscR alter iron and Fe-S cluster metabolism respectively in response to changes in the labile iron pool by regulation the expression of target genes. Therefore we monitored the expression of several promoters that are regulated by Fur and IscR to determine if nickel exposure alters the labile iron pool (C. L. Washington-Hughes, unpublished data). The *fepA-lacZ* fusion is repressed by Fe(II)-Fur under iron-replete conditions, however this repression is lost (leading to increased transcription of *fepA* and an increase in iron uptake) under low iron conditions. In control cells with no added nickel, expression of *fepA-lacZ* was high early in lag phase but rapidly dropped as the cells progressed through lag phase and into early exponential phase (by about 4 hours in this media) (Fig. 3.5A). This expression profile indicates that the cells are initially iron deprived when diluted into fresh media but the labile iron pool is replenished during lag phase by increased iron uptake in preparation for the exit to

exponential phase. In contrast, *fepA-lacZ* activity remains high throughout lag phase in the cells stressed with 50μM Ni(II) (Fig. 3.5A), indicating that the labile iron pool remains chronically low in the presence of nickel stress due to the low overall levels of intracellular iron.

The Fe-S cluster bound (holo) form of the IscR metalloregulatory protein represses its own transcription (and that of the downstream *iscSUA-hscBA-fdx-iscX* operon) when Fe-S cluster biogenesis is adequate for cellular needs.[18,23,24] When Fe-S cluster biogenesis is disrupted (by iron starvation for example), the cluster-free apo-form of IscR no longer represses the *iscR* promoter and the *isc* system is transcriptionally induced.[18,24-26] In control cells with no added nickel, expression from an *iscR-lacZ* fusion showed a similar pattern to that of *fepA-lacZ*, with initially high expression gradually decreasing throughout lag phase and into early exponential phase (Fig. 3.5B). In contrast, the addition of 50μM Ni(II) leads to constitutively high *iscR-lacZ* expression throughout lag phase, indicating a failure to maintain adequate Fe-S cluster biogenesis in the presence of nickel stress (Fig. 3.5B). This result is also consistent with the reduced activity of the [4Fe-4S] 6-phosphogluconate dehydratase (Edd) in the presence of nickel (Fig. 2.9).

Finally, the *sufABCDSE* system is used for stress-responsive Fe-S cluster biogenesis in *E. coli*. The *sufA* promoter is activated by OxyR and IHF under H_2O_2 stress, activated by apo-IscR under conditions that disrupt Fe-S cluster metabolism, and is regulated by Fur in response to iron.[18,24-27] The *sufA-lacZ* fusion can therefore be used to monitor these integrated stress responses. In control cells with no added nickel, expression from a *sufA-lacZ* fusion was initially high in early lag phase but decreased

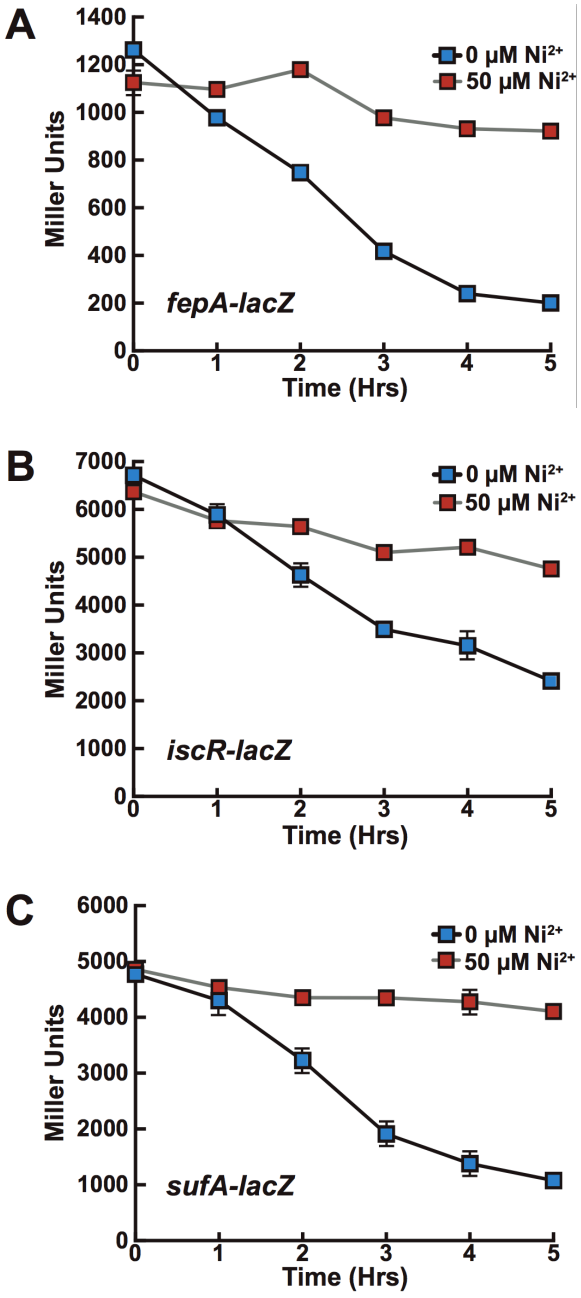

Figure 3.5. **Nickel induces the Fur and IscR regulons**. *E. coli* MG1655 strains with single copy chromosomal *lacZ* fusions were cultivated according to Scheme S1. 50μM $NiCl_2$ was added at the time of inoculation into the gluconate media (red squares) and compared to control cells grown in the same media without nickel exposure (blue squares). β-galactisidose activity was measured and is shown as Miller Units. All measurements were repeated in triplicate (n = 3) and error bars indicate one standard deviation from the mean value.

over time through the entry into early exponential phase (Fig. 3.5C). As seen with *fepA-lacZ* and *iscR-lacZ*, constitutively high *sufA-lacZ* expression is seen throughout lag phase upon addition of 50μM Ni(II), indicating disruption of Fe-S cluster biogenesis by nickel stress (Fig. 3.5C). To verify the increased expression of *suf* during nickel stress, RT-PCR also was performed on *sufA* mRNA. The results confirmed that *sufA* mRNA levels were two-fold higher in nickel-exposed cells as opposed to control cells grown without nickel (data not shown).

Whole cell electron paramagnetic resonance (EPR) was utilized to directly measure the effect of nickel stress on the size of the labile iron pool. The labile iron pool was quantified by formation of an EPR-active iron(III)-desferrioxamine (DFO) chelate inside cells (Fig. 3.6A).[16] In wild type control cells with no exposure to nickel, the labile (DFO-chelated) iron concentration was 31.9μM ± 1.5μM or approximately 12.6% of the total iron by 2hrs into lag phase (Fig. 3.6B). The labile iron concentration in cells exposed to 50μM Ni(II) was 3-fold lower (10.9μM ± 4.0μM) (Fig. 3.6B). These results support the promoter-*lacZ* fusion data, showing that total and labile intracellular iron is decreased and that the cells are iron deficient under nickel stress in lag phase.

To test if increasing intracellular iron stores prior to nickel exposure helps to alleviate nickel toxicity, 50μM $FeCl_3$ was added to the M9 glucose minimal media growth step prior to the shift into gluconate minimal media. ICP-MS analysis showed that 50μM $FeCl_3$ supplementation during the overnight growth in glucose minimal media allowed the wild type cells to increase their total cellular iron content by over 10-fold, from 32μM to 373μM (Fig. 3.7). When cells with the increased iron stores were transferred into gluconate media with Ni(II), the prolonged lag phase was shortened for

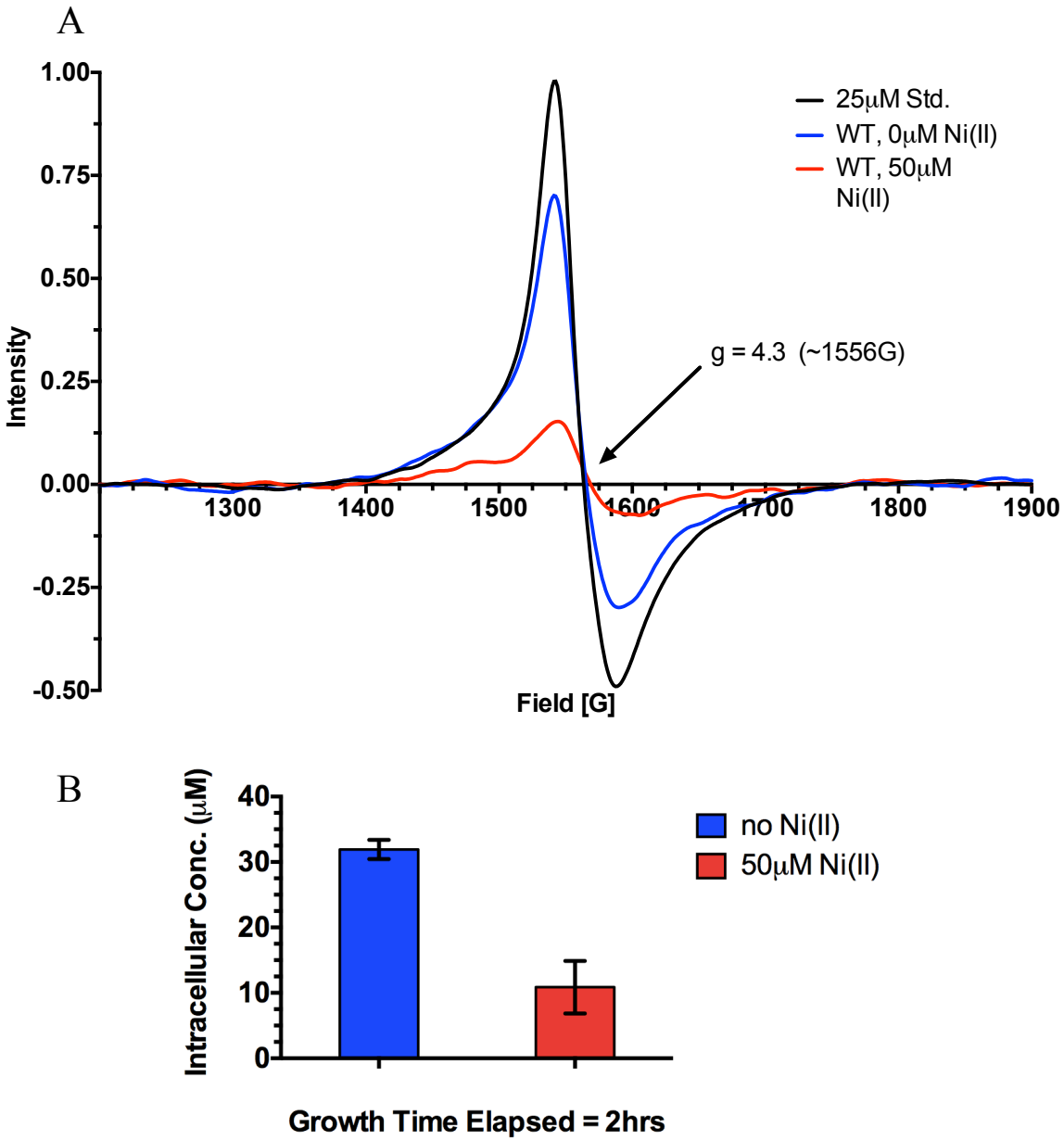

Figure 3.6. **Labile iron pools are diminished by nickel exposure during lag phase**. (A) Individual EPR spectra of the Fe(III)-DFO complex, showing an EPR signal with a calculated g-value of 4.3, from a 25μM Fe(III)-DFO standard (dotted line), from whole cells in lag phase without nickel exposure (solid line), or from whole cells in lag phase following nickel exposure (dashed line with grey fill). (B) Intracellular, DFO-accessible (labile) iron concentrations quantified from the data in panel A and normalized to cell volume and number. Cells for A and B were collected after 2hrs after inoculation into gluconate minimal media with or without 50μM $NiCl_2$. All samples were prepared in triplicate (n = 3) and error bars indicating one standard deviation from the mean value.

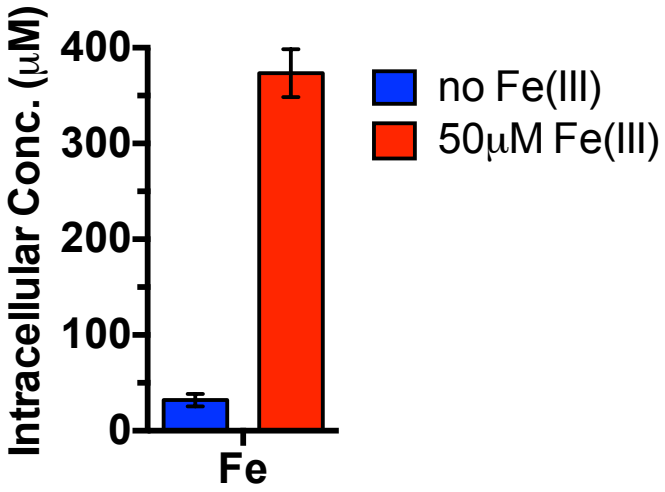

Figure 3.7. **Exposure to excess iron during the pre-stress growth increases total intracellular levels**. ICP-MS data demonstrating the extent of "iron-loading" in cells during growth in the glucose pre-stress minimal media prior to nickel exposure. All growths and samples for ICP-MS were repeated in triplicate (n = 3) and error bars indicate one standard deviation from the mean value.

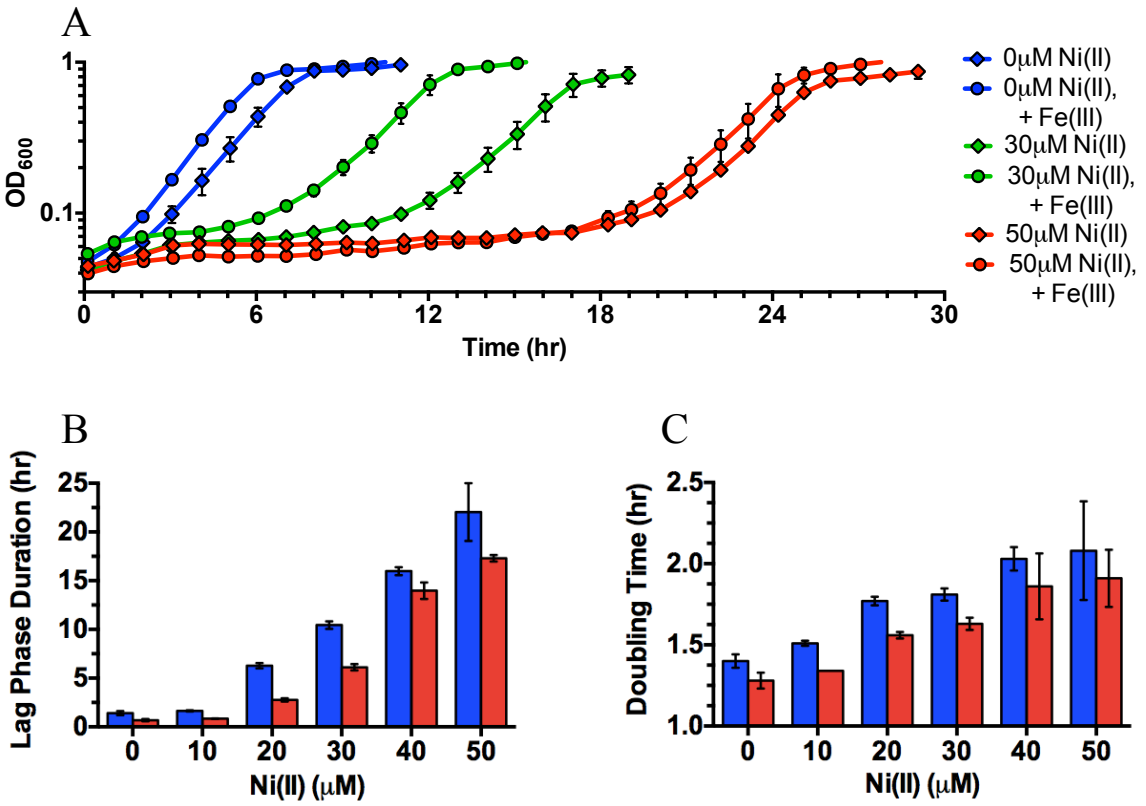

Figure 3.8. **Iron loading prior to nickel exposure partially alleviates nickel toxicity**. Wild-type MG1655 were grown to stationary phase with 50μM $FeCl_3$ in glucose minimal media prior to dilution into gluconate minimal media with increasing concentrations of $NiCl_2$. (A) Wild-type MG1655 cells were cultured according to Fig. 2-4 without prior iron supplementation (diamonds) or with 50μM $FeCl_3$ added during the pre-stress glucose growth (circles). Increasing concentrations of $NiCl_2$(aq) were added to the gluconate growth media (at the time of inoculation. Cultures were monitored by absorbance at 600nm each hour until stationary phase. Growth was monitored over time and the lag phase duration (B) and doubling times (C) of the various cultures were calculated from growth curve data. All growths were repeated in triplicate (n = 3) and error bars indicate one standard deviation from the mean value.

cells grown in intermediate concentrations of nickel (Fig. 3.8A,B). The cells with higher intracellular iron stores also showed a shorter doubling time at intermediate nickel exposure compared to control cells (Fig. 3.8C). This result is consistent with the observation that iron uptake or iron utilization may be disrupted by nickel exposure during lag phase, especially in iron-limited media. Based on the increase in intracellular zinc observed in nickel-exposed cells (Fig. 3.4B), we also tested if increasing intracellular stores of zinc could rescue the cells from nickel toxicity. The minimal media growth step was supplemented with 50μM $ZnCl_2$ prior to the shift into gluconate minimal media with nickel. We did not observe any change in lag phase duration or doubling time for nickel-treated cells with prior zinc supplementation (data not shown). Thus, prior supplementation with iron but not zinc helps to protect the cell from subsequent nickel toxicity in lag phase

Nickel toxicity disrupts enterobactin metabolism. The disruption of iron homeostasis and Fe-S cluster biogenesis caused by nickel exposure may stem, at least in part, from the failure of cells to accumulate iron during lag phase (Fig. 3.4A). Nickel exposure induced several genes regulated by the Fur regulon (Fig. 3.5A-C), but the increased expression of iron acquisition genes is apparently not sufficient to overcome the block to iron uptake (Fig. 3.4A). Mobilization and uptake of ferric ion from minimal media requires the siderophore enterobactin in *E. coli*. To test if disruption of enterobactin metabolism could be linked to impaired iron uptake in nickel-exposed cells, we measured the production of enterobactin and its associated hydrolysis products by the wild type strain in gluconate minimal media with or without nickel exposure (C. L. Washington Hughes, unpublished data). Since enterobactin and its hydrolysis products

are catechol siderophores, extracellular catechol production was monitored over time in spent media from control and nickel treated cells (Fig. 3.9).[20] Spent media from wild type cells cultured in gluconate minimal media with 50μM Ni(II) showed decreased levels of catecholate compounds compared to wild type control cells with no nickel added (Fig. 3.9A). Since nickel induces the Fur regulon (Fig. 3.5A-C), the lack of catechol compounds in the media could be due to accelerated uptake of the catechol enterobactin by increased expression of the FepA transport system. However, a Δ*fepA* deletion strain, which synthesizes and secretes enterobactin but cannot efficiently transport the ferric-bound form back into the cell also showed similar decreases in catechol accumulation in the media upon nickel exposure (Fig. 3.9B). This result indicates that enhanced clearance of enterobactin from the media does not explain the loss of catechol compounds in the wild type strain upon nickel exposure.

In order to identify the specific catecholate species altered in the spent media, enterobactin and its hydrolysis products were purified from spent media using FPLC according to previously published protocols (Fig. 3.9C).[22] LC-ESI-MS was used to confirm the expected mass of each purified species (data not shown). To maximize detectable media levels of enterobactin, the Δ*fepA* deletion strain was utilized. The enzymatic hydrolysis of cyclic enterobactin has been described previously.[22] The enzymatic breakdown of the enterobactin compound (Peak 4, Fig. 3.9C,D) produces a linear (2,3-dihydroxybenzolyserine)$_3$ trimer form with a hydroxylated R-group on the last serine (Peak 2, Fig. 3.9C,D), a (2,3-dihydroxybenzolyserine)$_2$ dimer (Peak 1, Fig. 3-9C,D), and a 2,3-dihydroxybenzolyserine monomer (Peak 3, Fig. 3.9C,D). Due to the basic conditions of the procedure used to separate the various breakdown products, a

A

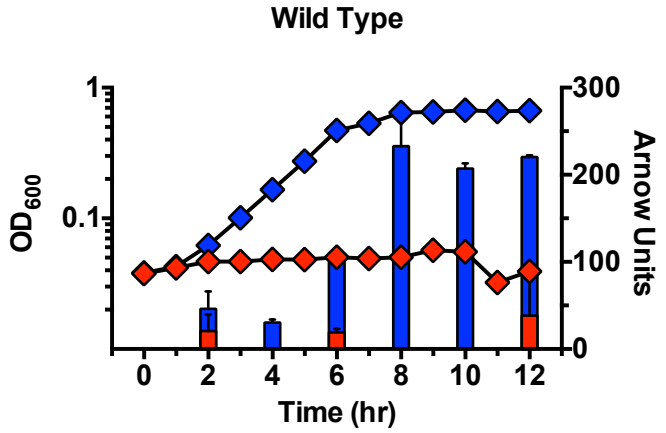

B

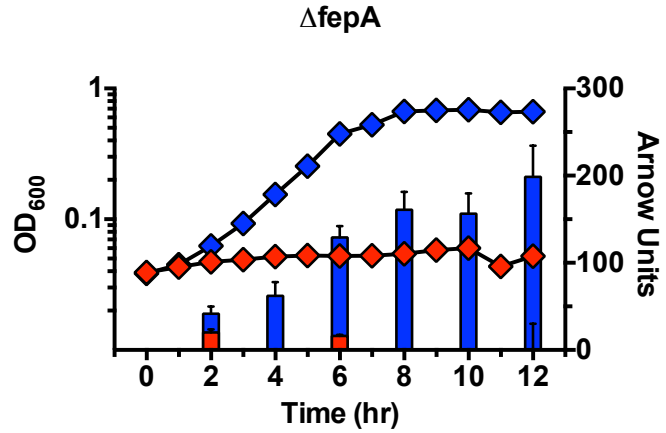

C

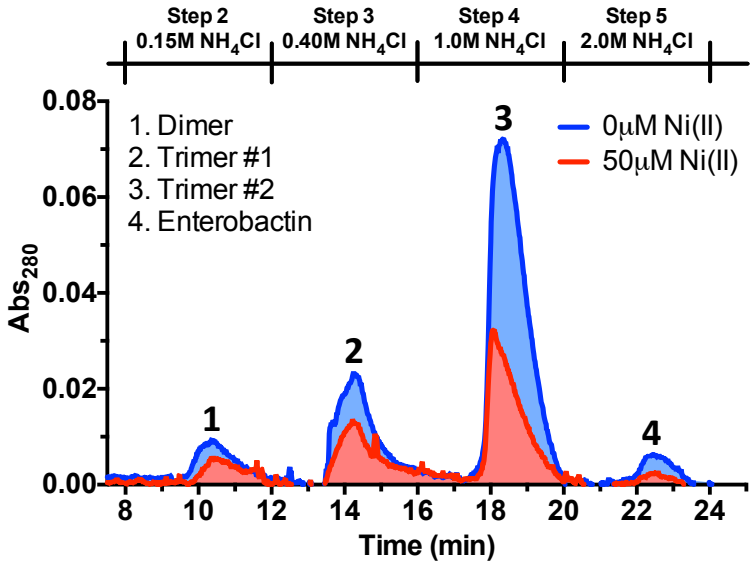

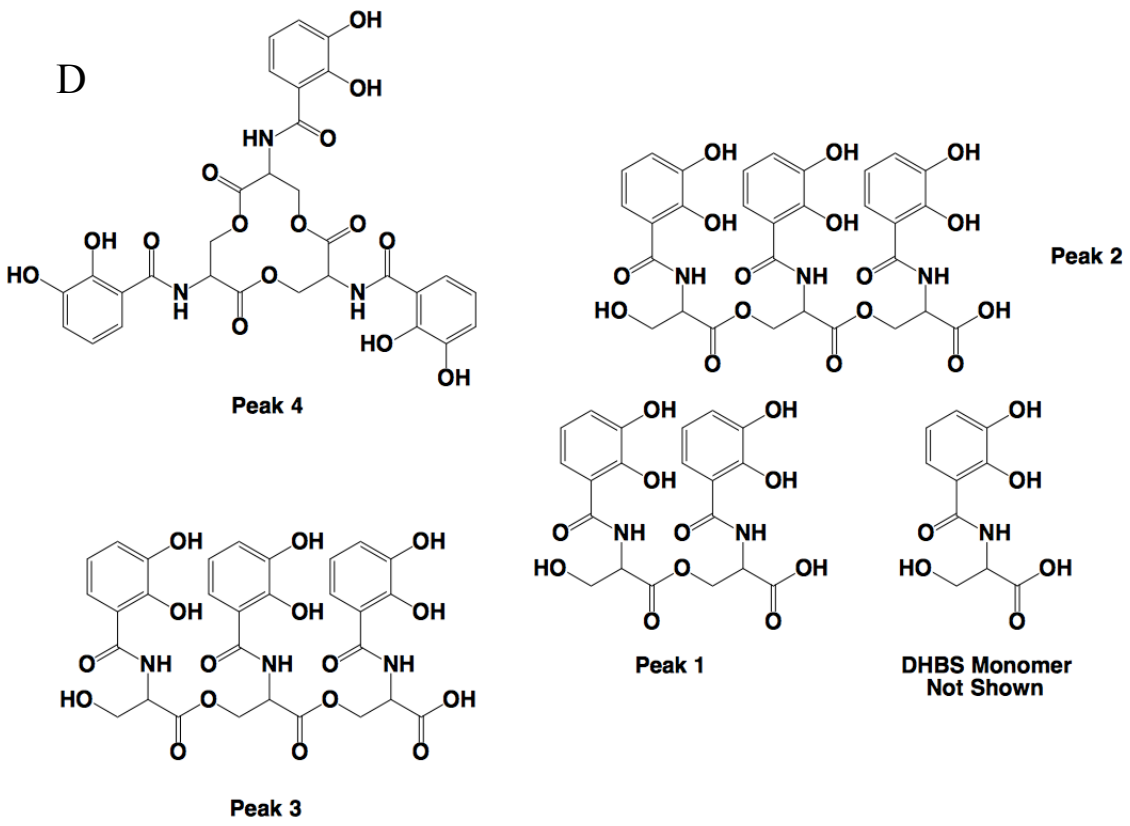

Figure 3.9. **Nickel disrupts the metabolism of the catecholate siderophore enterobactin during lag phase**. (A) Wild-type MG1655 or (B) MG1655 Δ*fepA* cells were grown according to the scheme in Scheme S1, with no added nickel (blue) or 50μM $NiCl_2$ (red). The Arnow Assay quantified total catecholate production over time (right axis, bars). Catecholate measurements are overlaid with growth data from the same cultures (left axis, diamonds). All growths were repeated in triplicate (n = 3) and error bars indicate one standard deviation from the mean value. (C) Spent media from Δ*fepA* cultures with no added nickel (blue traced line) or 50μM $NiCl_2$ (red traced line) was filtered and separated by FPLC. Elution steps are shown across the top axis and elution times are shown across the bottom axis**.** (D) The derived organic structures for the isolated numbered peaks in Panel C.

second, distinct linear (2,3-dihydroxybenzolyserine)$_3$ trimer was formed with a methylene R-group on the last serine (Peak 3, Fig. 3-9C,D).[28] These hydrolysis products are normally found in the extracellular environment where they can also function as lower affinity iron chelators for iron uptake.[29] Enterobactin and all of its hydrolysis products were reduced in cultures exposed to 50μM nickel (Fig. 3.9C). The four proteins EntCEBA together form the pathway for synthesis of enterobactin from the chorismate precursor.[30] To test if enterobactin deficiency may contribute to nickel toxicity, the enterobactin biosynthesis genes *entCEBA* were provided on a low-copy plasmid (pWSK29) fused behind the T7 promoter, and the *entCEBA* operon was constitutively expressed during growth.[21] Additional copies of the *entCEBA* plasmid provided partial rescue of nickel toxicity (Fig. 3.10). In sum, our data indicates that nickel exposure may target enterobactin metabolism, which in turn limits *E. coli* iron uptake in minimal media during the lag phase, leading to a iron starvation stress and disruption of Fe-S cluster metabolism.

3.4 Discussion

The lag phase is a sensitive period of metal homeostasis. The lag phase is a critical period of bacterial adaptation to new environments. Recent work has shown that during lag phase in LB, *S. enterica* Typhimurium increase the uptake of iron, calcium, and manganese in parallel with increases in the proteins responsible for energy production and protein expression in order to successfully move into the exponential phase of growth.[13] In contrast, other important metals in *S. enterica* Typhimurium, such as molybdenum, nickel, and cobalt, were lower during the lag phase but were

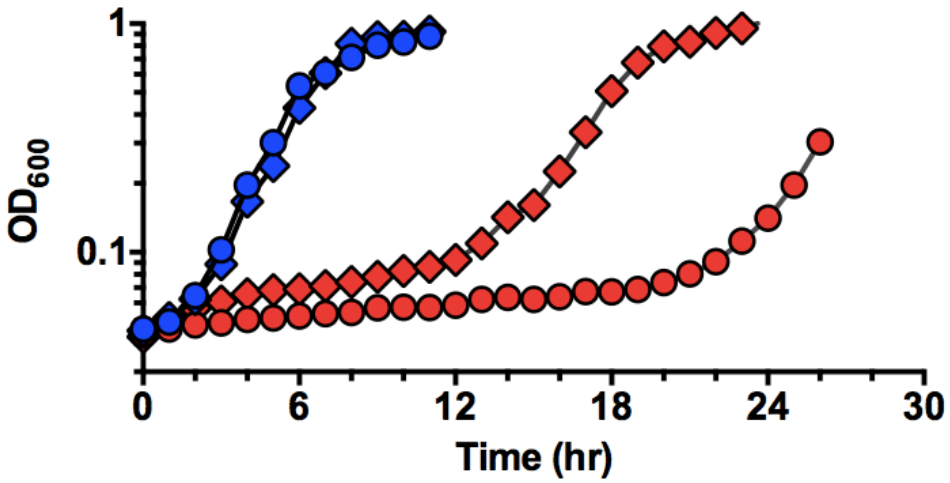

Figure 3.10. **Constitutive expression of the *entCEBA* gene products alleviates nickel toxicity**. The *entCEBA* genes were attached behind a T7 promoter and did not require induced expression. The strains MG1655 pWSK29 (diamonds) and MG1655 pEnt1 (circles) were cultured with no added nickel (blue) or 50μM $NiCl_2$ (red). All growths were repeated in triplicate (n = 3), and error bars indicate one standard deviation from the mean value.

accumulated in the stationary phase. Lastly, zinc was shown to decrease through the lag phase, from 133μM at the time of inoculation to 66μM at the end of the lag phase, but levels returned to initial levels by the stationary phase.[13] Here we also observed a close correlation between intracellular iron accumulation and the exit from lag phase into early exponential phase in *E. coli* when cells are grown in M9 minimal media (Fig. 3.4A). It appears that intracellular iron concentrations must reach a certain threshold in preparation for exponential growth. In iron depleted minimal media, this pool of intracellular iron is diluted as cells proceed to divide throughout exponential phase and into stationary phase (data not shown). Furthermore, when cells are cultured in M9 minimal media with glucose and 50μM Fe(III) overnight, the resulting final optical densities are nearly twice as high suggesting that the lack of basal iron levels in M9 minimal media leave the cells starved for iron (data not shown). In this media, iron is clearly a key limiting nutrient for bacterial adaptation and growth.

Iron homeostasis is a target of nickel toxicity. The growth scheme utilized in our study emphasizes the importance of lag phase adaptation after a metabolic shift from glucose to gluconate. Under these conditions, nickel exposure reduces intracellular iron levels in *E. coli*, leading to an extended lag phase prior to entering exponential growth (Figs. 2.5A and 3.4A). We also found that nickel diminishes activity of the [4Fe-4S] enzyme 6-phosphogluconate dehydratase and nickel induces Fur and IscR-regulated target promoters (Figs. 2.8 and 3.5A-C). Nickel sensitivity also is further enhanced if the SufABCDSE stress-response Fe-S cluster biogenesis machinery is missing.[11] Nickel toxicity can be partially alleviated by increasing intracellular iron stores prior to nickel exposure (Fig. 3.8A-C). These results clearly demonstrate that nickel can either directly

or indirectly perturb iron metabolism *in vivo* during lag phase. Unlike the more thiophilic metals Ag(I) and Cu(I), nickel does not directly attack mature Fe-S cluster metalloenzymes.[31] This observation and our iron accumulation results indicate that nickel disruption of iron metabolism is likely due to limiting iron accumulation during lag phase, especially in iron-poor minimal media. Nickel toxicity is further enhanced when the cell is forced to undergo metabolic adaptation to a new carbon source that requires de novo synthesis of iron metalloenzymes (such as Edd, 6-phosphogluconate dehydratase, in this case).

The block in iron accumulation may explain the lack of Edd activity, which contains a catalytic [4Fe-4S] cluster vital to its activity and is known to be susceptible to metal toxicity.[31,32] As demonstrated earlier, this enzyme is key to gluconate metabolism through the Entner-Doudoroff pathway and its activity is absent when cells are exposed to high levels of nickel (Fig 2.8). However, it was implied that nickel exposure does not inhibit protein translation as a whole nor is it bactericidal (Fig 2.9 and Fig. 2.15). Therefore, the deficiency of Edd activity could possibly be due to a lack Fe-S clusters available for assimilation into Edd during synthesis. However, while nickel has been revealed to inhibit other enzymes *in vitro*, it is unable to directly inhibit the Edd enzyme through destruction of its Fe-S cluster under similar conditions.[33] This result suggests an earlier step in iron uptake or Fe-S cluster biogenesis is targeted by nickel rather than the mature Fe-S enzyme.

We also observed increased zinc uptake in response to nickel stress. Previous results showing that the zinc-dependent enzyme FbaA is sensitive to nickel stress suggest that the increased zinc uptake may be a physiological response to disruption of zinc

metalloproteins by nickel in *E. coli*. However, under our growth conditions, specific nickel inhibition of FbaA does not appear to be a main cause of the extended lag phase during nickel stress. Gluconate does not require FbaA for its utilization in the Entner-Doudoroff pathway. Furthermore, there does not appear to be significant requirement for FbaA to recycle fructose 6-bisphosphate produced by the Pentose Phosphate pathway in the lag phase. Deletion of *gnd* to block the entry of carbon into the PPP does not rescue lag phase nickel toxicity even though it clearly rescues nickel toxicity during exponential phase growth (Fig. 2.8).[34] Possibly, carbon entering the PPP in lag phase produces NADPH and then exits the oxidative branch as ribose-5-phosphate rather than being fully recycled to fructose-6-phosphate and glyceraldehyde 3-phosphate via the non-oxidative branch. This possibility seems logical since lag phase cells require both nucleotide precursors and biosynthetic reducing power in preparation for entry into the exponential phase of growth. In our case, the increased zinc uptake during nickel stress may occur due to disruption of other zinc metalloproteins in lag phase, although this hypothesis remains to be tested.

Nickel-dependent disruption of enterobactin metabolism. Due to the aqueous chemistry of Fe(III) at neutral pH, ferric ion uptake is likely mediated through the enterobactin pathway in the minimal media used in this study. Enterobactin is a catecholate siderophore synthesized by *E. coli* to tightly bind ferric iron, thereby preventing the formation of insoluble ferric hydroxide or ferric phosphate complexes, which would otherwise be favored in M9 minimal media during aerobic growth.[35-37] The specific mechanism by which nickel perturbs enterobactin metabolism is still unclear. The results presented here suggest that nickel directly or indirectly decreases enterobactin

production or secretion (Fig. 3.9A-D). Incubation of purified ferric enterobactin with 50μM Ni(II) in M9 minimal media did not result in any degradation of enterobactin, indicating that nickel does not catalyze extracellular hydrolysis of enterobactin under these conditions (data not shown). However, *in vivo* nickel may destabilize enterobactin intermediates, inhibit a component of the non-ribosomal peptide synthesis apparatus used to produce enterobactin in *E. coli*, or prevent efficient intracellular enterobactin degradation and recycling. The fact that nickel export (via RcnA) is required for eventual adaptation to nickel stress and exit from lag phase further confirms that the failure to accumulate iron likely stems from disruption of intracellular targets of nickel in the *E. coli* cytoplasm. Studies are underway to further identify the specific targets of nickel toxicity involved with enterobactin metabolism. In conclusion, this study has demonstrated that iron metabolism is a major target of nickel toxicity in *E. coli* during lag phase adaptation.

3.5 References

1. Thomson, A. J. and Gray, H. B. (1998) Bio-inorganic chemistry. *Curr Op Chem Biol* 2, 155-158.

2. Finney, L. A. and O'Halloran, T. V. (2003) Transition metal speculation in the cell: insights from the chemistry of metal ion receptors. *Science* 300, 931-936.

3. Macomber, L. and Hausinger, R. P. (2011) Mechanisms of nickel toxicity in microorganisms. *Metallomics* 3, 1152-1162.

4. Andrews, S. C., Robinson, A. K., Rodriguez-Quinones, F. (2003) Bacterial Iron Homeostasis. *FEMS Microbiol Rev* 27, 215-237.

5. Winterbourn, C. C. (1995) Toxicity of iron and hydrogren peroxide: the Fenton Reaction. *Toxicol Lett* 82, 969-974.

6. Bullen, J. J., Rogers, H. J., and Griffiths, E. (1978) Role of iron in bacterial infection. *Current Topics in Microbiol Immunol* 80, 1-35.

7. Harris, W. R., Carrano, C. J., Cooper, S. R., Sofen, S. R., Avdeef, A. E., McArdle, J. V., and Raymond, K. N. (1979) Coordination Chemistry of Microbial Iron Transport Compounds. 19. Stability Constants and Electrochemical Behavior of Ferric Enterobactin and Model Complexes. *J Am Chem Soc* 101, 6097-6104.

8. Escolar, L., Pérez-Martín, J. and de Lorenzo, V. (1999) Opening the Iron Box: Transcriptional Metalloregulation by the Fur Protein. *J Bacteriol* 181, 6223-6229.

9. Mills, S. A. and Marletta, M. A. (2005) Metal Binding Characteristics and Role of Iron Oxidation in the Ferric Uptake Regulator from *Escherichia coli*. *Biochem* 44, 13553-13559.

10. Miethke, M. Hou, J., and Marahiel, M. A. (2011) The Siderophore-Interacting Protein YqjH acts as a Ferric Reductase in Different Iron Assimilation Pathways in *Escherichia coli*. *Biochem* 50, 10951-10964.

11. Wang, S., Wu, Y. and Outten, F. W. (2011) Fur the the novel regulator YqjI control transcription of the ferric reductase gene *yqjH* in *Escherichia coli*. *J Bacteriol* 193, 563-574.

12. Baranyi, J. and Roberts, T. A. (1994) A dynamic approach to predicting bacterial growth in food. *Int J Food Microbiol* 23, 277-294.

13. Rolfe, M. D., Rice, C. J., Lucchini, S., Pin, C. Thompson, A., Cameron, A. D. S., Alston, M., Stringer, M. F., Betts, R. P., Baranyi, J., Peck, M. W., and Hinton, J. C. D. (2012) Lag phase is a distinct growth phase that prepares bacteria for exponential growth and involves transient metal accumulation. *J Bacteriol* 194, 686-701.

14. Roth, V (2006) Doubling Time. (http://www.doubling-time.com/compute.php)

15. Volkmer, B. and Heinemannn, M. (2011) Condition-dependent cell volume and concentration of *Escherichia coli* to facilitate data conversion for systems biology modeling. *PLoS One* 6, e23126.

16. Keyer, K. and Imlay, J. A. (1996) Superoxide accelerates DNA damage by elevating free-iron levels. *Proceedings of the National Academy of the Sciences of the United States of America 93*, 13635-13640.

17. Popescu, C. V., Bates D. M., Beinert, H., Munck, E. and Kiley, P. J. (1998) Mössbauer spectroscopy as a tool for the study of activation/inactivation of the

transcription regulator FNA in whole cells of *Escherichia coli*. *Proc Natl Acad Sci USA* 95, 13431-13435.

18. Giel, J. L., Rodlonov, D., Liu M., Blattner, F. R., and Kiley, P. J. (2006) IscR-depdendent gene expression link iron-sulphur cluster assembly to the control of O_2-regulated genes in *Escherichia coli*. *Mol Microbiol* 60, 1058-1075.

19. Miller, J. H. (1972) Experiments in the molecular genetics. Cold Spring Harbor Laboratory, Cold Spring Harbor, NY.

20. Arnow, L. E. (1937) Colorimetric determination of the components of 3,4-dihydroxyphenylalanine-tyrosine mixtures. *J Biol Chem* 118, 531-537.

21. Ma, L. and Payne, S. M. (2012) AhpC is required for optimal production of enterobactin by *Escherichia coli*. *J Bacteriol* 194, 6748-6757.

22. O'Brien, I. G., and Gibson, F. (1970) The structure of enterochelin and related 2,3-dihydroxy-N-benzoylserine conjugates from *Escherichia coli*. *Biochim Biophys Acta* 215, 393-402.

23. Ayala-Castro, C., Saini, A., Outten, F. W. (2008) Fe-S Cluster Assembly Pathways in Bacteria. *Microbiol Mol Biol Rev* 172, 110-125.

24. Yeo, W. S., Lee, J. H., Lee, K. C., and Roe, J. H. (2006) IscR acts as an activator in response to oxidative stress for the *suf* operon encoding Fe-S assembly proteins. *Mol Microbiol* 61, 206-218.

25. Nesbit, A.D., Giel, J. L., Rose, J. C., and Kiley, P. J. (2009) Sequence-specific binding to a subset of IscR-regulated promoters does not require IscR Fe-S cluster ligation. *J Mol Biol* 387, 28-41.

26. Outten, F. W., Djaman, O., and Storz, G. (2004) A suf operon requirement for Fe-S cluster assembly during iron starvation in *Escherichia coli*. *Mol Microbiol* 52, 861-872.

27. Patzer, S. I. and Hantke, K. (1999) SufS is a NifS-like protein, and SufD is necessary for stability of the [2Fe-2S] FhuF protein in *Escherichia coli*. *J Bacteriol* 181, 3307-3309.

28. O'Brien, L. G. and Gibson, F. (1970) Biologically active compounds containing-2,3-dihydroxybenzoic acid and serine formed by *Escherichia coli*. *Biochim Biophys Acta* 201, 453-460.

29. Hancock, R. E., Hantke, K., and Braun, V. (1977) Iron transport in *Escherichia coli* K12: 2,3-Dihydroxybenzoate-promoted iron uptake. *Arch Microbiol* 114, 231-239.

30. Gehring, A. M. Bradley, K. A., Walsh, C. T. (1997) Enterobactin Biosynthesis in *Escherichia coli*: Isochorismate Lyase (EntB) is a Bifunctional Enzyme that is Phosphopantetheinylated by EntD and then Acylated by EntE using ATP and 2,3-Dihydroxybenzoate. *Biochem* 36, 8495-8503.

31. Xu, F. F. and Imlay, J. A. (2012) Silver(I), mercury(II), cadmium(II), and zinc(II) target exposed enzymic iron-sulfur clusters when they toxify *Escherichia coli*. *Appl Environ Microbiol* 78, 3614-3621.

32. Djaman, O., Outten, F. W., and Imlay, J. A. (2004) Repair of Oxidized Iron-Sulfur Clusters in *Escherichia coli*. *J Biol Chem* 279, 44590-44599.

33. Kalliri, E., Gryska, P. A., and Hausinger, R. P. (2005) Kinetic and spectroscopic investigation of CoII, NiII, and N-oxalylglycine inhibition of the FeII/alpha-ketoglutarate dioxygenase, TauD. *Biochem Biophys Res Commun* 338, 191-197.

34. Macomber, L., Elsey, S. P., and Hausinger, R. P. (2011). Fructose-1,6-bisphosphate aldolase (class II) is the primary site of nickel toxicity in *Escherichia coli*. *Mol Microbiol* 82, 1291-1300.

35. Wookey, P. and Rosenberg, H. (1978) Involvement of inner and outer membrane components in the transport of iron and in colicin B action in *Escherichia coli*. *J Bacteriol* 133, 661-666.

36. Pierce, J. R., Pickett, C. L., and Earhart, C. F. (1983) Two *fep* genes are required for ferrienterobactin uptake in *Escherichia coli* K-12. *J Bacteriol* 155, 330-336.

37. Ozenberger, B. A., Nahlik, M. S., and McIntosh, M. A. (1987) Genetic organization of multiple *fep* genes encoding ferric enterobactin transport functions in *Escherichia coli*. *J Bacteriol* 169, 3638-3646.

CHAPTER 4

THE FERRIC REDUCTASE YqjH IS REQUIRED FOR THE DEVELOPMENT OF NICKEL RESISTANCE IN *ESCHERICHIA COLI* AND IS A POTENTIAL ZINC METALLOENZYME

Abstract

Bacterial iron homeostasis utilizes a unique set of ferric ion chelators called siderophores, which greatly increase the solubility of the ferric ion. These compounds represent some of the most powerful iron-chelating species, with log stability constants for ferric ion ranging from the high 20s to approximately 40-50. In order to assimilate the iron provided by siderophores, bacteria have evolved a family of siderophore-interacting proteins designed to extract the ferric ion center. The protein YqjH has been identified as a putative ferric siderophore reductase. Currently, the overall role of this enzyme in the iron homeostasis system of *E. coli* remains ambiguous. Previous studies have shown that YqjH regulated by both iron and nickel homeostasis and establish a link between these two metals. New data suggests that the development of nickel resistance is tied to YqjH. Furthermore, evidence has been observed that YqjH may also function as a zinc metalloenzyme, where the Zn(II) ion may play a role in the catalytic cycling of YqjH. The presence of Zn(II) drastically enhances the reductase activity of YqjH during the reduction of ferric EDTA. The YqjH catalytic cycle also includes a semiquinone

intermediate during its catalytic cycle. This semiquinone state has been observed to preferentially bind Zn(II) over the oxidized by a factor of approximately 2. Additionally, the presence of zinc ion slows the formation of the semiquinone state when the oxidized protein is reduced by single electron reduction with sodium dithionite. Though preliminary, the evidence is intriguing and suggests further study to determine the exact manner and mechanism through which Zn(II) interacts with YqjH and enhances the ferric reductase activity.

4.1 **Introduction**

The transition metal iron and its vital role in bacteria have already been discussed in detail in the previous chapters, in addition to the systems that control iron homeostasis. Given its natural abundance and the major dependence of bacteria on this transition metal, bacteria still face the universal struggle to maintain sufficient levels of iron for optimal growth. This is due to several reasons, but largely depends on the growth conditions faced by bacteria. Due to the oxidative nature of Earth's atmosphere, iron primarily exists in the +3 (ferric) oxidation state, and has a molar solubility of approximately 1 x 10^{-18} M at physiological pHs.[1] This value is far to low for optimal bacterial growth, which require solubilized iron to be in the range of 10^{-7} to 10^{-5} M.[1]

Regardless of the conditions or environment bacteria may encounter, bacteria are often left to scavenge iron from any source available to maintain a sufficient intracellular quota. Bacteria have developed the use of a variety ferric chelating compounds, call siderophores, to answer their iron needs. Siderophores are highly efficient, low molecular

weight (< ~1 kDa) ferric ion scavenging compounds synthesized by bacteria, fungi, and plants during iron-limited periods of growths. Siderophores exhibit high affinities for iron in the ferric state, with log stability/formation constants that are typically 20 and higher.[1,2] Siderophores are also categorized into several different classes, with the two most common being the hydroxamates and catecholates. Archetypes for these classes are ferrichrome and enterobactin, respectively.[2,3] The classes of siderophore differ by their binding motifs and structures, but all bind the ferric ion in an octahedral, hexadentate complex.[2,4] However, siderophores with mixed motifs are synthesized as well, such as Mycobactin T produced by *Mycobacterium tuberculosis* for iron acquisition.[5,6]

In order to extract the iron center from siderophore complexes for assimilation, bacteria encode enzymes called siderophore-interacting proteins (SIPs) that function as ferric reductases. These proteins utilize redox-active prosthetic groups, such as flavins and Fe-S clusters, to electrochemically reduce ferric ions to the ferrous state thereby promoting release from the siderophore. In order to perform this step, the proposed SIP must have a reduction potential on par with potential of a ferric siderophore complex. One of the first characterized SIPs was ViuB from *Vibrio cholera.* ViuB is necessary for the uptake and utilization of the endogenous *V. cholera* siderophore vibriobactin.[7] *E. coli* K12 can import exogenous ferric siderophore complexes, such as copragen, ferrichrome, rhodotorulic acid, and ferrioxamine B.[1] *E. coli* also encodes the hydroxamate siderophore reductase FhuF. FhuF has shown the ability to extract ferric ion centers from a variety of hydroxamate siderophore complexes, such as ferrioxamine B, copragen, and ferrichrome, through electrochemical reduction.[8] The reduction potentials of ferrioxamine B (-468mV ± 15), copragen (-447mV ± 7), and ferrichrome (-400mV ± 10) are near the effective

redox potential range of FhuF (-241mV ± 25 to -369mV ± 25).[9-12] Additional studies have also shown that D*fhuF* strains grew more slowly when supplemented with ferrioxamine B only.[8] Curiously, the FhuF protein contains also a [2Fe-2S] cluster and requires the SufD protein for stability.[13] SufD is a member of the *sufABCDE* operon, which encodes a series of proteins responsible for Fe-S cluster synthesis during oxidative stress and iron limitation.[14] These data demonstrates the importance of FhuF to *E. coli* cannot be understated during periods of iron limitation, as it enables *E. coli* to use exogenous siderophores as iron sources and literally steal iron from other bacteria.

Most bacteria also endogenously synthesize at least one siderophore unique to that species. For example, *E. coli* K12 endogenously synthesizes the siderophore enterobactin, which displays one of the lowest dissociation constants for ferric ion at approximately 1 x 10^{-49} M.[15] In addition, *E. coli* encodes the transporters EntS and FepA, which function for the secretion and subsequent uptake of the ferric enterobactin complex, respectively (Fig 4.1).[16,17] These two proteins are also regulated by the Fur protein, and are induced during iron starvation but are repressed with iron sufficient conditions (Fig 4.1).[18-22] Currently, no SIP has been observed to directly reduce the intact ferric enterobactin complex. This is likely due to its uncharacteristically low redox potential, approximately -750mV.[23] This places enterobactin out of the effect redox range of most SIPs.

Recently, a putative ferric reductase, YqjH, has been found in *E. coli*, and has demonstrated an ability to reduce ferric ion (bound in several complexes) to ferrous iron.[24,25] YqjH has a high homology to the siderophore ViuB in *Vibrio cholerae*, suggesting that it too may interact with a siderophore complex *in vivo*.[24,25] However, the

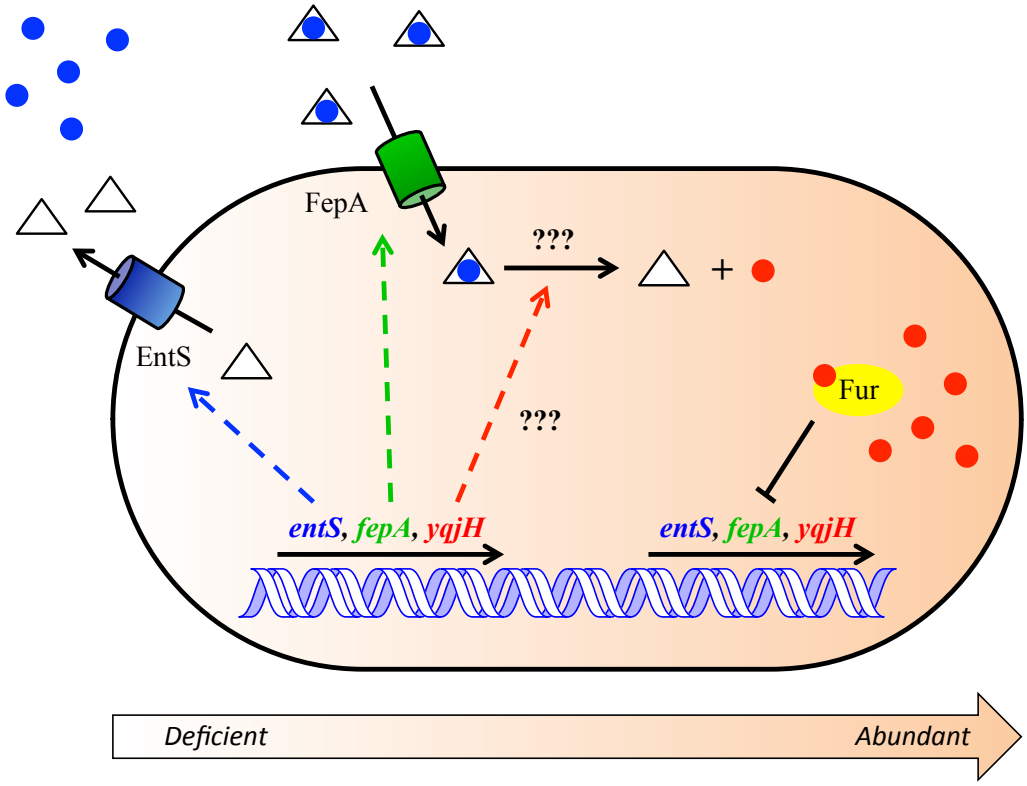

Figure 4.1. **An overview of iron homeostasis relating Enterobactin with YqjH**. The *entS*, *fepA*, and *yqjH* genes are expressed during periods of iron deficiency. EntS and FepA are involved in the export desferrienterobactin (white triangles) and the uptake of ferric enterobactin (white triangles with blue dot), respectively. The release of ferric iron (blue dots) and subsequent reduction to ferrous iron (red dot) is less understood and the role of YqjH in this process remains unclear. During periods with sufficient intracellular iron levels, the *entS*, *fepA*, and *yqjH* genes are repressed by Fe(II)-Fur regulation.

role of YqjH concerning iron homeostasis has yet to be clarified. Furthermore, a native ferric substrate has also not been fully confirmed, but recent data suggests the siderophore enterobactin may fulfill this role.[24] Enterobactin utilizes a system of catechol functional groups to coordinate a single ferric ion at the center and maintains one of the highest known affinities for ferric iron (Fig. 3.2). However, no known siderophore-interacting ferric reductase has shown the natural ability to electrochemically reduce the ferric ion center of intact enterobactin to date, primarily because of the exceedingly low reductive potential (approximately -750mV at a pH of 7) of the intact complex with ferric iron.[23] However, *E. coli* also encodes the enzyme ferric enterobactin esterase, Fes, which catalyzes the hydrolysis of the trilactone backbone of enterobactin, forming a mixture of linear dihydroxybenzoylserine compounds.[15] Once hydrolyzed, the affinity for ferric ion is significantly decreased, and YqjH has been demonstrated to have a high specific activity for reducing the linear dihydroxybenzoylserine compounds.[24]

The junction of iron and nickel homeostasis has recently been demonstrated with YqjH. YqjH has been demonstrated to fall under the Fur regulon, where its expression was repressed by Fur at sub-micromolar concentrations when grown in glucose M9 minimal media.[25] Simultaneously, YqjI, a protein divergently transcribed from YqjH, regulated YqjH expression as well in the presence of sub-micromolar levels nickel under the same media conditions. The deletion of the *yqjH* gene further resulted in hypersensitive phenotype to nickel toxicity.[25] This deletion also slowed growth of the mutant when supplemented solely with the iron-loaded dihydroxybenzoylserine compounds.[24] These results raised the possibility that nickel directly targets iron homeostasis in bacteria, as seen in eukaryotes.

The catalytic cycle of YqjH involves a multi-step, multi-electron transfer to and from a non-covalently attached FAD cofactor, which remains with the protein and doesn't dissociate from YqjH at any step, and ultimately reduces two equivalents of a ferric iron source compound. Initially, YqjH is reduced from a fully oxidized state (YqjH-FAD_{ox}) to a fully reduced hydroquinone state (YqjH-FAD_{hq}) via a 2-electron transfer from NADPH to the FAD cofactor. The oxidized NADP+ dissociates from the protein, allowing an equivalent of ferric ion to bind to YqjH and be reduced down to the ferrous state via a single electron transfer, while simultaneously oxidizing the FAD cofactor. This first oxidation step (E_1) forms the stable FAD semiquinone (YqjH-FAD_{sq}) species. The fully oxidized protein and cofactor is then fully reformed by a second oxidation step (E_2) where another single electron is transferred to reduce a second equivalent of the ferric ion substrate (Fig. 4.2).[24] The first oxidation step (E_1) of the redox couple, YqjH-FAD_{sq}/FAD_{hq}, has a redox potential of -431 ± 16mV; the second oxidation step (E_2) of the redox couple, YqjH-FAD_{ox}/FAD_{sq}, has a reported redox potential of -202 ± 9mV.[24] The increasing potential from E_1 to E_2 suggests that YqjH function is likely more suited to the passing of electrons to the ferric ion source from the NADPH substrate; as opposed to the production of NADPH as with structurally similar proteins like FNR.[24,26] For comparison, the redox potential of the 2-electron transfer step (E_m) for the redox coupling of YqjH-FAD_{ox}/FAD_{hq} was measured to be -312 ± 7mV, making the 2-electron reduction a favorable step by the $NADP^+$/NADPH redox couple ($E° = -370mV$) at physiological conditions.[24]

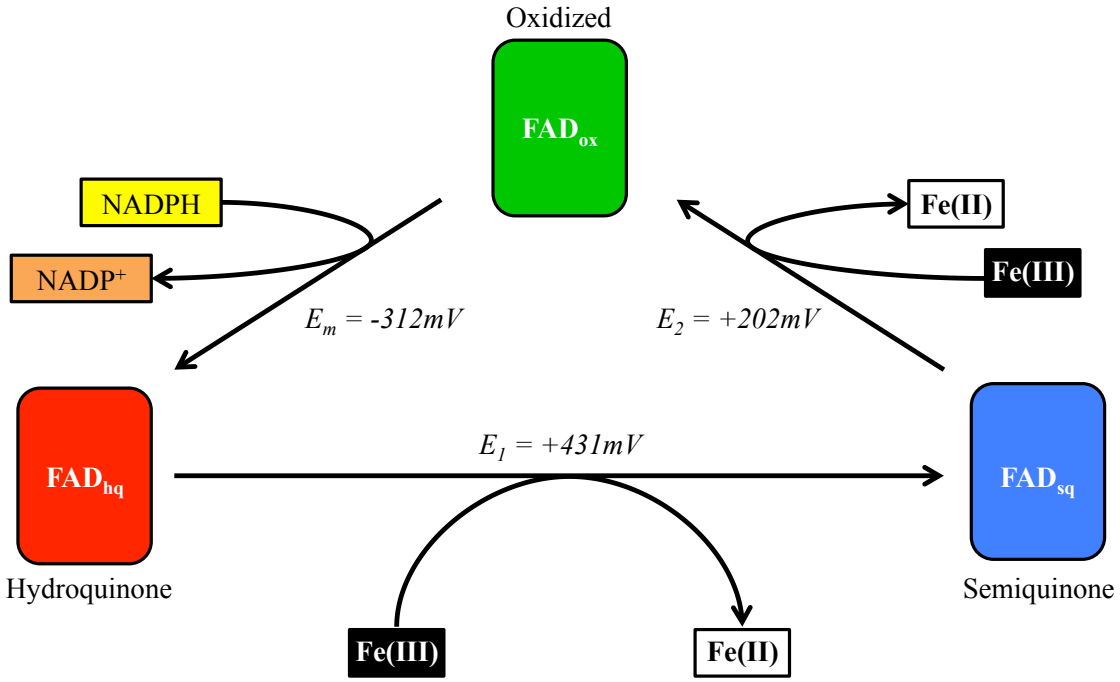

Figure 4.2. **The proposed catalytic cycle of YqjH**. The FAD cofactor of YqjH is responsible for the catalytic activity of the enzyme. It is reduced by a 2-electron transfer step from NADPH, creating the YqjH-FAD_{hq} state (red shading). From this point, two, single electron transfer steps oxidize the enzyme back to the YqjH-FAD_{ox} state (green shading). A semiquinone intermediate, YqjH-FAD_{sq} (blue shading), is formed and consumed between each of the oxidation steps. (Abbreviations: hq = hydroquinone, sq = semiquinone, ox = oxidized).

4.2 Materials and Methods

Bacterial Strains, Growth Media, and Growth Conditions. Strains used in this study are all derivatives of the parent wild-type strain E. *coli* MG1655 (Table 4.1). An individual colony was transferred from fresh Lennox broth (LB) agar plates into a 4mL volume of LB and grown for 4 to 5hrs at 37°C with shaking at 200rpm. Cells from this culture were pelleted and washed twice in sterile 1X M9 minimal media salts; and the OD_{600} was normalized to 1.0. Normalized cells were diluted 1:200 into M9 glucose minimal media containing 1X M9 minimal salts (BD Difco), 0.2% (w/v) glucose (Acros Organics), 0.2% (w/v) magnesium chloride, 0.1mM calcium sulfate, and 0.5µg/mL Thiamine HCl (Sigma-Aldrich). Cultures were incubated overnight for 18 – 20hr, at 37°C and 200rpm, then washed and pelleted twice in sterile 1X M9 salts as described above. The resulting cell suspensions were normalized to an OD_{600} of 2.0 and diluted 1:50 into M9 gluconate minimal media with 0.2% (w/v) potassium gluconate (Alfa Aesar) to give an initial OD_{600} of 0.04. Nickel chloride (Sigma-Aldrich) was added to a specified final concentration in the M9 gluconate minimal media, from 0µM up to 50µM. Other reagents added to M9 glucose or M9 gluconate media are described in the appropriate figure legends. All cultures were culture as above unless otherwise indicated (Fig. 2-4). Cell growth was monitored by UV-Vis absorption at 600nm and plotted versus time (in hours).

Development of nickel resistance strains. To ascertain if resistance to nickel toxicity had developed, wild-type MG1655 and MG1655 ΔyqjH::amp^R cells were initially exposed to 50µM Ni(II) and then collected after each growth had entered the

Table 4.1. **Bacterial Strains and Plasmids utilized in this study**.

Strain or Plasmid	Relevant Genotype or Phenotype	Reference or Source
E. coli Strains		
MG1655	Wild Type, *E. coli* K12 F-, λ^-, *ilvG- rfb*-50 *rph*-1	Laboratory Strain
GTF002	MG1655 Δ*yqjH::kan*^{R}	25
GTF004	BL21 (DE3)	Laboratory Strain
GTF008	DH10β *yqjH*_pet21a::amp^R	25
GTF015	BL21 (DE3) *yqjH*_pet21a::amp^R	This Study
GTF038	MG1655 50μM Ni-treated	This Study
GTF046	MG1655 Δ*yqjH::kan*^{R} 50μM Ni-treated	This Study
Plasmids		
pET_21a	Empty vector, amp^R	This Study

stationary phase. Collected cells were plated on LB plates without nickel and incubated overnight at 37°C. A single colony was transferred into 2mL LB, and cultured overnight at 37°C and 200rpm. Glycerol stocks were made from these cultures and stored at -80°C. Further experiments requiring these "Ni-adapted" strains (specified by the concentration of Ni(II) exposure) were conducted following the same growth scheme described above, with each strain exposed to a specified level of nickel.

YqjH over-expression and whole cell lysate preparation. A yqjH_pET21a plasmid expression vector utilized for these studies was constructed by Wang et al.[25] The yqjH gene was fused into the pET21a vector, downstream to a T7 promoter with the plasmid also encoding for an Amp^R gene. The *yqjH_pET21a* plasmid was transformed into *E. coli* BL21(DE3) chemically competent cells from DH5a for over-expression and purification of YqjH. Transformed cells were plated on LB agar plates infused with 100mg/L Ampicillin and incubated overnight at 37ºC. Isolated colonies were inoculated into 2.0mL LB with 100mg/L Ampicillin, for an overnight growth at 37ºC and 200rpm. A 0.50mL amount of overnight growth was inoculated into 50mL of fresh LB with 100mg/L Ampicillin, and incubated overnight at 37ºC and 200rpm. From the 50mL growth, 20.0mL were used to inoculate the final culture growth of 2.00L with 100mg/L Ampicillin.

The 2.0L growths were incubated at 37ºC and 200rpm; once the culture OD at 600nm reached a minimum of 0.3-0.4, the YqjH plasmid was over-expressed via induction with 1.00mL of 0.5 M Isopropyl-b-D-1-thiogalactopyranoside (IPTG) per liter of bacterial culture. Cultures were incubated for an additional three hours at 37ºC and 200rpm. Cells were then pelleted and collected by centrifugation at 6000rpm at 4ºC and

lysed on ice by sonication (50% intensity, 3min, 1sec ON/1sec OFF) under aerobic conditions. The lysed solution was treated with 1.00g of Streptomycin sulfate salt for every 100mL of cell lysis solution and the pH was balanced to 7.5. Cell debris was cleared away by centrifugation at 13,000rpm for 30 minutes and the resulting supernatant was collected and pooled together. The prepared cell lysate was filtered through a 0.22μm polyethersulfone, syringe-driven filter and kept on ice until ready for purification and column chromatography.

YqjH purification and storage. YqjH protein was purified from the cleared cell lysate was performed by ion-exchange first, followed by purification by hydrophobicity, and lastly by size exclusion columns on a Bio-Rad *Biologic DuoFlow*™ FPLC chromatography system. Selected fractions after each column were analyzed by SDS-PAGE for purity and to approximate the quantity of YqjH. Fractions exhibiting the highest purity and quantity were pooled together after the each column based on the performed SDS-PAGE analysis. After the final column and the selected fractions were concentrated to a final volume of approximately 1.0-1.5mL. Aliquots with an approximate volume of 25uL of the resulting concentrated solution were flash-frozen in liquid N_2 and stored at -80ºC until ready for use. Protein concentration was determined by using the Bradford Assay with a BSA calibration curved. The purified YqjH was also check for enzyme activity and FAD_{ox} content.

Ferric Reductase Assays. The enzymatic assay used for the following experiments was previously described by Wang et al. and modified as necessary.[25] All reagents and reaction mixtures were prepared under anaerobic conditions in a 50mM Tris-HCl, 100mM NaCl (pH 7.5) buffer, then sealed prior to removal from the anaerobic

chamber for enzymatic analysis by UV-Vis spectrometry. Ferric EDTA salt was used as a ferric ion source and added to a final concentration of 2mM, unless otherwise noted. NADPH was utilized as a 2-electron source for reduction of the FAD_{ox} cofactor of YqjH, and added to a final concentration of 500µM. Ferrozine was added to measure Fe(II) production by the reaction by enabling a colorimetric change.[27] Specific activities were determined by monitoring peak evolution at 562nm by UV-Vis spectroscopy over time. The final Δ562nm was used to calculate the specific activity for YqjH using Equation 1, below, where *C* = the concentration of YqjH in mg/mL, *t* = time of reaction in minutes, *V* = total reaction volume in mL, and $\varepsilon_{FeFz} = 27.9 mM^{-1}x\ cm^{-1}$, correlating to the ferrous-ferrozine (FeFz) complex at 562nm.[27]

Equation 1: Specific Activity = $(\Delta Abs_{562})/[C * t * V * \varepsilon_{FeFz}]$

To determine the effect of various divalent metal cations on the overall activity of YqjH, a specified cation was added into the reaction mixture with identical concentrations of NADPH, a Fe(III) ion source, and Ferrozine as previously described above. All reaction assays were carried out in 500µL total volume. Each cation selected was first tested individually at a concentration of 50µM to determine any effect on the activity of the YqjH enzyme. From this, cations showing the greatest effect were added to the reaction mixture at various concentrations. To serve as a control for interference in the assay, Fe(III) ion reduction in the presence of the same cation was also measured without the presence of the YqjH enzyme. Additionally, several different counter anions

were tested with the same cation pairing. The specific activities in the presence of a cation were calculated as described previously in Equation 1 above.

All divalent cations were stringently analyzed to determine the effect, if any, the cation may have on the ferrous ion indicator Ferrozine, whether by interfering with the complexation of Ferrozine to Fe(II) or by binding with Ferrozine itself. A 20μM concentration of a specified metal was equilibrated with 100μM Ferrozine in MQ H_2O for 10min and the absorbance was measured at 400, 500, 562 (for the ferrous-ferrozine complex), and 600nm. To determine if the metal interfered with the binding of ferrous ion to ferrozine, a 50μM concentration of the metal in question was first equilibrated with 100μM Ferrozine for one minute. To each sample, ferrous ammonium sulfate was added to a final concentration of 50μM. Each sample was diluted twice to give a final sample volume of 1000μL, with each metal present having a final concentration of 25μM. Absorbance at 562nm was measured at 30sec, 1, 2, 5, and 10min after mixing.

Circular Dichroism Studies of YqjH. CD Spectroscopy was used to elucidate the underlying secondary structures of YqjH through comparison to other proteins of known structure; e.g. other flavoproteins.[28] To study $YqjH_{ox}$ secondary structure, in the regions of 190-250nm, a 5μM fully oxidized sample of YqjH in 1mM Tris-HCl (pH 8.5) buffer was prepared. The far-UV spectrum of YqjH was also studied while in the presence of Zn(II) (added as zinc sulfate) to try and determine the effect of Zn(II) on YqjH or its FAD cofactor.

UV-Vis spectroscopy Studies of the YqjH semiquinone state. The formation of the semiquinone state of the flavin cofactor was studied via UV-Vis spectroscopy. All reagents were made fresh the day of the assays. A control sample was made by

incubating a 40µM sample of YqjH with 4mM dithionite in 20mM HEPES, 10% Glycerol, and pH'd to 7.5. To study the effects of Zn(II), another sample was made by incubating a 40µM sample of YqjH with 4mM dithionite and 400µM $ZnSO_4$, simultaneously, in 20mM HEPES, 10% Glycerol, and pH'd to 7.5. All samples were prepared under anaerobic conditions using a Coy anaerobic chamber. All buffers and reagents were made fresh and prepared anaerobically; time was allowed for oxygen gas to diffuse out of the solutions. The assays were performed under anaerobic conditions to prevent any adversary effects by oxidation, by either prematurely oxidizing the dithionite reagent or oxidizing YqjH back to the fully oxidized state. Time was started at the time of mixing. For scanning, 100µL aliquots of the specified mixture were removed from the anaerobic chamber and immediately scanned. Scans from 200nm to 800nm were taken at 5, 10, 20, and 30min.

Electron Paramagnetic Resonance Studies for YqjH reduction with Zn(II) and Dithionite. The effect of Zn(II) on the formation of the semiquinone state of YqjH ($YqjH_{sq}$) was further studied via Electron Paramagnetic Resonance (EPR). All samples were prepared under anaerobic conditions using a Coy anaerobic chamber. All buffers and reagents were made fresh and prepared anaerobically; time was allowed for oxygen gas to diffuse out of the solutions. A control sample of 100µM oxidized YqjH ($YqjH_{ox}$) was prepared in 20mM HEPES, 10% Glycerol, and pH'd to 7.5. Reduced samples were produced by incubating 100µM YqjH with 10mM Dithionite, with or without 1mM $ZnSO_4$. The mixtures were transferred after 20min incubation at room temperature into a 4mM x 250mm, thin-walled quartz EPR tube from Wilmad Glass (707-SQ-250M) (and

carefully flash frozen using N_2(l). All samples were stored in N_2(l) until ready for scanning. A blank was prepared using buffer only.

All EPR scans were performed on a Brüker EMX Plus instrument, at 4K with a receiver gain of 30dB and modulation amplitude of 10.0G. Instrument attenuation was set at 20, 23, 25, or 27dB for determining a power saturation curve. A total of 10 scans per narrow field sweep (2600G to 4100G) and 3 scans per wide field sweep (500G to 4500G) were each averaged together. The YqjH semiquinone radical was detected at a g-value of 2.005 (at approximately 3342G).

Inductively Coupled Plasma Mass Spectroscopy. Fresh aliquots of purified YqjH were analyzed *in vitro* for their metal content in both the oxidized and semiquinone states after incubation with $ZnSO_4$. All blanks, controls, and samples were prepared under anaerobic conditions and incubated in 50mM Tris-HCl, 100mM NaCl, 5% Glycerol, pH'd to 7.5. A 25µM sample of YqjH protein was incubated for 10min with or without 2.5mM sodium dithionite and with or without 250µM $ZnSO_4$. After the allotted time for incubation, mixtures were desalted through a 5mL HiTrap Desalting column from GE Health Care Life Sciences. Appropriate blanks and controls were also constructed to counter basal levels of selected metals for analyses and to ensure that excess zinc was washed away after the desalting. Volumes of 0.50mL were collected as fractions, and a Bradford Assay was used to determine the protein concentration for each. The third fraction was found, in all cases, to contain a significant majority of the treated protein samples. Therefore, all the third fraction of all blanks and controls was selected for ICP-MS analysis for comparison purposes.

Using this third fraction, an aliquot of each YqjH sample was diluted with an identical volume of trace-metal grade HNO_3 (distilled on site at the Center for Elemental Mass Spectrometry (CEMS), University of South Carolina), giving a final ratio of 1:1 sample to acid and an initial dilution of 2x. Samples were digested at room temperature for 36hrs. After the digestion, each sample was diluted 1:10 into MQ H_2O (18MΩ), ensuring a final acid matrix of 3.5%. Blanks consisting of the buffer only diluted 40x with 3.5% trace-metal grade HNO_3 in MQ H_2O (18MW) were made and prepared in the same manner as the cell samples. Standard element solutions (Inorganic Ventures) were also prepared in the same final acid matrix of 3.5% to establish a limit of detection and a calibration curve for determining the concentrations of each metal analyzed. The isotopes of biologically relevant transition metals with masses of ^{56}Fe, ^{58}Ni, ^{64}Zn, ^{55}Mn, and ^{63}Cu were selected for analysis based on natural abundances. Samples were analyzed under medium resolution to resolve polyatomic interferences (e.g. $^{40}Ar^{16}O$ for ^{56}Fe) on a Thermo Element 2 High Resolution ICP-MS instrument operated by CEMS at the University of South Carolina. A cyclonic spray chamber (Elemental Scientific) was used for delivery of sample into the instrument. Molar amounts of each metal were calculated for each control and sample. After blank correction, the molar ratio of each metal to YqjH was calculated.

4.3 Results

The nickel-sensitive ΔyqjH mutant does not develop resistance to nickel toxicity. Previously, it was observed that wild type strains exposed to 50μM Ni(II) eventually adapted to the nickel stress, exited the lag phase of growth, and grew to

stationary phase (Fig. 2.6A). Simultaneously, these cells developed a permanent resistance to nickel toxicity (Fig. 2.12). Furthermore, this developed nickel resistance was also only observed in cells exposed 50μM Ni(II), where as wild type cells exposed to levels of nickel lower than 50μM did not develop any such permanent resistance and the lag phase duration was similar to wild type cells with no previous exposure.

Recent studies demonstrated that a MG1655 ΔyqjH mutant was hypersensitive to nickel when compared to the wild type strain.[25] The mutant was cultured as according to the growth scheme described in Chapter 2 (Fig. 2.4). The ΔyqjH::amp^R strain was selected due to this previously observed hypersensitivity to nickel and that the regulation YqjH is influenced by both nickel and iron. Cultures were exposed with either no nickel exposure or with 50μM Ni(II) exposure in gluconate M9 minimal media. Wild type MG1655 cultures, with or without 50μM Ni(II) were used as control growths for comparison purposes. The ΔyqjH::amp^R strain was observed to slightly more sensitive to 50μM Ni(II) under these growth conditions, as compared to the MG1655 wild type strain (Fig. 4.3). In controls without any nickel exposure, both strains grew equally well with no apparent differences, indicating that the deletion of the YqjH carried no effect on overall cellular growth. After culturing the ΔyqjH mutant in the gluconate M9 minimal stress media to stationary phase, with or without 50μM Ni(II) exposure, a sample of a nickel-exposed growth was plated on to fresh LB plates as described above. This new 50μM Ni-treated (50μM Ni-T) ΔyqjH mutant strain was then re-cultured to determine the presence of any resistance to nickel toxicity, as according to growth scheme described in Chapter 2 (Fig. 2.4). MG1655 wild type cells treated and collected in the same manner were cultured simultaneously for comparison purposes and as a control. As previously

observed, MG1655 wild type cells with prior exposure to 50μM N(II) (50μM Ni-T) were shown to be very resistant to nickel exposure (Fig. 4.4). In contrast, the 50μM Ni-treated ΔyqjH::amp^R strain was observed to not be resistant to 50μM Ni(II), and the growth mimicked the native ΔyqjH::amp^R strain growths exposed to 50μM N(II) initially (Fig. 4.3). These results indicate that the permanent resistance observed in the MG1655 wild type strains after an initial exposure to 50μM Ni(II) is possibly linked to the presence and function of YqjH. However, with the role of YqjH still unknown, it is hard to surmise the mechanism of the resistance development.

Zn(II) enhances YqjH reductase activity. A set of divalent metal cations was selected to determine any effect each ion would have on the ferric reductase activity of YqjH. The transition metals Mn(II), Ni(II), Cu(II), and Zn(II) were selected for study based on the Irving-Williams series and Mg(II) and Ca(II) were selected based on their importance in some biochemical reactions as stabilizing cations and previously observed enhancement on ferric siderophore reductase activities.[29,30] The presence of the Zn(II), Mn(II), and Cu(II) were observed to enhance the specific activity of YqjH (Fig. 4.5A, Table 4.2). Contrary to these effects, the cations Mg(II), Ca(II), and Ni(II) were observed to have little to no effect. The fold-change in specific activity was compared against a standard YqjH sample with no divalent cation added. Furthermore, the specific activities of YqjH in the presence of a specified cation were adjusted against a respective control made without the YqjH enzyme but with identical concentrations of the divalent cation. This also provided a method to ensure there wasn't any non-specific activity caused by the presence of the divalent metal. Most controls demonstrated that there was no significant level of non-specific activity; suggesting any enhancement of activity was due

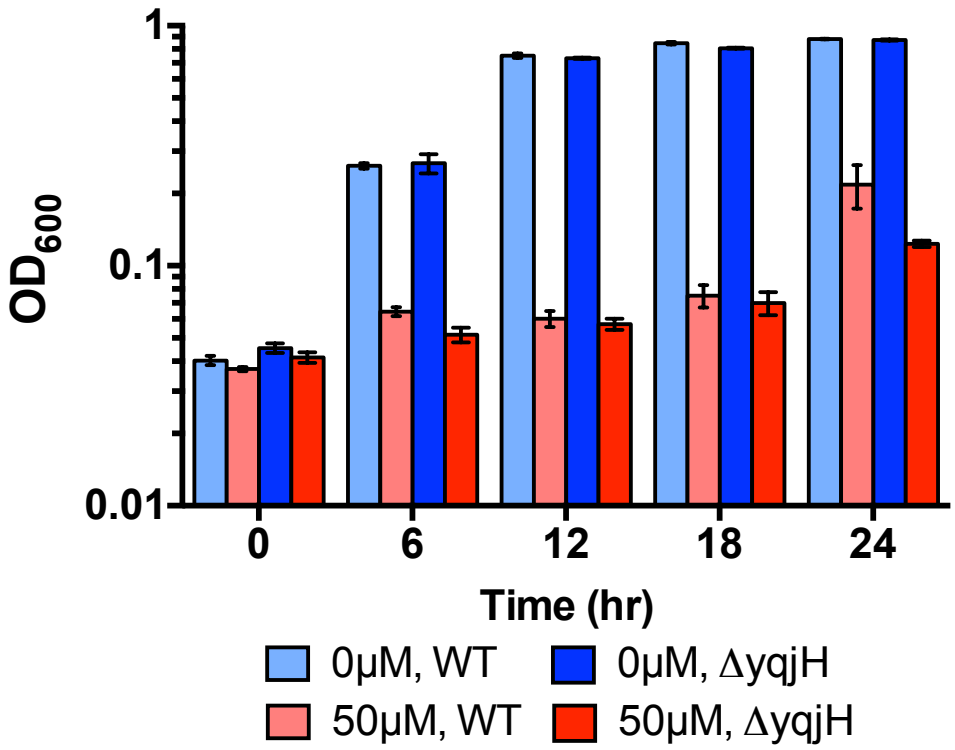

Figure 4.3. **The *yqjH* deletion mutant is only slightly more sensitive to nickel toxicity**. The Δ*yqjH::Amp*^{R} strain was cultured as according to the growth scheme in Figure 2.4. The *yqjH* deletion mutant was just slightly more sensitive than the wild type cultures. All assays were measured in triplicate (n = 3) with standard deviations reported.

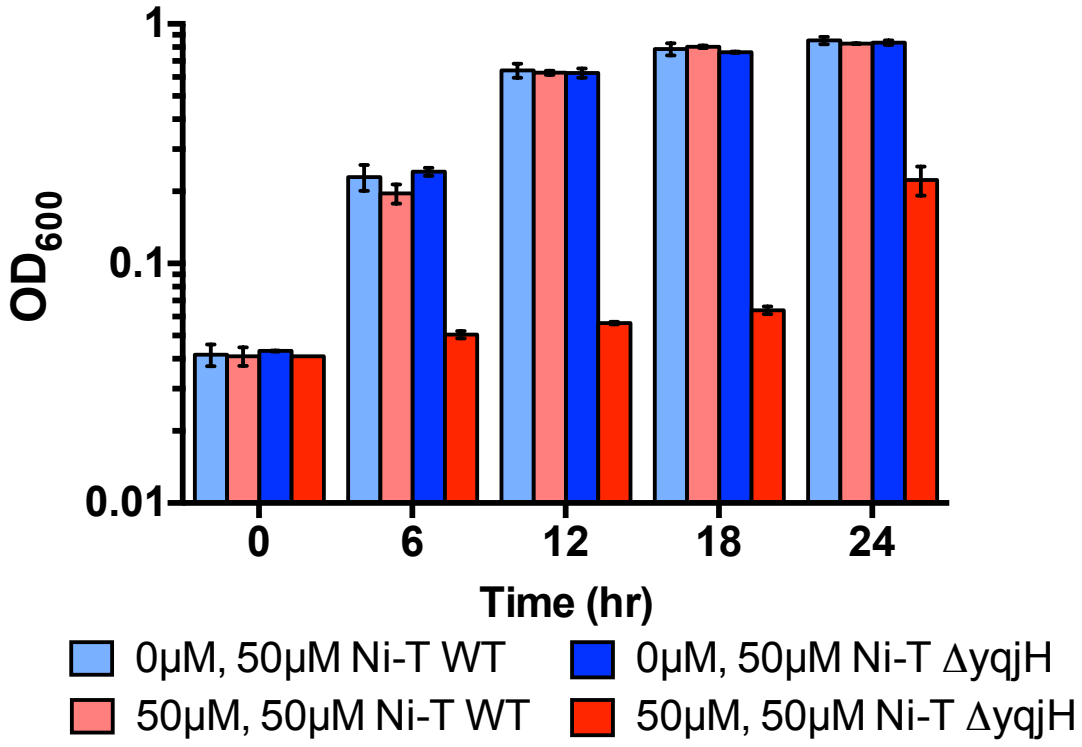

Figure 4.4. **The *yqjH* deletion mutant did not develop any resistance to nickel toxicity**. The nickel-sensitive Δ*yqjH::Amp*^{R} strain was cultured according the growth scheme in Figure 2.4. After the growths had sufficiently reached the stationary phase, cells samples were collected and passed several times on LB media. The resulting 50μM Ni-treated (50μM Ni-T) Δ*yqjH::Amp*^{R} strain was re-cultured according the growth scheme in Figure 2.4, without nickel (dark blue shading) or with 50μM Ni(II) (dark red shading). A 50μM Ni-treated (50μM Ni-T) Δ*yqjH::Amp*^{R} strain was cultured simultaneously as a control, without nickel (light blue shading) or with 50μM Ni(II) (light red shading). All assays were measured in triplicate (n = 3) with standard deviations reported.

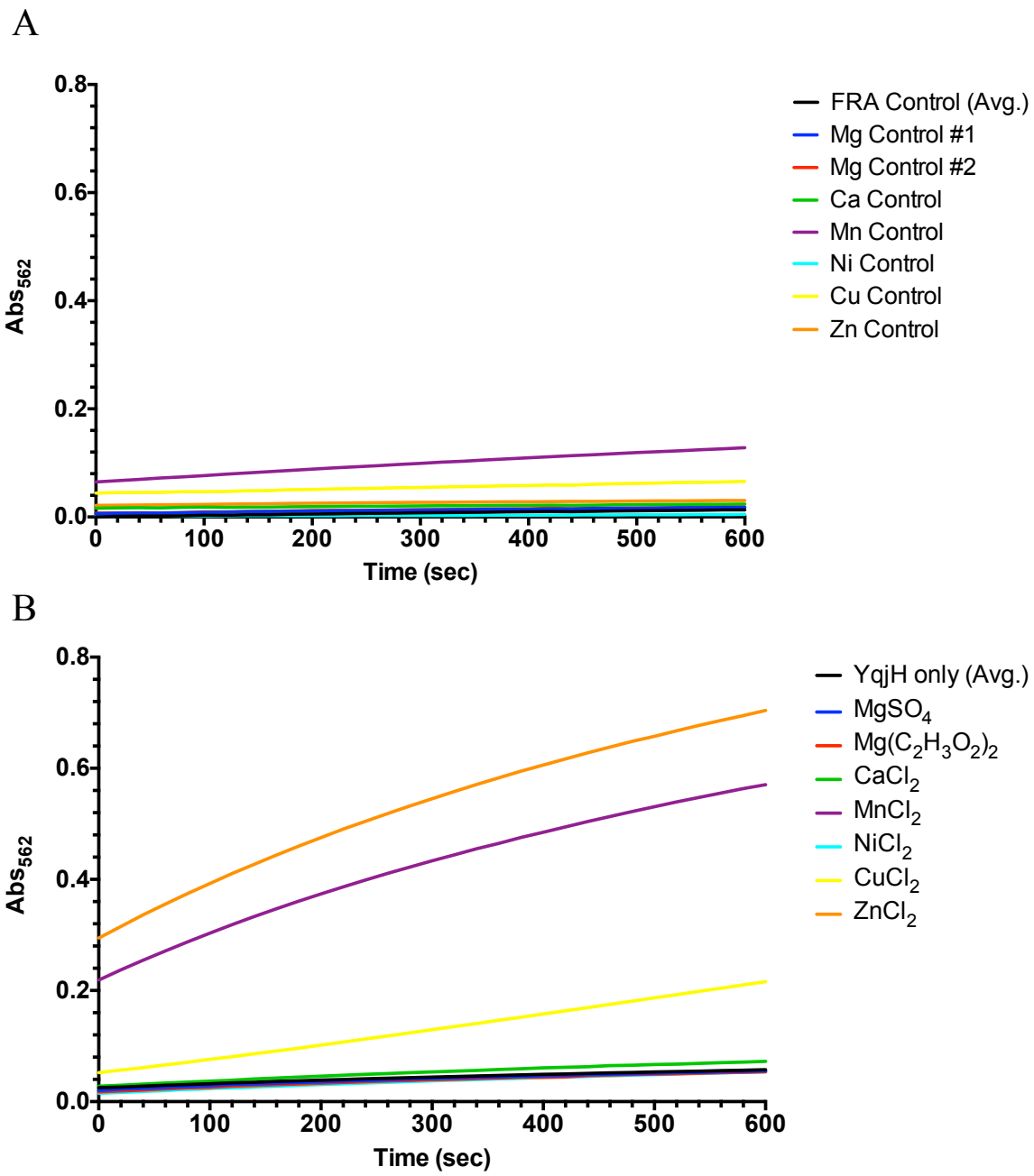

Figure 4.5. **The effect several divalent transition metal cations on the ferric reductase activity of YqjH**. (A) The specific activity of YqjH as a ferric reductase was measured in the presence of various divalent, transition metal cations. (B) Control assays, without YqjH enzyme, were analyzed with each divalent cation to determine the presence of any non-specific activity of the specified cation.

Table 4.2. The effect of select transition metals on YqjH ferric reductase activity

Atomic Number	Cation	Specific Activity - Fold Change -	EDTA Complex Log Stability, K_f	Radius (pm)		Reduction Half Reaction	Potential, $E°_{red}$ (V)
				Neutral	Cation		
12	Mg^{2+}	1.1 ($MgSO_4$) 1.1 ($MgAcetate_2$)	8.69	150	72	$Mg^{2+} + 2e^- \rightarrow Mg(s)$	- 2.372
20	Ca^{2+}	1.5	10.7	180	100	$Ca^{2+} + 2e^- \rightarrow Ca(s)$	- 2.868
25	Mn^{2+}	10.7	13.6	140	67	$Mn^{2+} + 2e^- \rightarrow Mg(s)$	- 1.185
26	Fe^{2+} **Fe^{3+}**	- **1.0**	14.3 **25.7**	140	61 **55**	$Fe^{2+} + 2e^- \rightarrow Fe(s)$ $Fe^{3+} + e^- \rightarrow Fe^{2+}$	- 0.447 + **0.771**
28	Ni^{2+}	1.1	18.6	135	69	$Ni^{2+} + 2e^- \rightarrow Ni(s)$	- 0.257
29	Cu^{2+}	3.9	18.8	135	73	$Cu^{2+} + 2e^- \rightarrow Cu(s)$ $Cu^{2+} + e^- \rightarrow Cu^+$	+ 0.342 + 0.153
30	Zn^{2+}	15.3 ($ZnSO_4$) 12.4 ($ZnCl_2$)	16.5	135	74	$Zn^{2+} + 2e^- \rightarrow Zn(s)$	- 0.762

to the presence of the cation interacting with YqjH (Fig. 4.5B). However, the control assays involving the Mn(II) and Cu(II) ions did indicate some non-specific activity (Fig. 4.5B). All specific activity data was further summarized alongside the parameters and reduction potentials of each divalent cation for comparison purposes (Table 4.2).

Despite the observed enhancement of some of the selected divalent transition metal cations, it also had to be ensured that the selected cation played no role by interfering with the binding of the Fe(II) ion binding to the Ferrozine ligands, since the controls with the Mn(II) and Cu(II) ions did indicate some non-specific activity (Fig. 4.5A). Any decrease on the formation rate for the $[Fe(Fz)_3]^{4-}$ complex (via monitoring changes in absorbance at 562nm) was determined by mixing a select cation with ferrozine prior to the addition any Fe(II), mimicking the ferric reductase assay conditions. These values were compared to the formation rate of the $[Fe(Fz)_3]^{4-}$ complex in a control reaction without any interfering cations. Overall, only the Cu(II) and Ni(II) ions showed extreme amounts of interference towards the rate of formation of the $[Fe(Fz)_3]^{4-}$ complex (Fig. 4.6A). Finally, the total concentration of $[Fe(Fz)_3]^{4-}$ complex formed after 2min was compared to the control mixture, based off the absorptivity coefficient of $27.9 mM^{-1}cm^{-1}$ for the $[Fe(Fz)_3]^{4-}$ complex at 562nm and a maximum theoretical concentration of 20μM for the $[Fe(Fz)_3]^{4-}$ complex (Fig. 4.6B). Curiously, the Mn^{2+} cation, which showed a degree of non-specific activity, did not interfere with the binding of Fe(II) to ferrozine (Fig. 4.6A,B). One further step was taken to ensure the counter ion of the metal salt played no role in interference of ferrous iron binding to ferrozine. Various nickel and zinc salts were selected and the choice of counter ion did not show any effect on the interference (or lack thereof) of the metal cation (Fig. 4.6C). Overall, the Zn(II) cation,

A

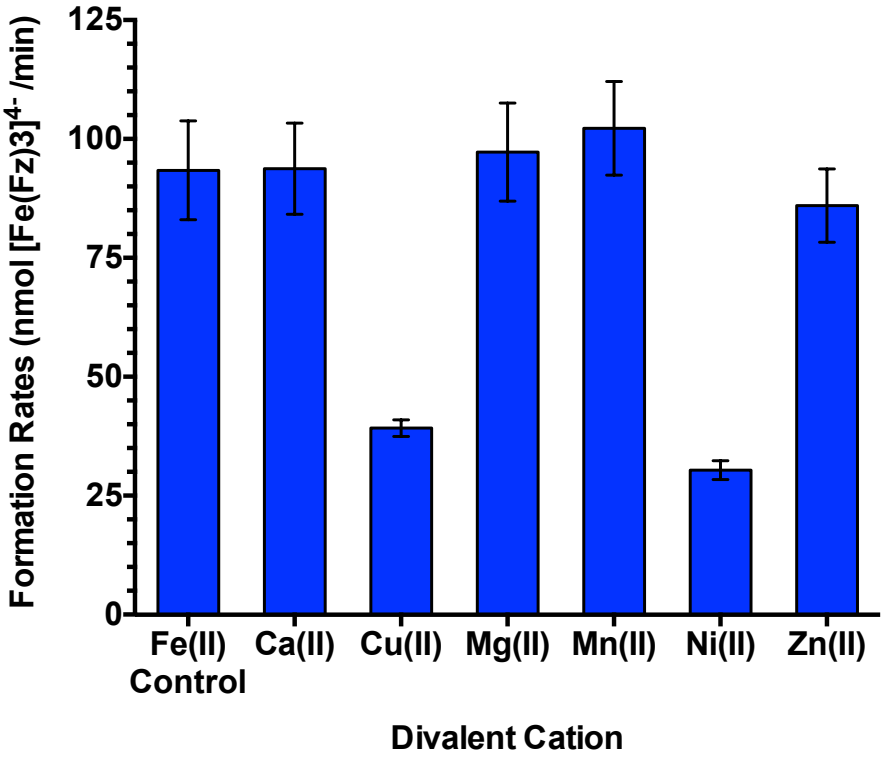

B

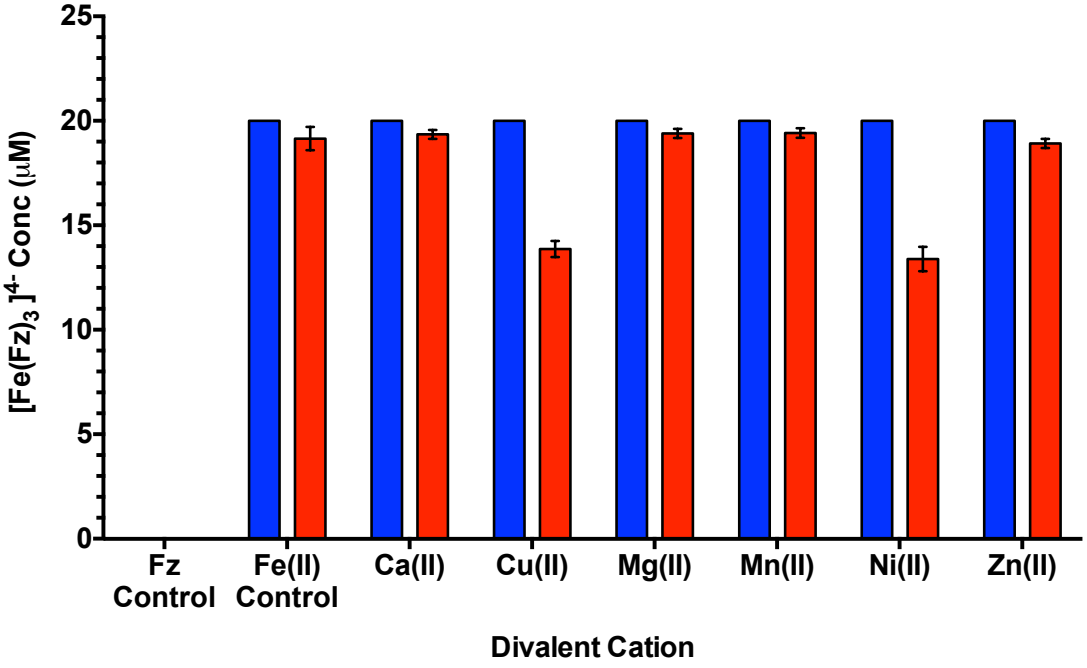

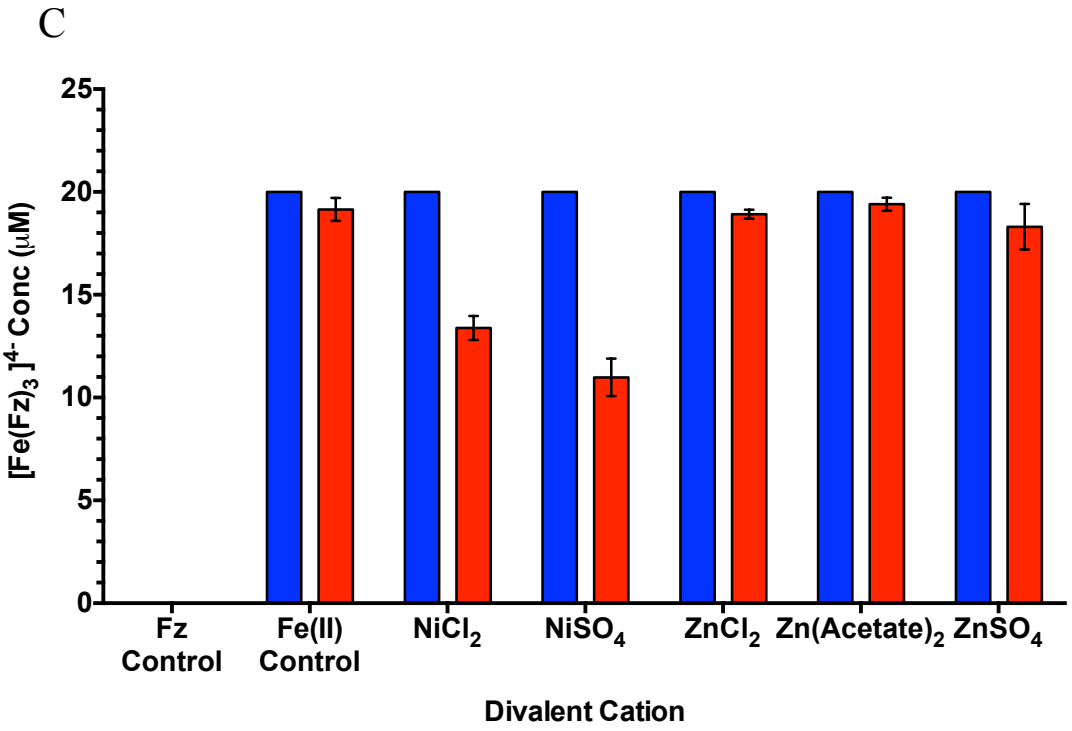

Figure 4.6. **Cu(II) and Ni(II) inhibited the formation of the $[Fe(Fz)_3]^{4-}$ complex, but Zn(II) does not**. The ferrozine chelator was incubated with a specific cation for 1min, before the addition of Fe(II) to a final concentration of 20μM. The change in absorbance at 562nm was measured by UV-Vis spectroscopy. (A) The formation of the $[Fe(Fz)_3]^{4-}$ complex was determined in the presence of various divalent, transition metal cations. (B) The total concentration of the $[Fe(Fz)_3]^{4-}$ complex was calculated after 2min of incubation with Fe(II) in the presence of various chloride salts. (C) The total concentration of the $[Fe(Fz)_3]^{4-}$ complex was calculated after 2min of incubation with Fe(II) in the presence of various Ni(II) and Zn(II) salts in order to determine any effect the counter ion had on ferrous ion binding of ferrozine. All assays were measured in triplicate (n = 3) with standard deviations reported.

which enhanced the ferric reductase activity of YqjH the greatest, showed no interference with ferrozine. This suggests that Zn(II) cation is possibly interacting with YqjH via an unknown mechanism to create the enhancement effect on reductase activity.

The presence of Zn(II) slows the reduction of the YqjH oxidized state to the semiquinone state. The lower redox potential of the first oxidation step (E_1), forming the semiquinone state, is more favorable as compared to the redox potential of the second oxidation step (E_2), which reforms the fully oxidized FAD cofactor (Fig 4.2). While the E_1 step has been proposed to feasibly overlap with the redox potential range for ferric enterobactin, this second final E_2 step is clearly not sufficiently low enough to be able to reduce another intact ferric enterobactin compound.[24] The observed enhancement of YqjH ferric reductase activity in the presence of Zn(II) ion presented an intriguing possibility. In theory, the zinc cation may then decrease the redox potential of the YqjH-FAD_{ox}/FAD_{sq} redox couple (bringing it closer to the redox potential of the E_1 step) and, therefore, increases YqjH's capability to pass an electron to a ferric ion center and enhances the activity of YqjH.

This warranted an analysis of the YqjH semiquinone state in the presence of zinc. A 40μM concentration of the YqjH enzyme was reduced with 4mM dithionite only as a control, and the formation of the semiquinone state was monitored via UV-Vis spectroscopy over time (Fig 4.7A). Maxima corresponding to semiquinone state were observed at 515 and 590nm; this broad absorbance band corresponds to a neutral FAD semiquinone species (Fig 4.8).[28] Additionally, the disappearance of the oxidized FAD cofactor was monitored at 450nm. The same assay was performed in the performed in the presence of 400μM $ZnSO_4$, with identical concentrations of YqjH and dithionite

A

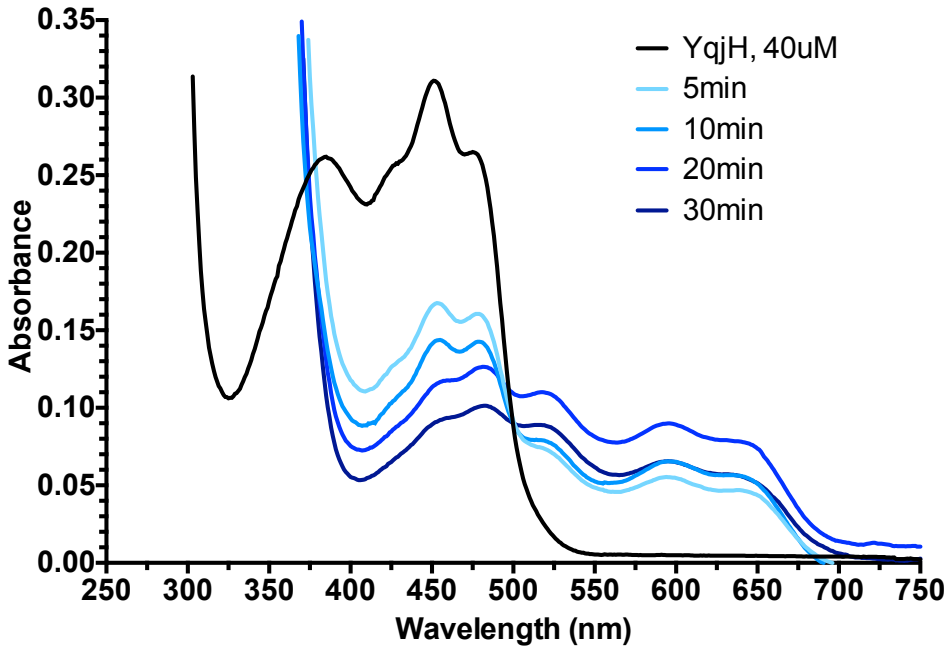

B

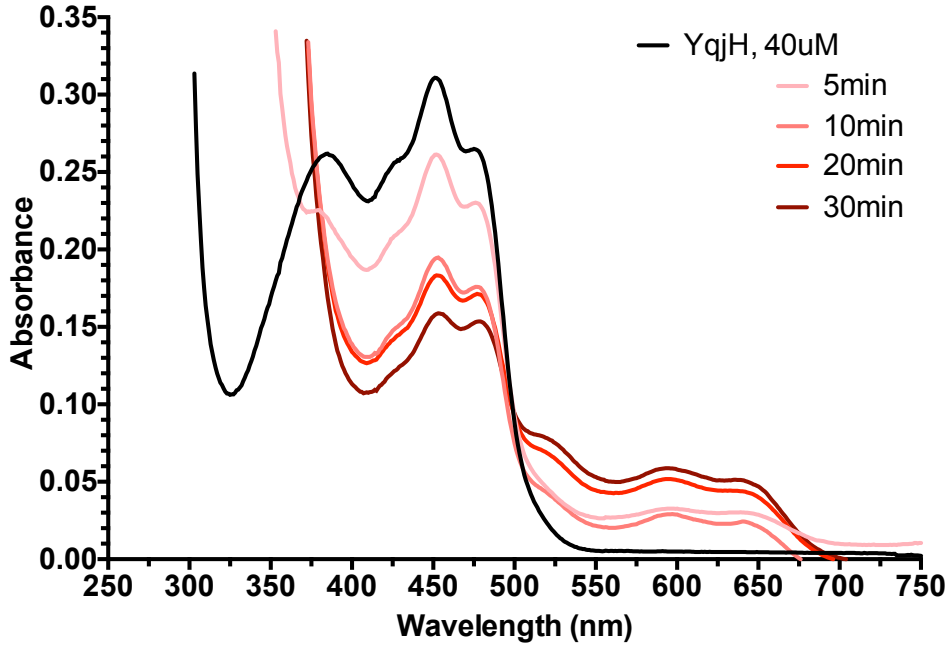

C

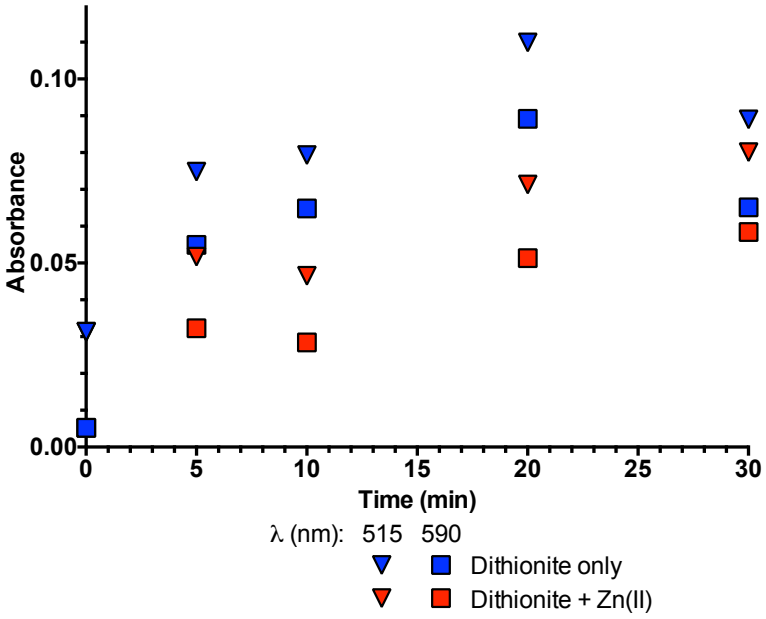

D

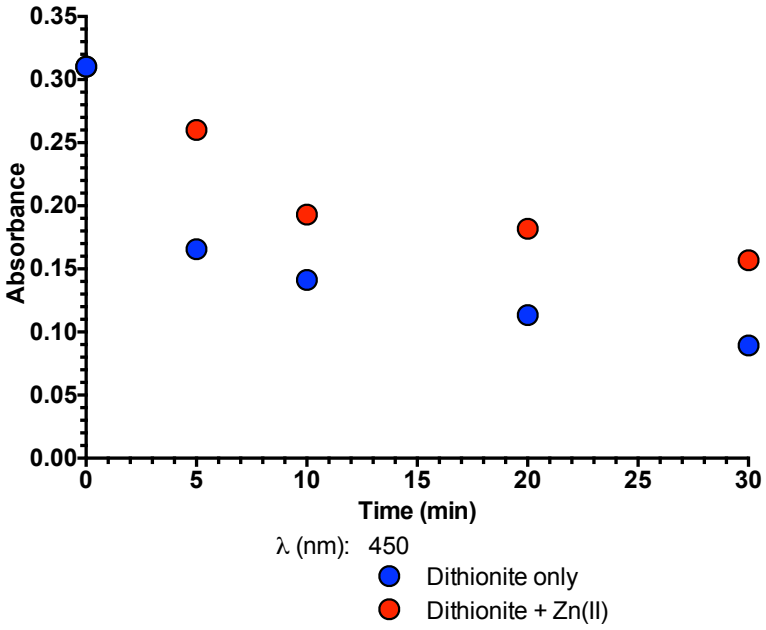

Figure 4.7. **Zn(II) ion slowed the formation of the YqjH-FAD$_{sq}$ state**. YqjH, 40µM, was incubated in the presence of 4mM dithionite, with (B, red traces) or without (A, blue traces) 400µM Zn(II). The black trace represents the fully oxidized protein, prior to the addition of any dithionite. Absorbance was measured from 200nm to 800nm over time by UV-Vis spectroscopy. (C) Absorbances at 515nm and 590nm, corresponding to the neutral semiquinone species, were monitored over time. (D) Absorbance at 450nm, corresponding to the oxidized peak of the FAD cofactor of YqjH, was monitored over time.

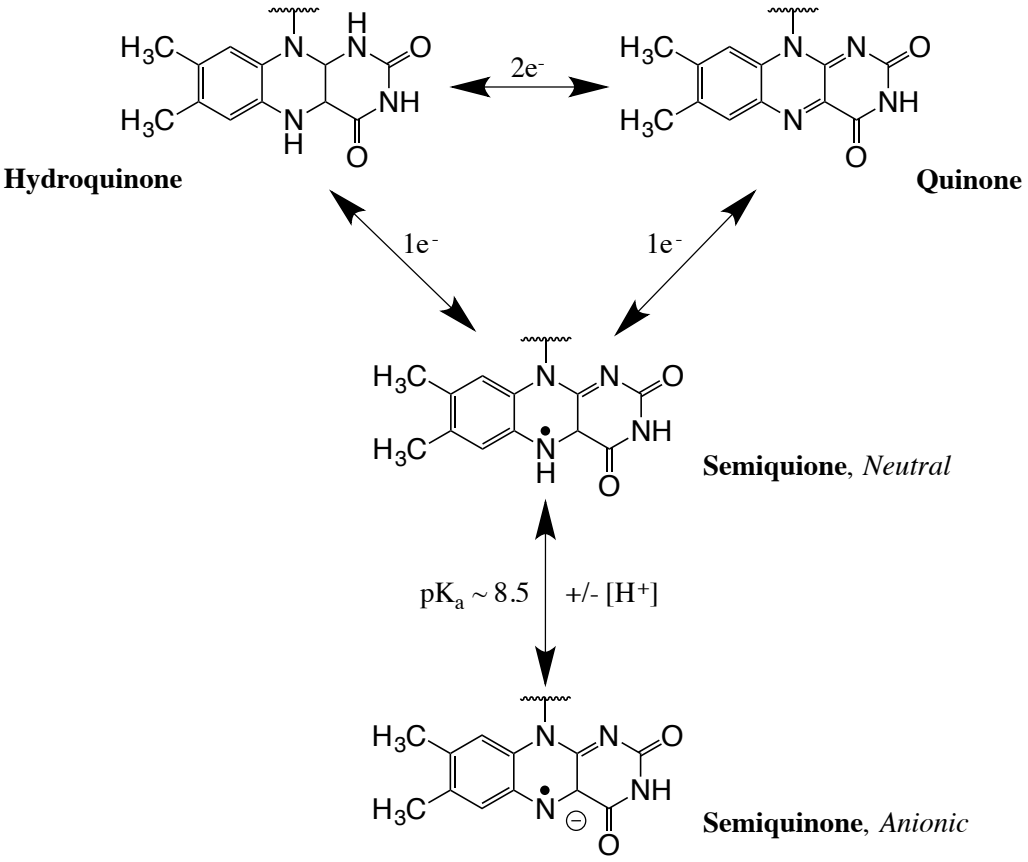

Figure 4.8. **The various redox states of a flavin compound**. Flavin cofactors can be used in either a 1- or 2-electron reaction, or a combination thereof. The flavin can exist in one of three redox states: oxidized (quinone), reduced (hydroquinone), or semiquinone. The charge of the semiquinone is largely dependent on pH and the protein environment.

reported above (Fig 4.7B). The control mixture of YqjH and dithionite only was observed to form more of the neutral semiquinone species, as compared to the sample mixture of YqjH with dithionite and zinc ion, over the same period of time. Subsequently, after 20min of incubation, the amount of neutral semiquinone in the control mixture with no zinc began to decline (Fig 4.7C). This suggests that excess dithionite had begun to further reduce the enzyme down to the hydroquinone state. The continued disappearance of the absorbance at 450nm further confirms this (Fig 4.7D). Conversely, the amount of neutral semiquinone in the zinc sample was still increasing and was even still lower in overall concentration compared to the control sample after at 30min. Overall, this indicates that presence of the zinc cation slowed the formation of the semiquinone state, possibly by altering the redox potential of the YqjH-FAD_{ox}/FAD_{sq} couple.

The formation and characteristics of the semiquinone state of YqjH in the presence of zinc were further analyzed by EPR for any change or difference as compared to previously published results.[24] The semiquinone state of a protein-associated flavin cofactor is a free radical species, with an average g-value of approximately 2.004 for the neutral semiquinone species and 2.003 for the anionic semiquinone species.[28] All mixtures were developed under anaerobic conditions and in the same buffer as the UV-Vis samples. A control mixture was prepared containing 100μM YqjH and 10mM dithionite only. A sample mixture was prepared with identical concentrations of YqjH and dithionite but included 1mM zinc sulfate. Each mixture was incubated for 20min, given that a maximum amount of semiquinone was formed by this time as observed by UV-Vis spectroscopy (Fig. 4.9). The control and sample mixtures were further compared

to a native, oxidized mixture of 100μM YqjH in buffer only. Both the control and sample mixtures of YqjH and dithionite, with or without zinc, developed the purported semiquinone state (Fig. 4.9). The total intensity of the semiquinone species was higher in the dithionite only control, indicating a higher amount of semiquinone formed compared to the sample incubated with zinc. This supports the earlier UV-Vis spectroscopy data, which also showed a higher amount of formed semiquinone in the dithionite only control. The dithionite only control and zinc sample were observed to have g-values of 2.00495 and 2.00503, respectively, at a field of 3342G (Fig. 4.9). The oxidized sample of YqjH showed no developed semiquinone. The line-width of each semiquinone species in the control and sample mixtures was 23G (2.3mT). These g-values and line-widths fall in line with previously reported values for YqjH.[24] Taken together, these characteristics support the presence of a neutral semiquinone state for YqjH.

The titration of YqjH with zinc does not alter the secondary structure of YqjH. The next step was to try and characterize how the zinc cation interacts with YqjH. Zinc was titrated into a mixture of 40μM YqjH up to several molar equivalents and monitored by CD spectroscopy (Fig. 4.10). The control mixture, with no zinc, was observed to represent anti-parallel b-sheets, in accordance with previously published data.[24,28] No changes in secondary structure in the far UV regions, between 190nm to 250nm, were observed up to 5 molar equivalents of zinc ion to YqjH protein. While still inconclusive, this does not necessarily mean the zinc ion doesn't cause an alteration to the protein secondary structure and further analysis is still required.

YqjH binds Zn(II) in the YqjH-FAD$_{ox}$ and YqjH-FAD$_{sq}$ states *in vitro*. If zinc is interacting with the YqjH in some manner, it was important to determine if the

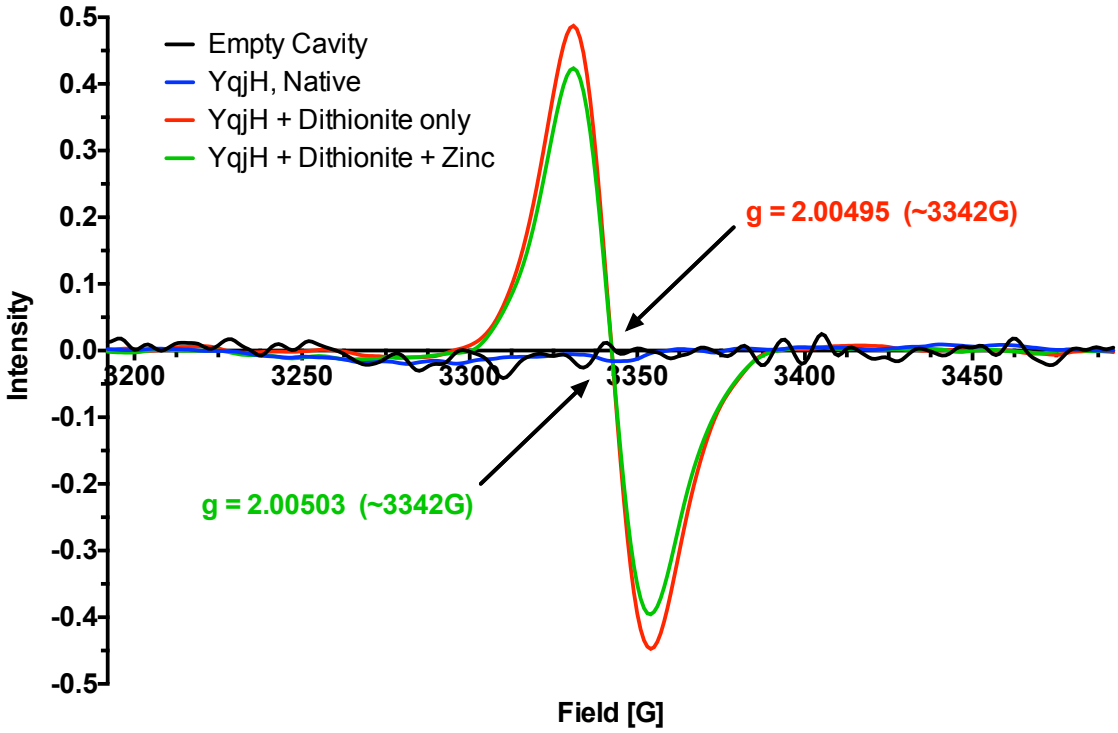

Figure 4.9. **EPR analysis of the YqjH-FAD$_{sq}$ state in the presence of zinc**. Samples were made in similar fashion with those analyzed by UV-Vis spectroscopy. EPR samples were made after 20min incubation with 10mM dithionite, with (green trace) or without (red trace) 1mM Zn(II). The blue trace represents an untreated, fully oxidized sample of YqjH. The black trace represents the empty cavity scan. All scans were measure at a temperature of 4-6K, a Gain of 30dB, an modulation amplitude of 10.0G, and attenuation of 25dB (0.6mW).

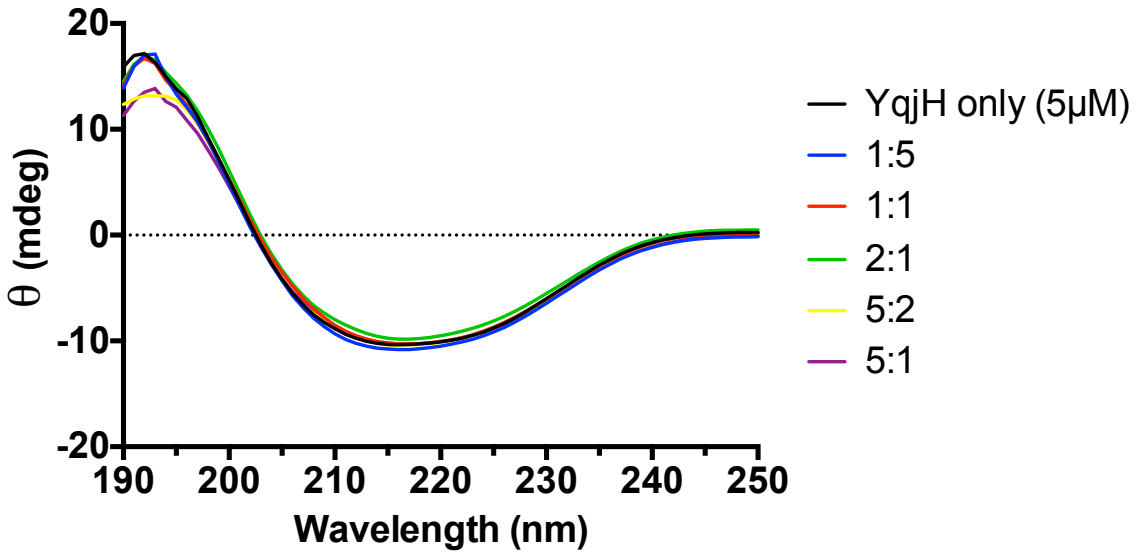

Figure 4.10. **The presence of zinc caused no change in the secondary structure of YqjH**. Zn(II) was titrated into a mixture of 5μM YqjH-FAD_{ox} up to 5 molar equivalents. Scans were performed under anaerobic conditions.

interaction was transient or more permanent. Freshly purified aliquots of 25µM YqjH enzyme were incubated with or without 2.5mM dithionite and with or without 250µM $ZnSO_4$ for 10min, then the enzyme was ran through a HiTrap desalting column (GE Health Care Life Sciences) to remove any free zinc ion and to eliminate any unreacted dithionite so as to prevent further reduction of the protein. Selected fractions were concentrated and digested for ICP-MS analysis. The obtained results show, surprisingly, that YqjH binds zinc in both the oxidized and semiquinone state (Fig. 4.11A). Other metals analyzed by ICP-MS included Fe, Ni, Mn, and Cu. The YqjH enzyme (no dithionite, no zinc) does not appear to bind any of these with any real affinity as purified (Fig. 4.11B). Additionally, it is important to note that the enzyme was also not incubated with excess levels of these ions so binding may still occur with YqjH in either redox state.

4.4 Discussion

YqjH plays a key role in the development of nickel resistance in *E. coli*. The mechanism through which nickel toxicity resistance had developed in the MG1655 wild type strain remains ambiguous. Therefore, the further study of selected mutant strains with known tie-ins to nickel homeostasis or that were observed to be more nickel sensitive could be used to elucidate the systems involved with the resistance mechanism. The MG1655 Δ*yqjH* mutant strain was determined to be nickel-sensitive, with the transcriptional regulation of the gene falling under the ferric uptake regulator, Fur,

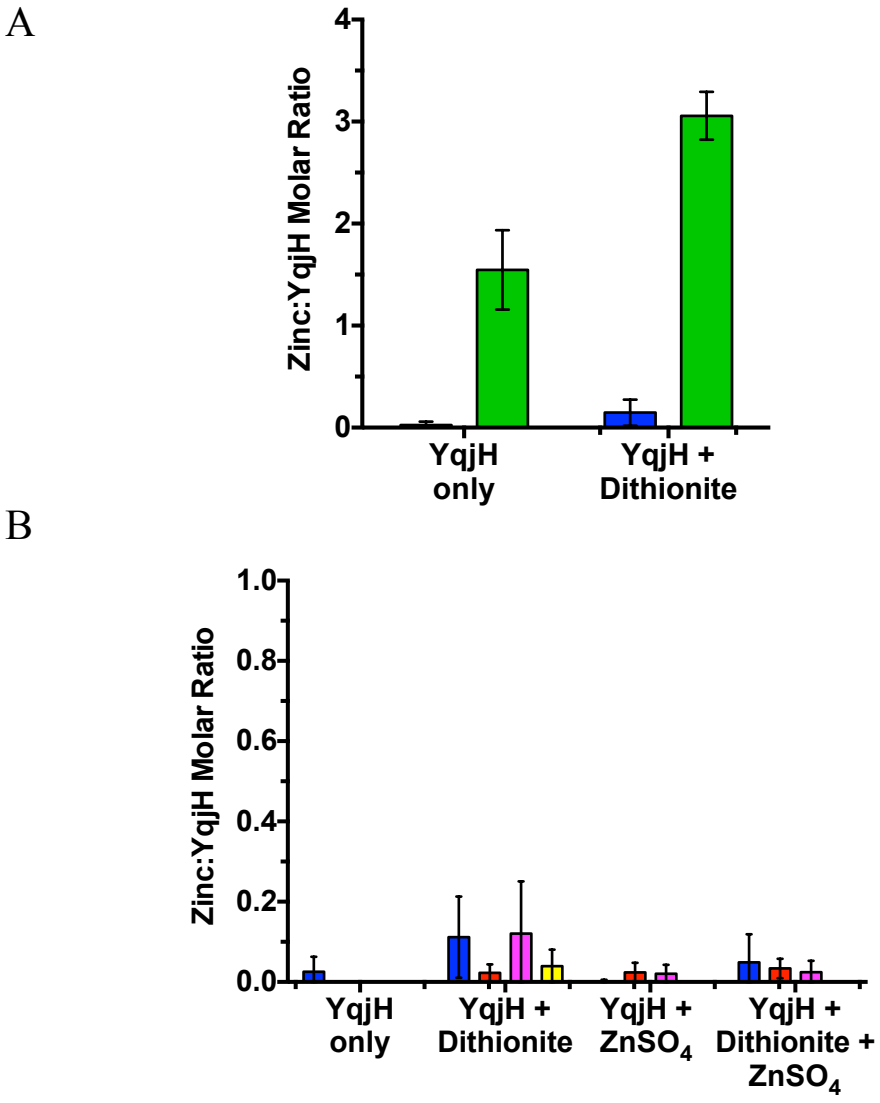

Figure 4.11. **YqjH in the oxidized and semiquinone states bind Zn(II)**. (A) 25μM YqjH was incubated with or without 2.5mM dithionite and with (green) or without (blue) 250μM Zn(II) for 10min. The samples were desalted to remove excess, unbound Zn(II) and to remove any dithionite to stop reduction. Fractions with the highest concentration of YqjH, as analyzed a Bradford Assay, were digest in 50% trace-metal grade nitric acid for 36hrs at room temperature, then analyzed for their metal content by ICP-MS. (B) The same samples were further analyzed for other biologically-relevant transition metals; iron (blue) nickel (red), manganese (magenta), and copper (yellow). Error bars represent the standard deviation between concentrated and nonconcentrated fractions

involved in iron homeostasis.[25] Additionally, transcription of *yqjH* is controlled by nickel homeostasis though regulation by the YqjI protein.[25] This dual regulation serves to suggest that iron and nickel homeostasis in *E. coli* is intertwined. Data reported in Chapters 2 and 3 supports this notion, demonstrating that nickel toxicity disrupts iron homeostasis during the lag phase of growth. Despite this understanding, the role of the YqjH enzyme, particularly in iron homeostasis, remains unknown. However, the development of resistance to nickel toxicity has now been linked to the presence of YqjH during toxicity (Fig. 4.3 and Fig. 4.4).

The zinc cation enhances YqjH reductase activity by possibly altering the redox potential of the YqjH-FAD$_{sq}$ intermediate. The enhancement of reductase activity by a divalent, cationic species is not without precedent. The siderophore reductase activity in *A. vinelandii* was shown observed to be enhanced by the presence of the Mg(II) cation.[30] Conversely, the presence of zinc, both during growth and *in vitro* assays, inhibited the ferric reductase activity with evidence of zinc acting as a mixed-type inhibitor.[30] The reductase activity of another recently reviewed ferric siderophore reductase, FscN, from *T. fusca*, which selectively reduces ferric ion chelated by the siderophore fuscachelin.[31] The FscN enzyme was also shown to bind a Zn(II) ion near the location of the flavin cofactor, but no reports concerning the effect of the zinc cation on the reductase activity of FscN were reported.[31] However, conjectures are made suggesting that the zinc ion may play a structural role. In the case of YqjH, this may too be a possibility. Finally, *E. coli* also encodes the gene *fhuF*, producing the hydroxamate siderophore iron reductase FhuF. This enzyme has been demonstrated to remove ferric ion from hydroxamate-type siderophores through a direct electrochemical reduction *in*

vitro.[8] However, there are no reports to suggest any enhancement of the reductase activity with the presence of a divalent metal cation.

The ferric reductase activity of YqjH was enhanced when the assay was performed in the presence of the zinc cation (Fig. 4.5A). Moreover, the presence of zinc ion was shown to act without any non-specific activity, nor was it observed to interfere with the binding of ferrous ion to the ferrozine chelator. The overall nature of this enhancement effect remains unclear, but the evidence presented here suggests that the relevant mechanism may involve an alteration in the redox potential of the YqjH-FAD_{sq} state. Several other cations, such as Cu(II), were shown to also enhance activity, but the cation's interference of the binding of Fe(II) to ferrozine was a cause for concern. Curiously, the presence of Mg(II) showed no significant enhancement of YqjH reductase activity. Finally, the presence of Ni(II), which positively controls YqjH transcription, had neither an enhancing nor inhibitive effect on YqjH activity. Whether or not this plays a role in the function of YqjH (e.g. during time of nickel stress) has yet to be determined.

A number of ferric compounds have been introduced as potential substrates for YqjH.[24,25] In some cases, a ferric siderophore reductase is specific to a single siderophore compound (e.g. FscN from *T. fusca*), in contrast to enzymes that show activity with a variety of ferric substrates (e.g. FhuF from *E. coli*). The siderophore enterobactin remains as the leading contender as the natural *in vivo* ferric ion substrate for YqjH, yet a number of obstacles have yet to be fully overcome. Most notably is the extremely low redox potential (as low as -750mV for the free, non-protein associated complexes) of the intact (cyclic) ferric enterobactin complex.[24] The complexation effect on redox potential

suggests that because enterobactin is one of the tightly-binding, stable ferric complexes, the standard reduction potential of the ferric ion is drastically lowered.[32] While the redox potential of flavoproteins varies widely (the redox potential of YqjH has been reported as -431mV), most fall within the range of -500mV to 80mV.[33] Therefore, flavoproteins such as YqjH, are often well outside the range for electrochemical reduction of the ferric center in enterobactin.

Given the extremely low redox potential of the intact ferric enterobactin complex, it seems that an additional mechanism may be involved that would increase the redox potential of the ferric enterobactin complex to bring it within range of the redox potential of YqjH in its fully reduced, hydroquinone state. The enzyme Fes, an esterase, is responsible for the hydrolyzation of cyclic enterobactin is suggested as one method for aiding in the extraction of ferric ion from the enterobactin complex.[34,35] Hydrolyzation of the tri-lactone, ester backbone of the enterobactin complex results in a variety of triscatecholate species that still chelate ferric ion (albeit less tightly), and have much higher redox potentials (that place them within range of the capabilities of the YqjH protein for reduction of the ferric center), and has already been demonstrated with YqjH.[24] Reductase activity with intact ferric enterobactin is practically nonexistent; whereas the hydrolyzed complex showed the greatest activity.[24,25]

The observed enhancement effect of Zn(II) on YqjH reductase activity has laid the groundwork for further study of this incidence. Further experimentation into the various redox states and potentials of the FAD cofactor are required, all the while in the presence of zinc. The mechanism of Zn(II) interaction would help to elucidate the possible role and function of YqjH in *E. coli* as well. Finally, the indication that YqjH

plays a role in the development of nickel toxicity resistance in *E. coli* suggests one possible role of this enzyme and ties nickel toxicity to iron homeostasis.

4.5 References

1. Andrews, S. C., Robinson, A. K., Rodriguez-Quinones, F. (2003) Bacterial Iron Homeostasis. *FEMS Microbiol Rev 27*, 215-237.
2. Nielands, J. B. (1981) Siderophores: Structure and Function of Microbial Iron Transport Compounds. *J Biol Chem* 270, 26723-26726.
3. Raymond, K. N., Dertz, E. A., and Kim, S. S. (2003) Enterobactin: An archetype for microbial iron transport. *Proc Natl Acad Sci* 100, 3584-3588.
4. Winkelmann, G. (2002) Microbial siderophore-mediated transport. *Biochem Soc Trans* 30, 691-696.
5. Snow G. A. (1965) Isolation and Structure of Mycobactin T, a Growth Factor from *Mycobacterium tuberculosis*. *J Biochem.* 97, 166-175.
6. Luo, M., Fadeev, E. A., and Groves, J. T. (2005) Mycobactin-mediated iron acquisition within macrophages. *Nat Chem Biol* 1, 149-153.
7. Butterton, J. R., and Calderwood, S. B. (1994) Identification, Cloning, and Sequencing of a Gene Required for Ferric Vibriobactin Utilization by *Vibrio cholerae*. *J. Bacteriol* 176, 5631-5638.
8. Matzanke, B. F., Anemüller, S., Schünemann, V., Trautwein, A. X., and Hantke, K. (2004) FhuF, part of a siderophore-reductase system. *Biochem* 43, 1386-1392.
9. Bickel, H., Hall, G., Keller-Schierlein, W., Prelog, V., Vischer, E., and Wettstein, A. (1960) Stoffwechselprodukte von Actinomyceten. 27. Mitteilung. Über die Konstitution von Ferrioxamin B. *Helv Chim Acta* 43, 2129-2138.
10. Cooper, S. R., McArdle, J. V., and Raymond, K. N. (1978) Siderophore electrochemistry: relation to intracellular iron release mechanism. *Proc Natl Acad Sci USA* 75, 3551-3554.
11. Wawrousek, E. F. and McArdle, J. V. (1982) Spectrochemistry of ferrioxamine B, ferrichrome, and ferrichrome A. *J Inorg Biochem* 17, 169-183.

12. Wong, G. B., Kappel, M. J., Raymond, K. N., Matzanke, B., and Winkelmann, G. (1983) Coordination chemistry of microbial iron transport compounds. 24. Characterization of coprogen and ferricrocin, two ferric hydroxamate siderophores. *J Am Chem Soc* 105, 810.

13. Patzer, S. I. and Hantke, K. (1999) SufS is a NifS-like Protein, and SufD is Necessary for Stability of the [2Fe-2S] FhuF Protein in *Escherichia coli*. *J Bacteriol* 181, 3307-3309.

14. Ayala-Castro, C., Saini, A., and Outten, F. W. (2008) Fe-S cluster assembly pathways in bacteria. *Microbiol Mol Biol Rev* 72, 110-125.

15. Lin, H., Fischbach, M. A., Liu, D. R., and Walsh, C. T. (2005) *In vitro* Characterization of Salmochelin and Enterobactin Trilactone Hydrolases IroD, IroE, and Fes. *J Am Chem Soc* 127, 11075-11084.

16. Ozenberger, B. A., Nahlik, N. S., and McIntosh, M. A. (1987) Genetic Organization of Mutiple *fep* Genes Encoding Ferric Enterobactin Transport Functions in *Escherichia coli*. *J Bacteriol* 169, 3638-3646.

17. Furrer, J. L., Sanders, D. N., Hook-Barnard, I. G., and McIntosh, M. A. (2002) Export of the siderophore enterobactin in *Escherichia coli*: involvement of a 43 kDa membrane exporter. *Mol Micriobiol* 44, 1225-1234.

18. Hunt, M. D., Pettis, G. S., and McIntosh, M. A. (1994) Promoter and operator determinants for fur-mediated iron regulation in the bidirectional fepA-fes control region of the *Escherichia coli* enterobactin gene system. *J Bacteriol* 176, 3944-3955.

19. Escolar, L., Pérez-Martin, J., and de Lorenzo, V. (1998) Binding of the Fur (ferric uptake regulator) repressor of *Escherichia coli* to arrays of the GATAAT sequence. *J Mol Biol* 283:537-547

20. Christoffersen, C. A., Brickman, T. J., Hook-Barnard, I., McIntosh, M. A. (2001) Regulatory architecture of the iron-regulated fepD-ybdA bidirectional promoter region in *Escherichia coli*. *J Bacteriol* 183, 2059-2070.

21. Lavrrar, J. L., Christoffersen, C. A., and McIntosh, M. A. (2002) Fur-DNA interactions at the bidirectional fepDGC-entS promoter region in *Escherichia coli*. *J Mol Biol* 322, 983-995.

22. Chen, Z., Lewis, K. A., Shultzaberger, R. K., Lyakhov, I. G., Zheng, M., Doan, B., Storz, G. and Schneider, T. D. (2007) Discovery of Fur binding sties clusters in *Escherichia coli* by information theory models. *Nucleic Acids Res* 35, 6762-6777.

23. Harris, W. R., Carrano, C. J., Cooper, S. R., Sofen, S. R., Avdeef, A. E., McArdle J. V., and Raymond, K. N. (1979) Coordination chemistry of microbial iron transport compounds. 19. Stability constants and electrochemical behavior of ferric enterobactin and model complexes. *J Am Chem Soc* 101, 6097-6104.

24. Miethke, M., Hou, J. Marahiel, M. A. (2011) The Siderophore-Interacting Protein YqjH Acts as a Ferric Reductase in Different Iron Assimilation Pathways of *Escherichia coli*. *Biochem* 50, 10591-10964.

25. Wang, S., Wu, Y. and Outten, F. W. (2011) Fur the the novel regulator YqjI control transcription of the ferric reductase gene *yqjH* in *Escherichia coli*. *J Bacteriol* 193, 563-574.

26. Carrillo, N. and Ceccarelli E. A. (2003) Open questions in ferredoxing-NADP+ reductase catalytic mechanism. *Eur J Biochem* 270, 1900-1915.

27. Stookey, L. L. (1970) Ferrozine – A new Spectrophotometric Reagent for Iron. *Anal Chem* 42, 779-781.

28. Chapman, S., & Reid, G. (1999). *Flavoprotein Protocols*. Totowa, NJ: Humana Press.

29. Irving, H. and Williams, R. J. P. (1984) Order of stability of metal complexes. *Nature 162*, 746-747.

30. Huyer, M. and Page, W. J. (1989) Ferric Reductase Activity in *Azobacter vinelandii* and its inhibition by Zn2+. *J Bacteriol* 171, 4031-4037.

31. Li, K., Chen, W., and Bruner, S. (2015) Structure and mechanism of the Siderophore Interacting Protein from the fuscachelin gene cluster of *Thermobifida fu*sca. *Biochem* 54, 3989-4000.

32. Rizvi, M. A. (2015) Complexation Modulated Redox Behavior of Transition Metal Systems (Review). *J Gen Chem* 85, 959-973.

33. Stankovich,M.T. (1991) Redox properties of flavins and flavoproteins ,in *Chemistry and Biochemistry of Flavoenzymes* (Müller, F., ed.), vol 1, CRC Press, Inc., Boca Raton, FL, pp. 401–425.

34. Langman, L., Young, I. G., Frost, G. E., Rosenberg, H. and Gibson, F. (1972) Enterochelin system of iron transport in *Escherichia coli*: mutations affecting ferric-enterochelin esterase.

35. Greenwood, K. T. and Luke, R. K. (1978) Enzymatic hydrolysis of enterochelin and its iron complex in Escherichia Coli K-12. Properties of enterochelin esterase. *Biochim Biophys Acta* 525, 209-218.

SUMMARY AND FUTURE DIRECTIONS

Nickel is an important trace metal for eukaryotic organisms, including mammals, and is considered to be essential. However, over-exposure to this metal is of a greater concern than its deficiency. Therefore, the study of nickel over-exposure and the mechanisms behind these detrimental effects on cellular health (both prokaryotic and eukaryotic) has increasingly become of more and more interest over the past few decades; despite the overall toxic effects being well-known for the better part of the last century. In order to fully understand these toxic effects and, perhaps more importantly, in order to develop possible treatments and increase prevention, a thorough understanding of the potential targets and mechanisms of toxicity is required. Prokaryotes such as *E. coli*, therefore make for an ideal and simple model for studying nickel toxicity.

It was important to develop a batch culturing method that would expose new targets of nickel toxicity, specifically in during the lag phase of growth. This growth scheme would also be used as a way to standardize all cultures. After surveying a number of growth schemes, media components, and the resulting nickel toxicity phenotypes, it was determined that not only does the growth scheme and media components influence nickel toxicity, but that new, additional targets of nickel toxicity likely exist. Settling on a single growth scheme, we moved forward to explore nickel toxicity during growth on gluconate-infused minimal media, combined with a metabolic

stress caused by initially growing cells on glucose-infused minimal media. The observed nickel toxicity phenotype included a significantly increased lag phase duration, with a slightly increased doubling time. The increase in lag phase duration was determined to be a result of a metabolic block in gluconate metabolism; specifically the inhibition of 6-phosphogluconate dehydratase (Edd) activity in cells exposed to nickel during the lag phase. Additional data showed that nickel toxicity was dependent on intracellular uptake, and adaptation to the nickel stress was dependent on nickel efflux. Furthermore, by altering the timing of nickel exposure, we could alter the resulting toxicity phenotype. This suggested that while Edd may be a target during lag phase exposure to nickel, this might not be the case during exponential phase exposure. Therefore, the primary target(s) of nickel toxicity may depend on the growth phase of the cell.

Once Edd was determined to be a target of nickel toxicity during lag phase nickel exposure using our developed growth scheme, the next step was to determine the mechanism behind this inhibition. Given that Edd is an iron-dependent enzyme (specifically due to its 4Fe-4S enzymatic cluster), our first studies were to determine the effect of nickel on the iron metallome. Our data showed that nickel inhibits the accumulation of iron during the lag phase and diminished both the total and labile iron pools. Combined with our studies on the regulation of key iron homeostasis proteins, it was determined that cells are not only iron deficient but that they could also sense this deficiency. This could imply that the increase in lag phase duration is a result of the cell having to enter a kind of static mode until a sufficient amount of iron had been accumulated for proper metabolic activity.

Finally, an additional link between iron homeostasis and nickel toxicity has been demonstrated in the putative E. coli ferric reductase, YqjH. Despite the exact function and role of YqjH (concerning iron homeostasis) remaining ambiguous, the regulation of this enzyme is clearly under the control of both iron and nickel. In this aspect, it would appear that nickel regulates an enzyme involved in iron homeostasis, as opposed to the regulation of a protein involved in nickel homeostasis (such as RcnA and RcnR) by iron. This would certainly imply that there is, at some level, there exists a degree of cross talk between these two transition metals. We observed that the presence of YqjH plays an important role in the development of nickel resistance and the deletion of this enzyme resulted in no observable development of nickel resistance as compared to the wild type. This, therefore, implies that one possible role of YqjH is involved in adaptation of the cell to the nickel stress, possibly by aiding E. coli to accumulate iron during nickel exposure. This is supported by *in vivo* data published by Wang et al. showing YqjH is up-regulated in the presence of nickel, and that YqjH ferric reductase activity is not inhibited in the presence of nickel *in vitro*. However, given that a DyqjH mutant was still able to adapt to the nickel stress and ultimately exit the lag phase could further imply that the role of YqjH is not directly involved with the nickel stress, only the downstream (i.e. iron accumulation) effects.

Finally, the *in vitro* enhancement of YqjH ferric reductase activity in the presence of Zn(II) could potentially shed light on the utilization of intact enterobactin, a ferric siderophore, by *E. coli*. Interestingly enough, we observed that the presence of nickel was able to suppress either enterobactin synthesis or secretion; further tying the role of YqjH during nickel toxicity. The presence of zinc was shown to slow the formation of

the YqjH semiquinone state, an important step during its catalytic cycle, *in vitro*. This suggests that the presence of zinc could be possibly altering the redox potentials and capabilities of the YqjH enzyme. How such an incidence occurs remains to be determined.

To date, the mechanism of inhibition behind the identified target, Edd, remains unknown. This mechanism could fall within one of the mechanisms proposed by Macomber et al., or could be due to a novel mechanism, but this of course remains to be shown. The inhibition of this enzyme in the presence of nickel is an intriguing occurrence, given earlier evidence that nickel was unable to directly interfere with the mature, holo-Edd enzyme and its 4Fe-4S cluster. As nickel was shown to inhibit the uptake and accumulation of iron during the lag phase of growth, the inhibition of Edd could be due to a lack of viable Fe-S cluster synthesis (via a lack of the iron component). Future work may also focus on identifying any targets and mechanism of nickel toxicity that are involved in iron uptake. Therefore, additional protein targets beyond Edd would include the proteins and enzymes involved in 1) the synthesis of enterobactin, 2) the secretion of this siderophore into the extracellular media, and 3) the uptake of both the intact siderophore and its intermediate products; especially because there was an observed correlation between this siderophore compound and the presence of nickel.

Further work can also be done to explore the effect of nickel on the function of the Fe-S synthesis pathways, Isc and Suf. Given the connections and similarities between nickel and cobalt and the fact that cobalt inhibited function of the Isc pathway, nickel could also be interfering with these pathways by some unknown mechanism. Further evidence supporting this route was seen in the up-regulation of the Suf pathway; however

if this is due to an inhibition of the Isc pathway by nickel or a side effect of nickel toxicity due to low intercellular levels of iron remains to be determined. The toxic effects caused by nickel toxicity in *E. coli* may also be analogous to the targets and/or mechanisms of nickel toxicity observed in eukaryotic systems, where nickel has been observed to interfere with iron homeostasis as well.

APPENDIX A

NICKEL EXPOSURE DURING THE EXPONENTIAL PHASE ALTERS THE METABOLIC STATE OF *ESCHERICHIA COLI*

A.1 **Materials and Methods**

Bacterial Strains, Growth Media, and Growth Conditions. Where indicated cell growths for metal analysis and metabolomics studies were carried out using the previously described growth scheme in Figure 2.4. An individual colony was transferred from fresh Lennox broth (LB) agar plates into a 4mL volume of LB and grown for 4 – 5hrs at 37°C with shaking at 200rpm. Cells from this culture were pelleted and washed twice in sterile 1X M9 minimal media salts; then the OD_{600} was normalized to 1.0. Normalized cells were diluted 1:200 into M9 glucose minimal media containing 1X M9 minimal salts (BD Difco), 0.2% (w/v) glucose (Acros Organics), 0.2% (w/v) magnesium chloride, 0.1mM calcium sulfate, and 0.5µg/mL Thiamine HCl (Sigma-Aldrich). Cultures were incubated overnight for 18 – 20hr, at 37°C and 200rpm, then washed and pelleted twice in sterile 1X M9 salts as described above. The resulting cell suspensions were normalized to an OD_{600} of 2.0 and diluted 1:50 into M9 gluconate minimal media with 0.2% (w/v) potassium gluconate (Alfa Aesar) to give an initial OD_{600} of 0.04. Nickel (II) chloride (Sigma-Aldrich) was added to specified final concentrations in the

gluconate M9 minimal stress media. Other reagents added to glucose or gluconate M9 media are described in the appropriate figure legends.

Cell growth was monitored by UV-Vis absorption at 600nm and plotted versus time (in hours). Lag phase duration was determined using the online fitting program, DMFit (www.ifr.ac.uk/safety/DMfit), applying the no-asymptote fitted model and parameters.[1,2] Stationary phase OD_{600} measurements were omitted for best fit of the model. Doubling time of the cells during the exponential phase of growth, where the steepest linear fit line could be applied, was determined using the Online Doubling Calculator (http://www.doubling-time.com/compute.php).[3] All growths were cultured according to Figure 2.4, unless otherwise noted.

Metabolomics Analyses. Cells were cultured in LB and glucose minimal media as described previously in Figure 2-4. Cell cultures were then grown at 37°C, 200rpm in a 1.5L volume of M9 gluconate minimal media (in a 4.0L culture flask) to an OD_{600} of approximately 0.25-0.30. Once this OD was reached, nickel chloride was added to a final concentration of 50μM. All growths were performed in triplicate using 3 individual colonies. All growths were cultured on the same day to minimize variability between the triplicate samples.

The sampling procedure was adapted from Boroujerdi et al. along with other sources (Fig A.1).[4-6] At specified time points, a 200mL sample of each growth culture condition was removed from the main culture. The samples were measured out into a chilled glass beaker, and set on a stir plate in a 4°C cold room. A stir bar was added to aid with mixing. To each sample, approximately 75mL of $N_2(l)$ were added in 25mL increments. The increment additions were spaced 15-20sec apart to avoid cooling the

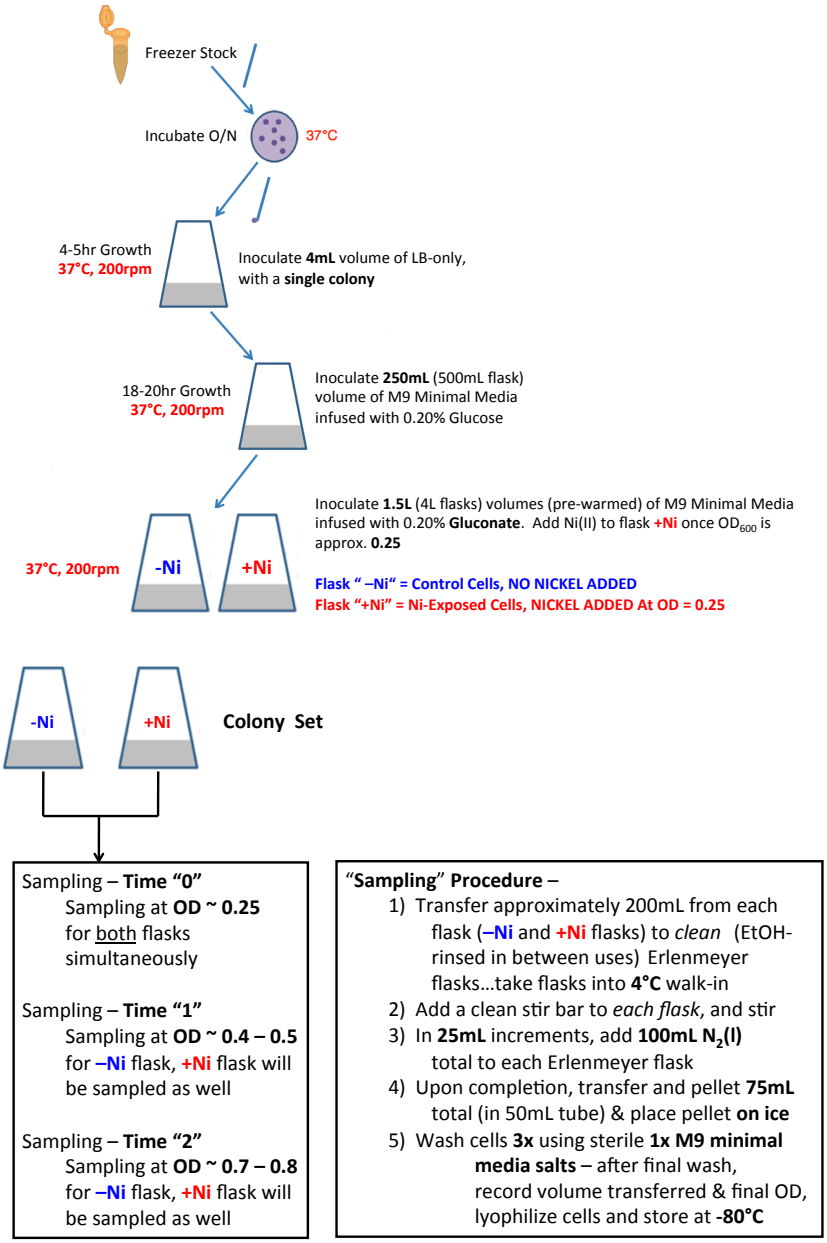

Figure A.1. **Description of Growths and Samplings for Metabolomics Analysis**. The above diagram visualizes the method utilized for culturing and sampling growths for metabolomics analysis. Three individual colonies were cultured, providing triplicate growths and every sample collected was performed in duplicate.

cells too quickly and forming ice crystals within the cells. After the additions, the culture temperature was cool to the touch. Two (2) 75mL samples of the cooled culture mixture were then centrifuged at 4000 x g for 20min, providing duplicate samples. The cell pellets were washed and pelleted three (3) times with cold 1x M9 minimal media at 16,000 x g for 1 minute each time. A final OD_{600} was measured for each sample, and recorded. A 900µL volume of resuspension was transferred to a pre-massed 1.5mL Eppendorf tubes and pelleted down at 16,000 x g. Samples were immediately lyophilized at ~140psi and -40°C overnight. The following day, the dried cell pellets were massed and recorded. The empty tube weight was subtracted out to give the final pellet mass (recorded as a dry mass). Final cell pellets were flash frozen in N_2(l) and stored at -80°C. Samples were sent do Arezue Boroujerdi, Ph.D. (Claflin University in Orangeburg, SC 29115) for processing, extraction, and NMR analysis.

Inductively Coupled Plasma Mass Spectrometry (ICP-MS). Cells were cultured in LB and glucose minimal media as described previously in Figure 2.4. Cell cultures were then grown in 1.5L M9 gluconate minimal media, with or without 50µM nickel chloride in a 4L culture flask at 37°C and 200rpm. 150mL samples were centrifuged at 3,000 x g for 20min and then pelleted three times at 16,000 x g with intermediate washing in 1mL sterile, ice-cold wash solution consisting of 50mM EDTA tetrasodium salt, 100mM oxalic acid, 100mM NaCl, and 10mM KCl, to remove any cell surface-associated metal ions. Washed cell pellets were re-suspended in a 1mL volume of ice-cold, sterile 1X M9 salts. A small portion of each sample was then diluted 40-fold to record the final OD_{600}. Cell re-suspensions were transferred to an acid-washed, Perfluoroalkoxy (PFA) microcentrifuge tube (Savillex Corporation) and centrifuged at

16,000 x g. After centrifugation, the supernatant was discarded and the cell pellets were frozen in liquid nitrogen. Cell pellets were stored at -80°C until ready for digestion and ICP-MS analysis.

Samples for ICP-MS were thawed for 15min on ice followed by drying at 80°C for 30min. A 400µL volume of trace-metal grade HNO_3 (distilled on site at the Center for Elemental Mass Spectrometry (CEMS), University of South Carolina) was added to each sample tube and digested at 80°C for 4hrs. After digestion, each sample tube was centrifuged for 1min at 16,000 x g and the supernatant was diluted 1:20 into MQ H_2O, giving a final acid matrix of 3.5%. Blanks consisting of 3.5% trace-metal grade HNO_3 only in MQ H_2O (18MΩ) were made and prepared in the same manner as the cell samples. Standard element solutions (Inorganic Ventures) were also prepared in the same final acid matrix of 3.5% to establish a limit of detection and a calibration curve for determining the concentrations of each metal analyzed. The isotopes of biologically relevant transition metals with masses of ^{56}Fe, ^{58}Ni, ^{64}Zn, ^{55}Mn, and ^{63}Cu were selected for analysis based on natural abundances. Samples were analyzed under medium resolution to resolve polyatomic interferences (e.g. $^{40}Ar^{16}O$ for ^{56}Fe) on a Thermo Element 2 High Resolution ICP-MS instrument operated by CEMS at the University of South Carolina. A cyclonic spray chamber (Elemental Scientific) was used for delivery of sample into the instrument. Final intracellular metal concentrations were calculated based on total cell numbers present in the EPR tube by using the OD_{600} and previously established cell number conversions.[7]

A.2 **Results and Discussion**

Exponential phase nickel exposure shifts the metabolic state of *E. coli* and stalls growth. Metabolomics is the characterization and quantification of the cellular metabolome (the collection of the low-weight compounds and metabolites produced and consumed by the cell) and is a useful tool for analyzing the metabolic state of cell during a defined physiological condition.[8] This technique therefore provides researchers a metabolic "snapshot" for insight into the effect a particular stress may have on the metabolic state. Metabolomics has quickly become a great tool for studying the effects of metal toxicity in bacteria.[9] However, this technique also brings along its own challenges. The metabolic state of microorganisms is heavily influenced by even small perturbations, and can quickly change when exposed to a stress. Therefore, the selection of the samples and the proceeding sample preparation for metabolomics analysis require quick and efficient methods in order to accurately capture this metabolic "snapshot".[5] The alterations of individual metabolites can also be further analyzed and quantified through NMR spectroscopy and the use of large libraries for identifying the specific metabolite(s). This is would be particularly useful in determining metabolic "blocks" in response to a particular stress and potentially help to identify enzymatic targets.

The effect of nickel toxicity on the metabolome of *E. coli* offered an intriguing aspect that could be analyzed by metabolomics. As with other "-omics" based methods, a large number of cells was required. To optimize the process, we started by exposing *E. coli* cells to nickel during the exponential phase of growth. Previously, the phenotypic changes in growth with exponential nickel exposure were much less severe, as compared

to lag phase exposure (Figs. 2.7, 2.10, A.2). In contrast to lag phase nickel exposure, the doubling time was drastically altered in wild type cells exposed to nickel during the exponential phase instead of the lag phase duration (Fig A.3). This comes as no surprise, since the extended lag phase phenotype is only observed with lag phase nickel exposure. Nonetheless, though less severe, exponential nickel exposure still negatively affect wild type cells.

MG1655 wild type cells were collected and prepared for metabolomics analysis through the methods described above (Fig A.1). Alterations in several metabolites were noted from prepared metabolomics samples exposed to the nickel stress, including several amino acids and central carbon metabolism intermediates (Fig. A.4). The intracellular amounts of alanine and glycine were lower in nickel-exposed cells (Fig. A.4). Interestingly, one of the reactions that produce alanine is performed by the desulfurase IscS, which catalyzes a sulfur transfer using cysteine as a substrate. IscS is responsible for the donation of sulfur into the Fe-S cluster synthesis pathway. Glcyine is also produced by the GlyA enzyme, which contains a PLP cofactor vital to its function in the synthesis of purines, thymidine, and other products. IscS also requires a PLP cofactor to function, suggesting a potential target of nickel toxicity. Furthermore, another metabolite, hypoxanthine, was determined to be higher in nickel-exposed cells. This particular binds to the PurR transcription factor and represses the transcription of the GlyA enzyme.[10] This may suggest that nickel could be targeting these two enzymes directly as well. Other metabolites, such as acetate and lactate, however, were observed to be higher (Fig. A.4). However, it is less clear how nickel may be affecting these two compounds.

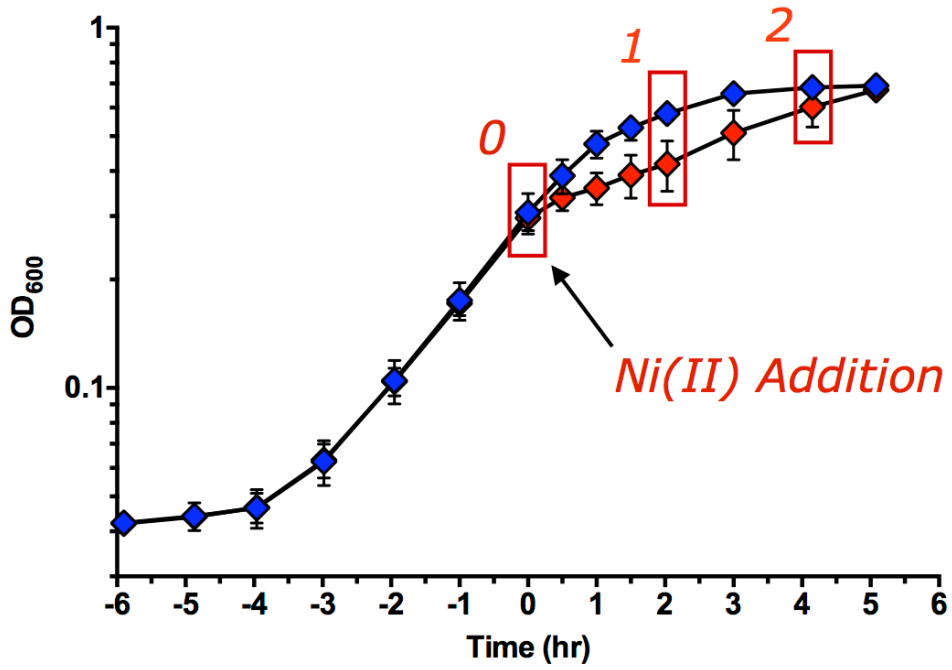

Figure A.2. **Nickel exposure during the exponential phase slowed bacterial growth**. MG1655 wild type cells were cultured as according to the growth scheme described in Figure 2-4. Growths were exposed to nickel during the lag phase, at an approximate OD_{600} of 0.25. All growths were performed in triplicate (n = 3). The boxed time points represent when a sample was taken for metabolomics processing and analysis.

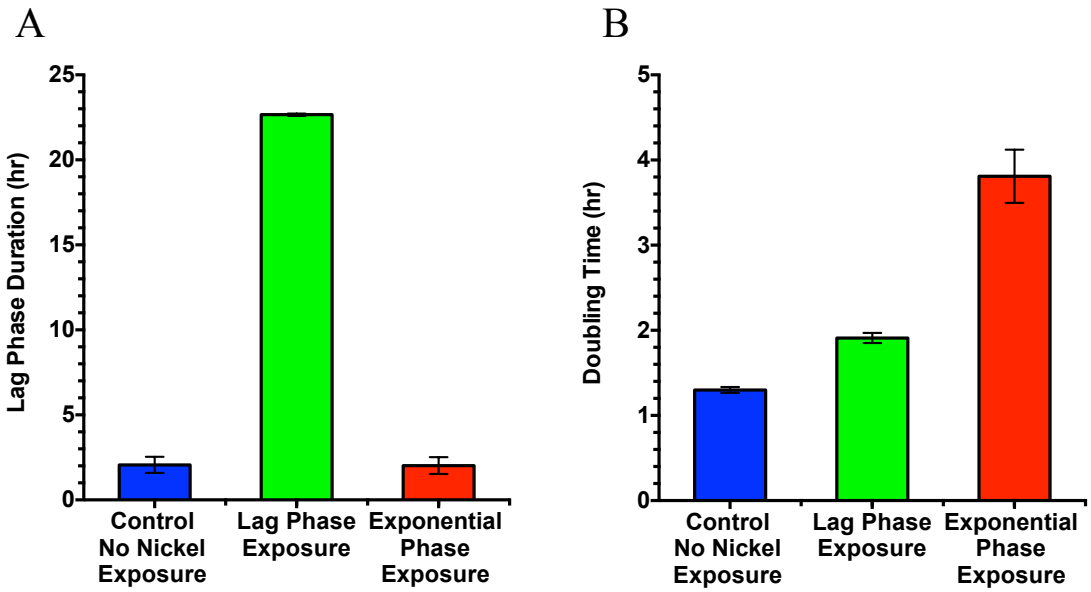

Figure A.3. **Nickel exposure during the exponential phase slows bacterial growth and alters the doubling time of the culture**. MG1655 wild type cells were exposed to nickel during the exponential phase and compared against control growths without the addition of nickel and to prior growths with nickel exposure during the lag phase. All growths were performed in triplicate (n = 3). (A) The lag phase duration of the cultures with the delayed nickel exposure (red bar) showed no change as expected and entered the exponential phase with the control growths with no nickel exposure (blue bar). Only when nickel exposure was performed during the lag phase (green bar) is any effect observed. (B) The doubling time (or the rate of growth) of the wild type cells exposed to nickel during the exponential phase was significantly slowed (red bar), as compared to the control cells (blue bar) without any nickel exposure. This comes in stark contrast to cells to cells exposed to nickel during the lag phase (green bar).

WT, - Ni	WT, + Ni
Alanine	Down
Acetate	Up
N-acetylaspartate	Down
Lactate	Up
Succinate	Down
Adenine	Up
Glycine	Down
Hypoxanthine	Up
Adenosine	Up/Down???
Formate	Up

Figure A.4. **Relative changes in the concentrations for select metabolites after nickel exposure during the lag phase**. Select metabolites were identified from metabolomics samples by proton NMR analysis. The amounts of each metabolite from the control (-Ni) cells were relatively compared to the amount of the same metabolite in nickel-exposed cells (+Ni). Nickel exposure was performed after cell cultures had reach and OD_{600} of approximately 0.25.

Principal component (PC) analysis was kindly performed by Boroujerdi et al. to statistically compare the individual metabolic states of samples at various stages of growth, as well as after exponential phase nickel exposure. Overlaid groups of the three time points of nickel-exposed cells were observed to be more static as compared to the control cell samples at identical time points (Fig. A.5A). While control cells showed a general shift in the metabolic state as the cells progress from the exponential phase into the stationary phase, nickel-exposed cells remained more metabolically-static. This is also represented 3-dimensionally, where control cells occupied various spaces as the cell progressed into stationary phase, whereas nickel-exposed cells remained in the same space (Fig A.5B). This suggests the nickel exposure forced the cells into a bacteriostatic-like state while coping with the nickel stress. This was observed phenotypically as well and supports the increase in doubling time (Figs. A.2, A.3). The statistical constants for the pairwise comparisons suggest that the two groups of samples, control cells versus nickel-exposed cells, were statistically different (Fig. A.6, data not shown).

Intracellular levels of iron are unaffected by exponential phase nickel exposure. In addition to analyzing the metabolome of *E. coli* during nickel stress, we also sought to characterize the metallome of select metals during the same stress period. ICP-MS remained best tool for achieving this. Previously, it was established that lag phase exposure to nickel inhibited the uptake of iron by *E. coli* and led to various downstream effects on the activity of an Fe-S cluster enzyme, Edd, the intracellular and labile iron pool concentrations, and the regulation of several Fur-controlled genes involved in iron uptake (Figs. 2.9, 3.4, 3.5, and 3.6). However, exponential phase nickel

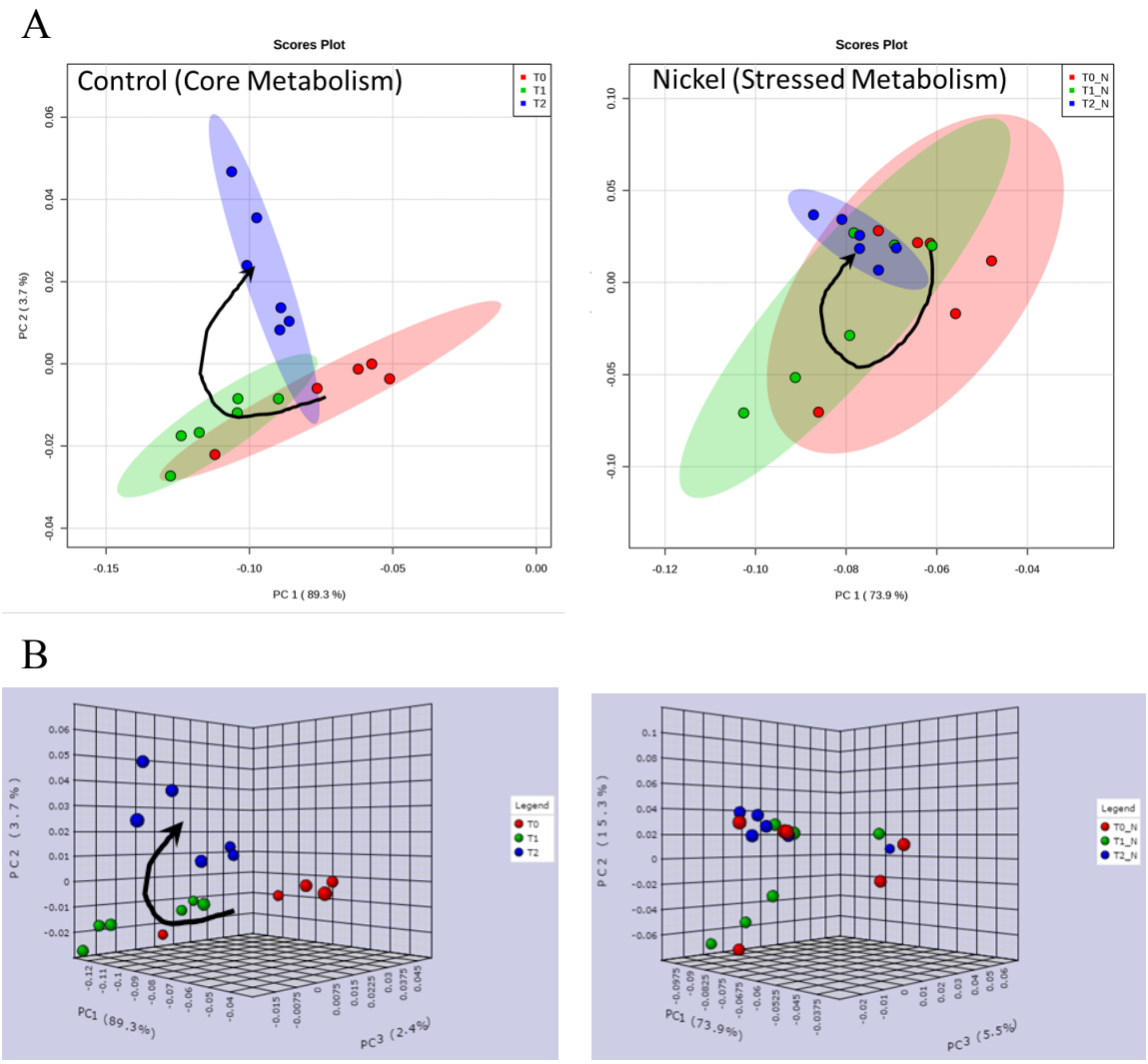

Figure A.5. **Exponential phase nickel exposure forced cells to enter a steady-state to cope with the nickel stress**. MG1655 wild type cells were exposed to nickel during the exponential phase and collected for metabolomics analysis. (A) Overlay of the three sampling times, T0 (red dots), T1 (green dots), and T2 (red dots) for Control (Core Metabolism) cells compared to Nickel (Stressed Metabolism) cell samples. (B) A 3D representation of the data from panel A. The arrow indicates the shifts in metabolism of the control (nickel free) cells as the culture moves from the exponential phase into the stationary phase. No such shift is observed with the nickel-exposed cells.

A

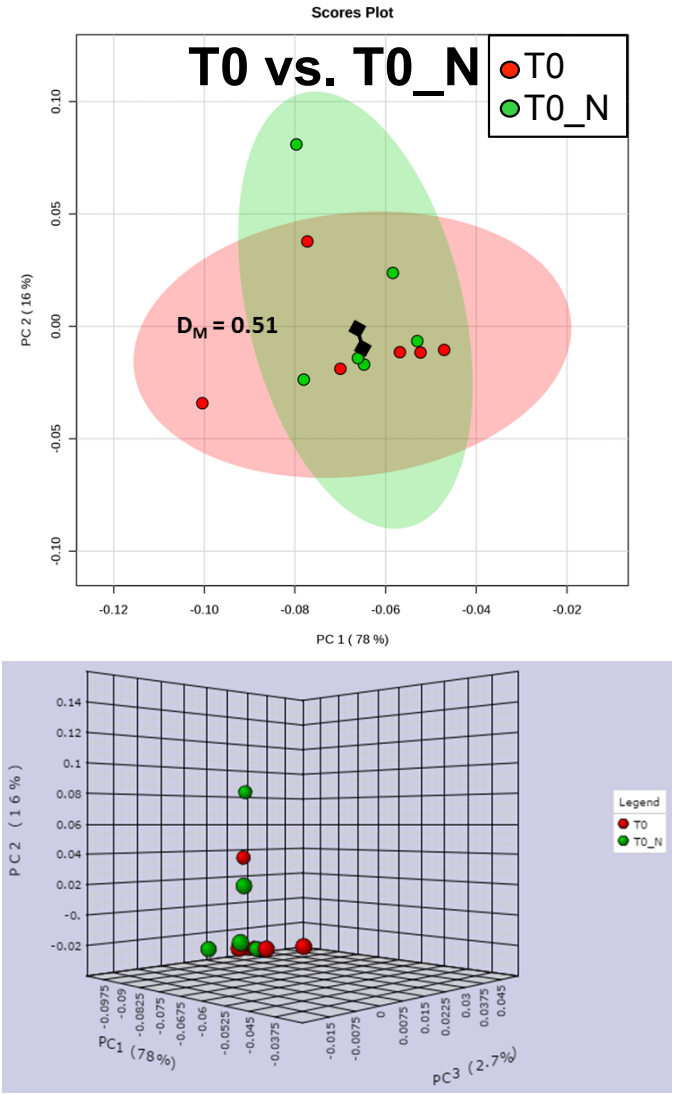

B

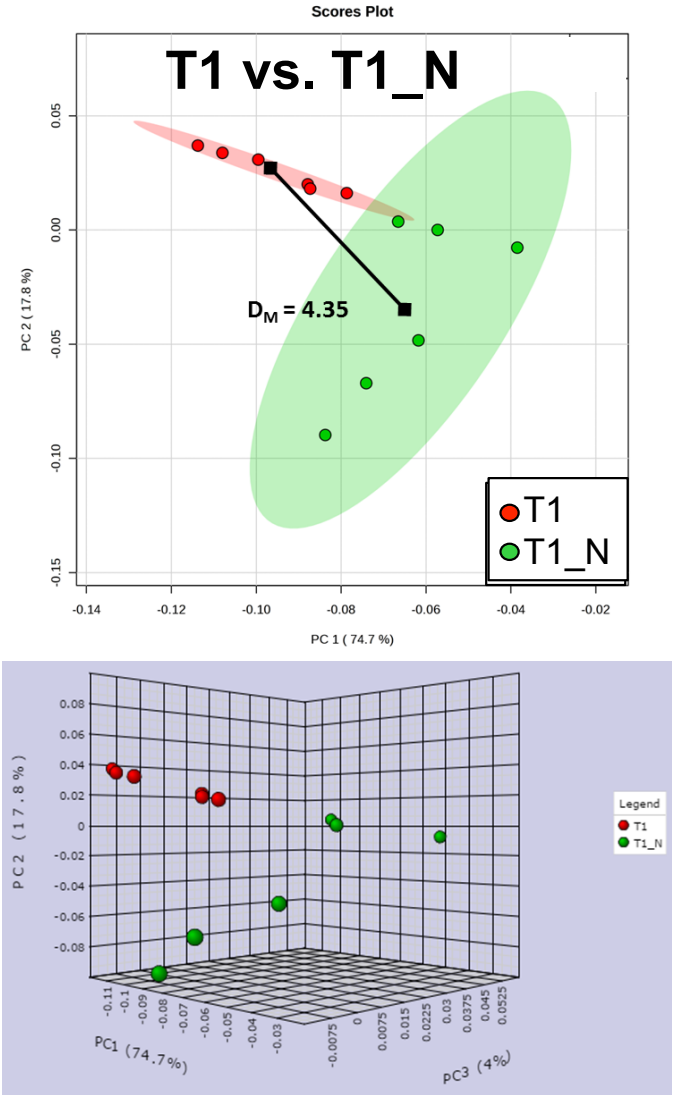

C

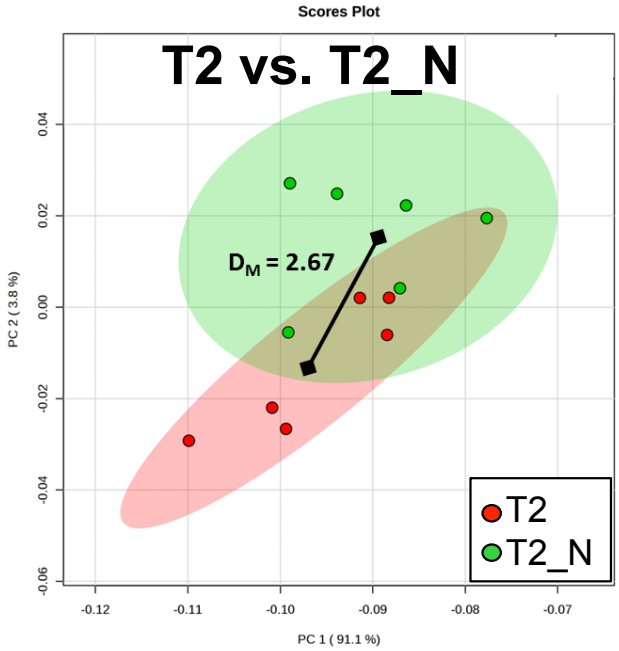

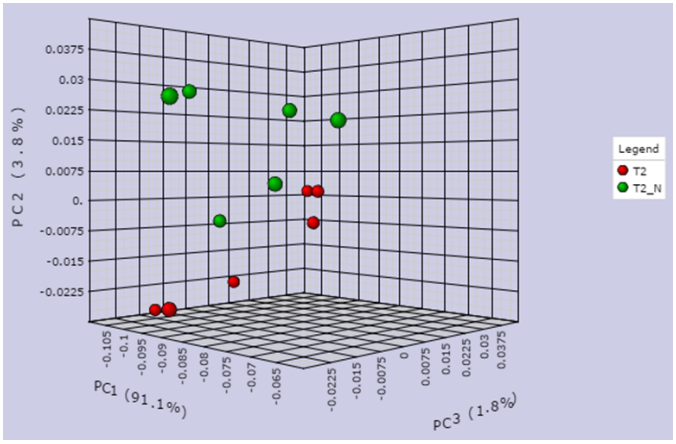

Figure A.6. **Nickel-exposed cells exist in different metabolic states after similar periods of incubation as compared to control cells**. Individual two-dimensional PC plots comparing control cells (red dots) and nickel-exposed cells (red dots). (A) Comparison of control cells (T0) and nickel-exposed cells (T0_N) at the first sampling time when nickel was added during the exponential phase. (B) Comparison of control cells (T1) and nickel-exposed cells (T1_N) at the first sampling time when nickel was added during the exponential phase. (C) Comparison of control cells (T2) and nickel-exposed cells (T2_N) at the first sampling time when nickel was added during the exponential phase.

exposure caused no significant differences in intracellular iron levels as compared to control cells (Fig. A.7A) Moreover, there was a drastic alteration in intracellular nickel levels in the nickel-exposed cells, as expected (Fig. A.7B). Finally, a similar affect was observed with intracellular zinc levels, given that they were slightly raised, as compared to the control cells (Fig. A.7C). Unlike the observations on iron homeostasis with nickel exposure during the lag phase, iron homeostasis appeared to be less of a target with exponential phase exposure. However, intracellular iron levels are known to decrease after exit from the lag phase.[2] This indicates that intracellular iron is in less demand during the exponential phase and is no longer a primary target of nickel toxicity at this stage. Coupled with the previous observations towards metabolites involved in nucleic and amino acid production, this may suggest that nickel is now targeting systems involved with sustain the rapid growth seen in cell cultures during the exponential phase.

A.3. **References**

1. Baranyi, J. and Roberts, T. A. (1994) A dynamic approach to predicting bacterial growth in food. *Int J Food Microbiol* 23, 277-294.

2. Rolfe, M. D., Rice, C. J., Lucchini, S., Pin, C. Thompson, A., Cameron, A. D. S., Alston, M., Stringer, M. F., Betts, R. P., Baranyi, J., Peck, M. W., and Hinton, J. C. D. (2012) Lag phase is a distinct growth phase that prepares bacteria for exponential growth and involves transient metal accumulation. *J Bacteriol* 194, 686-701.

3. Roth, V (2006) Doubling Time. (http://www.doubling-time.com/compute.php)

4. Boroujerdi, A. F. B., Vizcaino, M. I., Meyers, A., Pollock, E. C., Huynh, S. L., Schock, T. B., Morris, P. J., and Bearden, D. W. (2009) NMR-based microbial metabolomics and the temperature-dependent coral pathogen *Vibrio coralliilyticus*. *Environ Sci Technol* 43, 7658-7664.

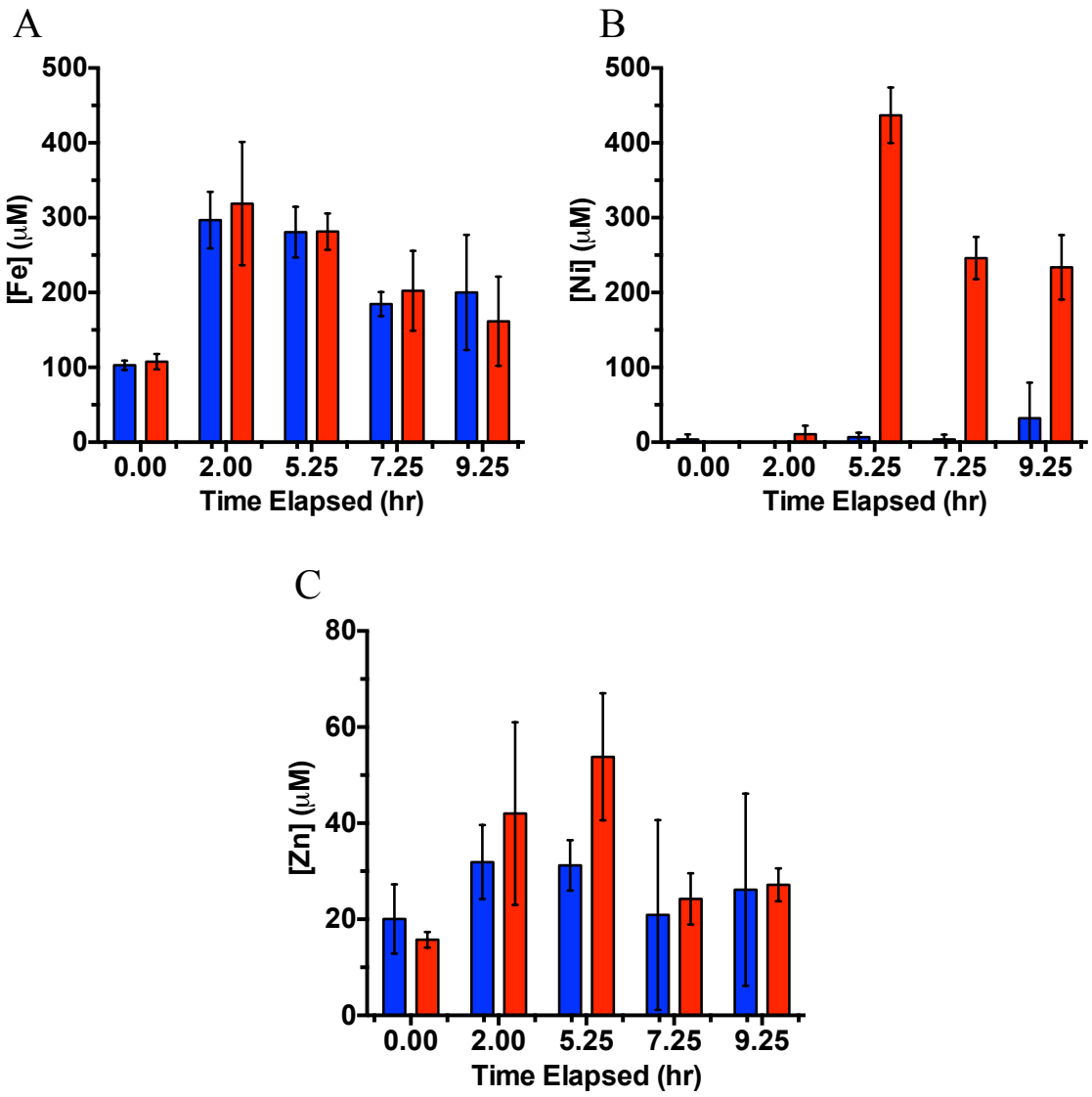

Figure A.7. **Intracellular iron levels remain similar in nickel-exposed cells as ompared to control cells when nickel is added during the exponential phase**. MG1655 wild type cells were cultured as according to the growth scheme in Figure 2-4. Select growths were exposed to nickel during the exponential phase at an OD_{600} of approximately 0.25, at a time of approximately 5.25hrs into the growth. Cells were collected for ICP-MS analysis at the specified times above. (A) Intracellular iron levels remained unchanged with nickel exposure (red bars) as compared to control, nickel-free cells (blue bars). (B) Nickel-exposed cells saw drastic increases in intracellular levels of nickel (red bars) as compared to the control cells (blue bars). Four hours after exposure, intracellular levels of nickel had fallen by approximately 50%. (C) Zinc levels in nickel-exposed cells (red bars) increased slightly after nickel exposure, but quickly matched control cells (blue bars) after two hours of growth.

5. Boroujerdi, A. F. B., Vizcaino, M. I., Meyers, A., Pollock, E. C., Huynh, S. L., Schock, T. B., Morris, P. J., and Bearden, D. W. (2009) NMR-based microbial metabolomics and the temperature-dependent coral pathogen *Vibrio coralliilyticus*. *Environ Sci Technol* 43, 7658-7664.

6. Alvarez-Sanchez, B., Capote-Priego, F., Luque de Castro, M. D. (2010) Metabolomics analysis I. Selection of biological samples and practical aspects preceding sample preparation. *Trends in Anal Chem* 29, 111-119.

7. Alvarez-Sanchez, B., Capote-Priego, F., Luque de Castro, M. D. (2010) Metabolomics analysis II. Preparation of biological samples prior to detection. *Trends in Anal Chem* 29, 120-127.

8. Volkmer, B. and Heinemannn, M. (2011) Condition-dependent cell volume and concentration of *Escherichia coli* to facilitate data conversion for systems biology modeling. *PLoS One* 6, e23126.

9. Tremaroli, V., Workentine, M. L., Weljie, A. M., Vogel, H. J., Ceri, H., Viti, C., Tatti, E., Zhang, P., Hynes, A., Turner, R. J., and Zannoni, D. (2008) Metabolomics investigation of bacterial response to metal challenge. *Appl Environ Microbiol* 75, 719-728.

10. Boothe, S. C., Workentine, M. L., Weljie, A. M., and Turner, R. J. (2011) Metabolomics and its application to studying metal toxicity. *Metallomics* 3, 1142-1152.

11. Stelert, J. G., Kubu, C., and Stauffer, G. V. (1992) The PurR binding site in the *glyA* promoter region of *Escherichia coli*. *FEMS Microbiol* 78, 299-304.